This is a digital copy of a book that was preserved for generations on library shelves before it was carefully scanned by Google as part of a project to make the world's books discoverable online.

It has survived long enough for the copyright to expire and the book to enter the public domain. A public domain book is one that was never subject to copyright or whose legal copyright term has expired. Whether a book is in the public domain may vary country to country. Public domain books are our gateways to the past, representing a wealth of history, culture and knowledge that's often difficult to discover.

Marks, notations and other marginalia present in the original volume will appear in this file - a reminder of this book's long journey from the publisher to a library and finally to you.

Usage guidelines

Google is proud to partner with libraries to digitize public domain materials and make them widely accessible. Public domain books belong to the public and we are merely their custodians. Nevertheless, this work is expensive, so in order to keep providing this resource, we have taken steps to prevent abuse by commercial parties, including placing technical restrictions on automated querying.

We also ask that you:

+ *Make non-commercial use of the files* We designed Google Book Search for use by individuals, and we request that you use these files for personal, non-commercial purposes.
+ *Refrain from automated querying* Do not send automated queries of any sort to Google's system: If you are conducting research on machine translation, optical character recognition or other areas where access to a large amount of text is helpful, please contact us. We encourage the use of public domain materials for these purposes and may be able to help.
+ *Maintain attribution* The Google "watermark" you see on each file is essential for informing people about this project and helping them find additional materials through Google Book Search. Please do not remove it.
+ *Keep it legal* Whatever your use, remember that you are responsible for ensuring that what you are doing is legal. Do not assume that just because we believe a book is in the public domain for users in the United States, that the work is also in the public domain for users in other countries. Whether a book is still in copyright varies from country to country, and we can't offer guidance on whether any specific use of any specific book is allowed. Please do not assume that a book's appearance in Google Book Search means it can be used in any manner anywhere in the world. Copyright infringement liability can be quite severe.

About Google Book Search

Google's mission is to organize the world's information and to make it universally accessible and useful. Google Book Search helps readers discover the world's books while helping authors and publishers reach new audiences. You can search through the full text of this book on the web at `http://books.google.com/`

DIEGO
984

Digitized by Google

THE UNIVERSITY LIBRARY
UNIVERSITY OF CALIFORNIA, SAN DIEGO
Digitized by Google

UNIVERSITY OF CALIFORNIA, SAN DIEGO
3 1822 00567 7984

University of California, San Diego
Please Note: This item is subject to recall.
Date Due

MAY 0 4 1992	
~~DEC 2 3 2002~~	
DEC 0 5 2002 REC'D	
~~MAR 2 4 2008~~	
~~SEP 2 3 2008~~	
SEP 0 2 REC'D	
~~DEC 0 9 2008~~	

Cl 39a (4/91) UCSD Lib.

Digitized by Google

Digitized by Google

JASON

April 1979

Technical Report
JSR-78-07

THE LONG TERM IMPACT OF ATMOSPHERIC CARBON DIOXIDE ON CLIMATE

G. MacDonald, Chairman
H. Abarbanel
P. Carruthers
J. Chamberlain
H. Foley
W. Munk
W. Nierenberg
O. Rothaus
M. Ruderman
J. Vesecky
F. Zachariasen

Prepared for:

U.S. Department of Energy
Washington, D.C. 20545

Contract EY-76-C-03-0115, P.A. 136

SRI Project 5793

SRI International
1611 North Kent Street
Arlington, Virginia 22209

Digitized by Google

Digitized by Google

ABSTRACT

If the current growth rate in the use of fossil fuels continues at 4.3% per year, then the CO_2 concentration in the atmosphere can be expected to double by about 2035 provided the current partition of CO_2 between the atmosphere, biosphere and oceans is maintained as is the current mix of fuels. Slower rates of anticipated growth of energy use lead to a doubling of the carbon content of the atmosphere sometime in the period 2040 to 2060.

This report addresses the questions of the sources of atmospheric carbon dioxide, considers distribution of the present carbon dioxide among the atmospheric, oceanic and biospheric reservoir and assesses the impact on climate as reflected by the average ground temperature at each latitude of signficant increases in atmospheric carbon dioxide.

The oceans and the biosphere, including the soils, store very large amounts of carbon compared with that in the atmosphere. Small changes in these large reservoirs can have a major effect on the atmosphere. Neither the ocean-atmosphere nor the atmosphere-biosphere interfaces are well understood. In regard to the former we propose a new model for the mixing of carbon dioxide in the oceans. The proposed model explicitly takes into account the flow of colder/and or saltier water

Digitized by Google

to great depths. Such models provide a means for the evaluation of the oceanic carbon dioxide mixing without resort to the use of box model which with adjusted effective diffusion parameters. The atmosphere-biosphere interface is significantly more complex. It is clear, however, that data on several key questions are needed: (1) clear and detailed information on the rapid turnover time of life forms in the oceans (2) information on the possibility that biologically derived organic debris in shallow seas could be buried and thus effectively removed from the oceans (3) the reservoir of carbon in the soils is thought to be about five times the amount in the atmosphere but the fraction of that carbon which can communicate with the atmosphere is not known.

Increasing CO_2 in the atmosphere perturbs climate by altering the radiative properties of the atmosphere. The resulting climate change has been calculated through highly parameterized analytic models of the ocean-atmosphere system or by large computer models. We have adopted the first approach starting with an atmosphere locally in radiative equilibrium and then allowing meridional transport of heat. We have constructed two models for the case of radiative equilibrium treating the atmosphere as gray and dividing the infrared emission region into nine bands. The gray atmosphere model predicts an increase of average surface temperature of $2.8^{o}K$ for a doubling of CO_2, a result about a degree less than the nine band model. In the model the principal effect of increasing CO_2 is to enhance

Digitized by Google

the absorption by weak CO_2 bands in 8-12 micron region. Trace gases, CH_4, N_2O, NH_3, freons and hydrocarbons can also block off the atmospheric window.

An analytic model of the atmosphere has been constructed (JASON Climate Model). Calculation with this zonally averaged model shows an increase of average surface temperature of 2.4^{o} for a doubling of CO_2. The equatorial temperature increases by $0.7^{o}K$ while the poles warm up by 10 to $12^{o}K$.

The JASON climate model suffers from a number of fundamental weaknesses. The role of clouds in determining the albedo is not adequately taken into account nor are the asymmetries between the northern and southern hemisphere. We expect, however, that models intermediate between the large GCMs and the primitive analytic models can yield insights into the nature of climate change.

The warming of climate will not necessarily lead to improved living conditions everywhere. Changes in sea level, in agricultural productivity and in water availability can be anticipated, but the dimensions of their economic, political or social consequences can not.

Digitized by Google

Digitized by Google

CONTENTS

ABSTRACT i

LIST OF FIGURES vii

LIST OF TABLES ix

ACKNOWLEDGEMENTS xi

I THE IMPACTS OF INCREASING CARBON DIOXIDE: AN OVERVIEW . 1
(G. MacDonald)

A. Climate and Carbon Dioxide in Historical Perspective 3
B. Measured Changes in Atmospheric Carbon Dioxide . . 5
C. Fuel Sources of Carbon 9
D. The Carbon Mystery 14
E. Future Carbon Levels in the Atmosphere 17
F. Climate Change from Changing Carbon Dioxide . . . 18
G. Zeroth Order Calculations 21
H. First Order Models 23
I. Global Circulation Models 23
J. Impacts of Climate Change 24
K. Conclusions 27

REFERENCES FOR SECTION I 31

II THE OCEANS AS A SINK FOR CARBON DIOXIDE 33

A. Cold Ocean Sinks (M. Ruderman) 34
B. A Pipe Model of the Oceans (W. Munk) 40
C. Solutions to the Pipe Models (F. Zachariasen) . . 47

REFERENCES FOR SECTION II 59

Digitized by Google

CONTENTS (CONT)

III RADIATIVE LIMITES ON CLIMATE 61

A. Gray Homogeneous Model of the Atmosphere (J. Chamberlain) 62
B. A Simple Band Model for Infrared Emission from the Terrestrial Atmosphere (J. Vesecky) 80

REFERENCES FOR SECTION III 113

APPENDIX A to SECTION III (M. Ruderman) 115

IV CLIMATE MODELS 119

A. Energy Budget Climate Models (O. Rothaus) 119
B. JASON Climate Model (H. Abarbanel) 130
C. Sensitivity of Climate Models (W. Nierenberg) . . . 151
D. Sensitivity of Energy Budget Models to Changes in Albedo (P. Carruthers) 157

REFERENCES FOR SECTION IV 163

V RESEARCH NEEDS: A CRITIQUE OF "A COMPREHENSIVE PLAN FOR CARBON DIOXIDE EFFECTS RESEARCH AND ASSESSMENT 165

A. General 165
B. Priorities 167
C. Management Issues 169

Digitized by Google

LIST OF FIGURES

Figure I-1	ATMOSPHERIC CARBON DIOXIDE CONCENTRATION AT MAUNA LOA OBSERVATORY	6
Figure II-1	AN OCEAN PIPE MODEL	42
Figure II-2	THE GEOMETRY ILLUSTRATING THE USE OF THE PIPE MODEL	48
Figure II-3	MODEL FOR SOLUTION OF PIPE MODEL WITH A SINGLE SOURCE	52
Figure III-A	TEMPERATURE VERSUS CO_2 ABUNDANCE IN A GRAY MODEL IS IN GLOBAL RADIATIVE EQUILIBRIUM . .	72
Figure III-1	SCHEMATIC DIAGRAM OF TEMPERATURE PROFILE USED IN NINE-BAND IR EMISSION MODEL FOR THE TERRESTRIAL ATMOSPHERE	83
Figure III-2	INFRARED BAND ABSORPTION OF ATMOSPHERIC GASES	85
Figure III-3	THERMAL EMISSION FROM THE EARTH'S SURFACE AND ATMOSPHERE EMITTED VERTICALLY UPWARDS AND MEASURED BY HANEL et al. (1971) USING THE INFRARED INTERFEROMETER SPECTROMETER ON NIMBUS 4, (a) OVER SAHARA, (b) OVER MEDITERRANEAN AND (c) OVER ANTARCTIC	97
Figure III-4	ATMOSPHERIC RADIATION FLUX TO SPACE $F(T_s)$ . .	100
Figure IV-1	THE AVERAGE ANNUAL LATITUDINAL DISTRIBUTION OF THE COMPONENTS OF THE ENERGY BALANCE OF THE EARTH-ATMOSPHERE SYSTEM IN KLY $YEAR^{-1}$ (top) AND OF THE COMPONENTS OF THE POLEWARD ENERGY FLUX IN 10^{19} KCAL $YEAR^{-1}$(bottom)	137
Figure IV-2	PREDICTION OF THE JASON MODEL FOR VARIANCE IN TEMPERATURE WITH LATITUDE (O) AND A CO_2 CONCENTRATION OF 332 ppm	144
Figure IV-3	OBSERVATION DATA TAKEN FROM CESS (1976) FOR NORTHERN & SOUTHERN HEMISPHERES (O is the latitude)	145

Digitized by Google

Figure IV-4 PREDICTION OF THE JASON MODEL FOR VARIANCE IN TEMPERATURE WITH LATITUDE (O), AND ASSUMING A DOUBLING OF THE CO_2 CONCENTRATION FOR PRESENT LEVELS 146

Figure IV-5 SAMPLE PLOTS OF TEMPERATURE VARIATION FOR SAMPLE CASES 156

a) Change in A & B Factor = 0.98; No Ice Line . 156
b) Change in A & B Factor = 1.01; Sin Ice Latitude = 0.867 156
c) Change in A & B Factor = 1.00; Sin Ice Latitude = 0.935 156
d) Change in A & B Factor = 1.02; Sin Ice Latitude = 0.798 156

Digitized by Google

LIST OF TABLES

Table I-1	CHANGING CO_2 CONTENT OF ATMOSPHERE	7
Table I-2	ESTIMATED CARBON ADDED TO THE ATMOSPHERE BY THE BURNING OF FUELS IN GTONS	10
Table I-3	CARBON PRODUCED PER HUNDRED QUADS OF THERMAL ENERGY GENERATED	10
Table I-4	1975 WORLD PRODUCTION OF CARBON BY BURNING FOSSIL FUELS	11
Table I-5	WORLD-WIDE CARBON RELEASE IN THE YEAR 2000 . .	13
Table I-6	WORLD-WIDE CARBON RELEASE IN THE YEAR 2025 . .	13
Table I-7	APPROXIMATE MAGNITUDES OF THE RESERVOIRS OF CARBON IN GTONS	15
Table I-8	APPROXIMATE DATES FOR DOUBLING THE CARBON DIOXIDE CONTENT OF THE ATMOSPHERE	19
Table I-9	PROJECTED WORLD CARBON PRODUCTION BY USE OF RECOVERABLE RESERVES	20
Table I-10	PROJECTED WORLD CARBON PRODUCTION BY USE OF RECOVERABLE RESOURCES	20
Table III-1	ABSORBERS IN 8 - 12 μm WINDOW	68
Table III-2	BAND CHARACTERISTICS	84
Table III-3	EFFECTIVE HEIGHTS AND TEMPERATURES FOR THE SURFACE CONDITIONS OF FIG. III-3	99
Table III-4	LINEAR APPROXIMATION FOR $F(T_s')$ CENTERED ON λ°C, $F(T_s'$ in °C) = $A+BT_s'$	108
Table IV-1	SUMMARY OF ZONAL ANNUAL CLIMATOLOGICAL DATA FOR THE NORTHERN HEMISPHERE	133
Table IV-2	SUMMARY OF ZONAL ANNUAL CLIMATOLOGICAL DATA FOR THE SOUTHERN HEMISPHERE	134
Table IV-3	SENSITIVITY OF THE ICE LINE TEMPERATURE . . .	154

Digitized by Google

Digitized by Google

ACKNOWLEDGMENTS

The JASON 1978 Summer Study on carbon dioxide was assisted by numerous scientists, each of whose knowledge of the field far exceeds that of the contributors to this report. In particular, we wish to thank:

Wallace Broecker	Columbia University
Harmon Craig	Scripps Institute of Oceanography
Hans Oeschger	University of Bern
H. Gote Ostlund	University of Miami
Minze Stuiver	University of Michigan

for introducing us to the mysteries of carbon dioxide models and the role of the oceans in sequestering carbon dioxide. Their insights inspired us to pursue alternative ways of examining the pathways by which carbon dioxide enters into and mixes with the oceans.

Robert Chervin	National Center for Atmospheric Research
Lawrence Gates	Oregon State University
Gerald North	University of Missour
Michael Schlesinger	Oregon State University
Steven Schneider	National Center for Atmospheric Research

Digitized by Google

illuminated many of the problems of modeling the atmosphere for long-term climate changes. Their perceptive presentations convinced us to go back to basic principles and try to understand radiative equilibrium and energy budgets. We have tried.

As physicists, we welcomed the opportunity to provide the rationale that biology was not in any way of significance in understanding effects of carbon dioxide.

Melvin Calvin	University of California, Berkeley
Constance Delwicke	University of California, Davis
Boyd Strain	Duke University

convinced us that the biosphere plays a critical role in the carbon dioxide problem. We are now attempting to understand the carbon dioxide consequences of life in the oceans with its very small standing crop and very rapid turnover, and life on land where opposite conditions hold.

Charles David Keeling, whose observations have been and are crucial to all attempts at understanding the effects of carbon dioxide, not only provided us with his most recent data, but also gave us a critical view of current research efforts, a view that is reflected in many ways in our report.

Digitized by Google

Roger Revelle, more than twenty years ago, recognized the long-term significance of increasing atmospheric carbon dioxide by the burning of carbon based fuels. His early actions in heightening the scientific attention to the problem are consistent with this effort to focus JASONs to the biospheric contributions of carbon.

One of our colleagues, Freeman Dyson, has a deep concern about the consequences of a carbon dioxide increase. He has made numerous helpful comments on the draft report.

Digitized by Google

Digitized by Google

I THE IMPACTS OF INCREASING CARBON DIOXIDE: AN OVERVIEW

Events in the early 1970's illustrate the influence that small shifts in climate can have on world events. In 1972 the Soviet Union lost a significant portion of its winter wheat crop when the snows failed to provide adequate cover, and a sharp freeze destroyed the exposed seedlings. Later, the winter harvest was delayed as the summer moisture normally carried by the westerlies did not arrive in the Ukraine and in the late fall, the ripened crop was blanketed by snow. The Soviet Union rapidly entered the world grain market with major world-wide economic repercussions.

In the same time interval, the six West African countries south in the Sahel--Mauretania, Senegal, Mali, Upper Volta, Niger and Chad, were driven to the edge of economic and political ruin by a drought that began in 1968. The Sahelian drought and the Soviet grain failure received world-wide attention. The Ecuadorean rice failure of 1974, the Chinese droughts and floods of the same year and the 1973 droughts in Central America attracted less attention. However, all of these examples illustrate the fragility of the world's crop producing capacity, particularly in those marginal areas where small alterations in temperature and precipitation can bring about major changes in total productivity.

Digitized by Google

In 1977 and 1978, climatic conditions for agriculture largely returned to those of the 1950s and 1960s with agriculturally favorable weather prevailing in the Indian subcontinent, China, the Soviet Union, and the United States. Despite the improved world food situation, the lesson of the early 1970's remains, the heightened demands of an increasing population for food with a lowered availability of arable land and water make the world food supply vulnerable to climatic changes.

The climatic fluctuations of the past few decades are minor compared to those contained in the historical and geologic records. A warming comparable to the "altithermal" period of 4000 to 8000 years ago would bring about not only major shifts in agriculture, but would have significant demographic effects not only from the direct climatic changes, but also from shifts in sea level resulting from the melting of glacial ice.

The burning of carbon-based fuels employing current technology releases carbon dioxide into the atmosphere. Carbon dioxide is a relatively minor constituent in the atmosphere, having a concentration at present of 332 parts per million (ppm). Despite its small concentration, carbon dioxide exerts a major influence on the thermal structure of the atmosphere since the carbon dioxide molecule absorbs infrared radiation emitted by the earth's surface that otherwise would escape into space. Because of carbon dioxide's radiative properties, changes in the concentration of carbon dioxide changes the atmosphere's thermal properties, and in this fashion changes in carbon dioxide

Digitized by Google

concentration can produce changes in climate. While the general theory of the influence of carbon dioxide on climate is widely accepted by atmospheric scientists, there are disputes as to the magnitude and character of the climate fluctuations resulting from anticipated future burning of carbon based fuels.

Plants in photosynthesis fix carbon from carbon dioxide in the atmosphere. Changes in carbon dioxide concentration can be expected to alter biological productivity, but in ways that are not understood. The acidity of the buffered oceans depends in part on the atmospheric carbon dioxide concentrations and changes in this concentration could influence marine life. These examples emphasize that while climatic variations are likely to be the most important consequences of changes in carbon dioxide, other changes whose importance is presently not known, can be anticipated.

A. Climate and Carbon Dioxide in Historical Perspective

Tyndale[1] in 1861 first suggested that slight changes in atmospheric composition could bring about climatic variation. Tyndale's work was based on early experiments measuring the absorption of light as a function of gas density. Arrhenius[2] first calculated the influence of changes in carbon dioxide concentration on the surface temperature noting that enhanced absorption in the infrared should yield a higher surface temperature. For a three-fold increase in the atmospheric concentration

Digitized by Google

of carbon dioxide, Arrhenius in 1896 calculated a surface temperature rise of 9°C--a remarkable result considering the paucity of data. Today's estimate is 4 to 6°C. Arrhenius[3] and Chamberlain[4] speculated that the large variation in the earth's climate, and in particular the glacial epochs, could be due to changing carbon dioxide concentrations of the atmosphere resulting from geologic processes. The work of Arrhenius and Chamberlain greatly influenced the thinking about geologic changes in climate during the first half of the 20th Century. The critical role of the oceans in the global distribution of carbon dioxide was first demonstrated and explored by Tolman[5] in 1899.

Calendar in 1938 first recognized that man, through the burning of carbon-based fuels, was changing the composition of the atmosphere. The geophysical significance of the rise in atmospheric carbon dioxide was dramatically emphasized by Revelle and Suess[7]; "Human beings are now carrying out a large-scale geophysical experiment of a kind that could not have happened in the past nor be repeated in the future. Within a few centuries, we are returning to the atmospheres and oceans the concentrated organic carbon stored in the sedimentary rocks over hundreds of millions of years. This experiment, if adequately documented, may yield a far-reaching insight into processes determining weather and climate."

Revelle was instrumental in incorporating into the program of the International Geophysical Year, accurate and regular measurements

Digitized by Google

of the concentration of carbon dioxide. Keeling[8,9] has led a number of investigators in maintaining, over the past 20 years, continuous monitoring programs of atmospheric carbon dioxide at Mauna Loa, Hawaii, and the South Pole.

The impact of rising carbon dioxide levels on man were alluded to by Revelle and Suess and explicitly discussed in a report of the President's Science Advisory Committee[10] in 1965. The Arab Oil Embargo, President Nixon's Project Independence and the increased emphasis on the use of coal as a major energy resource has focused renewed attention on the possible consequences of increased levels of carbon dioxide in the atmosphere.

B. Measured Changes in Atmospheric Carbon Dioxide

Figure I-1 shows the record of a secular increase of atmospheric carbon dioxide obtained from a nearly continuous monitoring at Mauna Loa, a site at 3,400m altitude and well within the trade wind belt. The current content carbon as carbon dioxide in the atmosphere is about 702 x 10^9 metric tons (Gtons). Between about 87 and 140 Gtons of carbon has been added to the atmosphere since 1850 (See Table I-1). The uncertainty arises from the unknown level of carbon dioxide in the pre-industrial atmosphere (See, for example, Callendar[6]).

Digitized by Google

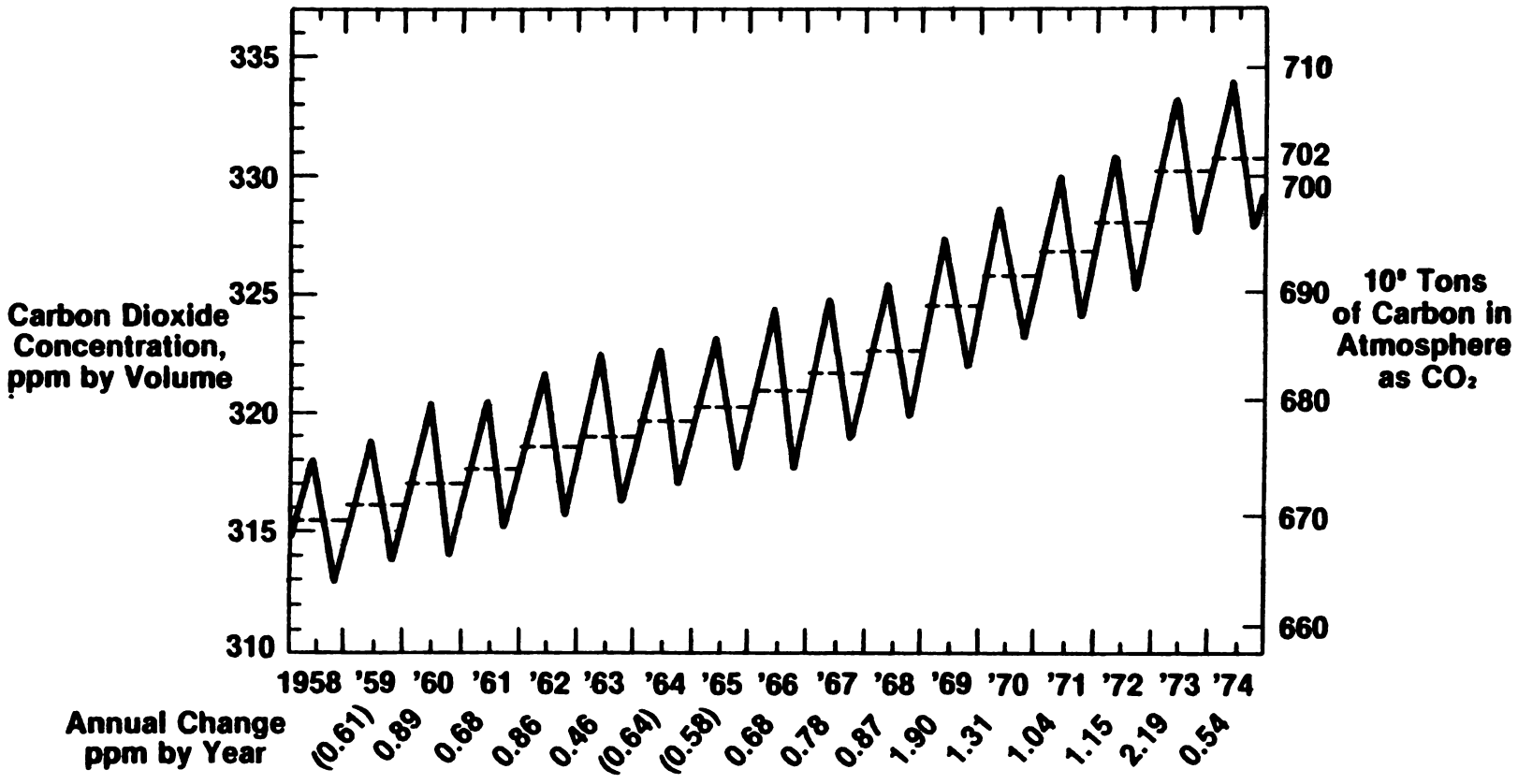

Figure I-1
Atmospheric Carbon Dioxide Concentration at Mauna Loa Observatory
(after Keeling, et al 8, 9)

Digitized by Google

TABLE I-1

CHANGING CO_2 CONTENT OF ATMOSPHERE

DATE	CONCENTRATION IN PPM BY VOLUME	MASS OF CARBON IN Gtons)
1850	265 - 290	562 - 615
1958	315.4	669
1975	330.9	702

Digitized by Google

A similar secular increase has been observed at the South Pole with the values lagging Mauna Loa by a few ppm in any given year. This lag is consistent with the interpretation that more than 90% of the increased carbon dioxide is introduced in the industralized Northern Hemisphere, and that there is a time lag in the mixing of the atmosphere between the hemispheres.

Shorter records from Point Barrow, Alaska[11] and from Scandinavin airplane flights[12] show similar secular trends. Superimposed on the secular trend is a regular annual variation of approximately 6 ppm at Mauna Loa, 1.6 ppm at the South Pole, and as high as 15 ppm at Point Barrow. In the Northern Hemisphere, the maximum in the annual variation is in spring and the minimum in late summer. The seasonal variation is usually attributed to seasonal changes in net photosynthesis and respiration of the biosphere[13] though variations in sea surface temperature may contribute since the dissolved carbon dioxide content of the oceans is temperature dependent.

Even with the limited number of observation stations, it is clear that the carbon dioxide content of the atmosphere has been rising and that the rate of increase has accelerated over the 20 years of accurate measurements. In the late 1950's, carbon in the form of carbon dioxide was being added at a rate of about 1 Gton per year, while today the rate is approximately two Gtons per year.

Digitized by Google

C. Fuel Sources of Carbon

Calender[6] first suggested that the burning of carbon-based fuels provided the major source for the increasing carbon dioxide content of the atmosphere. The burning of calcium carbonate to make quick lime in cement manufacture also adds carbon dioxide, but this contribution of carbon dioxide returns to cement once the cement and mortar are used. Table I-2 lists the carbon added to the atmosphere by the world-wide burning of carbon-based fuels for various years. Over the last 30 years, the fuel generated carbon has been increasing at an almost constant rate of 4.3% per year.

The cumulative contribution by fuel burning of carbon to the short-term carbon cycle for the period 1800 to 1978 is about 154.5 Gtons or about one-quarter of the pre-industrial atmospheric carbon content. However, as will be discussed, only a fraction of the carbon introduced into the atmosphere has remained airborne. Of the 154.5 Gtons, 27% or 42.5 Gtons have been added in the period 1970-1978.

The amount of carbon added to the atmosphere depends on the mix of carbon-based fuels. Table I-3 lists values for carbon added per hundred quads (1 quad - 10^{15} Btu) of thermal energy generated. The values are estimated averages since the heat content of the fuels vary, particularly for coal. The values for synthetic gas and oil derived from coal are even more uncertain because of the differences among possible gasification and liquefaction processes. The important point is that coal derived

Digitized by Google

TABLE I-2

ESTIMATED CARBON ADDED TO THE ATMOSPHERE BY THE BURNING OF FUELS IN GTONS[14]

YEAR	CARBON ADDED
1950	1.63
1960	2.61
1970	3.96
1975	4.87
1978*	5.54

*Estimated

TABLE I-3

CARBON PRODUCED PER HUNDRED QUADS OF THERMAL ENERGY GENERATED

FUEL	CARBON IN GTONS
Oil	2.0
Gas	1.45
Coal	2.5
Synthetic Gas or Oil Derived From Coal	3 - 4

Digitized by Google

TABLE I-4

1975 WORLD PRODUCTION OF CARBON
BY BURNING FOSSIL FUELS

FUEL	QUADS	PERCENT	GTONS OF CARBON
Oil	112	47%	2.24
Gas	49	20%	0.71
Gas (flared)	10	4%	0.14
Coal	70	29%	1.78
TOTAL	241	100%	4.87

4.87 Gigatons = 0.69% of total atmospheric carbon

Digitized by Google

synthetic fuels will release more carbon dioxide per unit of delivered thermal energy than will coal. The relative mix of carbon-based fuels and their contribution in 1975 to the atmospheric carbon load is shown in Table I-4.

Projection of future carbon loading of the atmosphere is clearly a hazardous venture depending on anticipated rates of energy usage in various parts of the world as well as on estimates of the mix of fuels employed by various countries. For example, the Soviet Union plans to increase the fraction of their total energy produced by natural gas from the present 22% to 40% in 1985[15]. The switch from coal and oil to gas will lower the amount of carbon introduced into the atmosphere per quad of energy used. Similarly, large scale introduction of nuclear or solar energy systems will further reduce the rate at which carbon is introduced.

If the use of carbon-based fuels continues to grow at a yearly rate of 4.3%, then 14.4 Gtons of carbon would be released as carbon dioxide in the year 2000, 34 Gton in 2025. For a continuing 4.3% rate of increase the cumulative total of carbon released by 2000 would be about 360 Gtons, by 2025, 840 Gtons. These estimates would probably be upper limits since energy growth rate will slow in the industrial world and the use of non-carbon fuels will increase. However, the extensive use of coal in the next 20 years could raise the yearly contribution somewhat (See Table 5).

Digitized by Google

TABLE I-5

WORLD-WIDE CARBON RELEASE IN THE YEAR 2000

WORLD CONSUMPTION OF CARBON BASED ENERGY IN QUADS	FUEL MIX IN PERCENT			CARBON RELEASE IN GTONS
	OIL	GAS	COAL	
600	50	20	30	12.2
	30	10	60	13.5
	30	50	20	10.9
700	50	20	30	14.0
	30	10	60	15.8
	30	50	20	12.7

TABLE I-6

WORLD-WIDE CARBON RELEASE IN THE YEAR 2025

WORLD CONSUMPTION OF CARBON BASED ENERGY IN QUADS	FUEL MIX IN PERCENT			CARBON RELEASE IN GTONS
	OIL	GAS	COAL	
770	20	0	80	18.4
	10	60	30	14.0
1150	20	0	80	27.5
	10	60	30	20.9

Digitized by Google

Table I-5 presents illustrative values of carbon release based on a low (600 quads) and high (700 quads) yearly of energy uses in the year 2000. Depending on the assumed carbon fuel mix the values range from twice to three times the current release rate. Similar estimates are shown in Table I-6 for the year 2025 where the annual energy use rate of 770 quad corresponds to a 1% yearly growth from a base of 600 quads in 2000, the 1150 quad figure corresponds to a 2% growth rate in use of carbon-based fuels from a base of 700 quads in the year 2000. The carbon release 45 years in the future could thus be three to six times the current rate and even greater if synthetic fuels are used in a significant way.

D. The Carbon Mystery

A comparison of the observed increase of atmospheric carbon (Figure I-1) with the release of carbon from burning fuels (Table I-4) shows that only about half of the fuel carbon remains airborne and thus capable of influencing climate. The usual assumption is that the oceans absorb the majority of the missing carbon though a portion may be taken up by the biosphere[16]. More recently, the possibility has been advanced that current land clearing with the subsequent oxidation of plant material and the removal of carbon using plants may be adding to the carbon content of the atmosphere in a significant way. An understanding of the distribution of carbon between the oceans, biosphere, sediments and atmosphere is of critical importance to the forecasting of future carbon levels in the atmosphere.

Digitized by Google

TABLE I-7

APPROXIMATE MAGNITUDES OF THE RESERVOIRS OF CARBON IN GTONS

• Sediments	
- Oxidized	5×10^7
- Reduced	2×10^7
• Igneous Rocks	3×10^6
• Oceans (deep)	4×10^4
• Oceans (mixed layer)	6×10^2
• Fuels	7×10^3
• Soils	3×10^3
• Biosphere (living)	8×10^2
• Atmosphere	7×10^2

Digitized by Google

The atmosphere is in fact the smallest of the major reservoirs of carbon as is illustrated in Table I-7. Further, the fluxes between the reservoirs are large. For example, the biosphere puts into the atmosphere approximately 160 Gton of carbon a year through respiration and decomposition of terrestrial and oceanic biota. The atmosphere returns an equal quantity through photosynthesis if equilibrium conditions are maintained. Small changes in the large reservoirs or in the rates of exchange between the reservoirs could bring about significant changes in atmospheric composition that would overwhelm the effects of burning carbon based fuels. Indeed, the older climate change hypothesis put forward by Arrhenius and Chamberlain were based on changes in the carbon content of the various reservoirs on geologic time scale.

The uncertainty in how much of the man-derived carbon goes rapidly into the oceans derives from the poorly understood mixing processes within the ocean. Numerous models of ocean-wide diffusive and convective exchange processes between adjoining vertical layers have been constructed to study the movement of carbon dioxide. The models and their supporting data on the movement of radioactive isotopes are not accurate enough to determine what fraction of the carbon released through fuel burning enters the ocean or whether additional carbon derived from land clearing and deforestation is also sequestered

Digitized by Google

in the oceans. In this report, Munk and Zachariasen (§ II-B) question the application of convection-diffusion models arguing that the movement of carbon dioxide in the oceans is influenced by processes at the ocean boundaries which alter the temperature and salinity (hence the density) and which affect how the newly formed water masses spread into the oceans.

The question as to whether the biosphere is a source or sink for carbon is similarly uncertain. The rates of land clearing, the resulting changes in biological productivity, the removal of organic material by sedimentation in the shallow oceans, the rates of exchange of carbon in soils with the atmosphere are all poorly known. Recent estimates suggest that the biosphere has been a moderate source of carbon in recent years, 1 to 3 Gtons/year[18], but much higher figures have been proposed as well as suggestions that the biosphere is a sink for carbon. Some oceanographers would argue that the ocean data are inconsistent with the hypothesis that the oceans take up half of the carbon supplied by fuel burning (2.5 Gtons/year) together with the 1 to 3 Gtons/year derived from changes in the biosphere.[19]

E. Future Carbon Levels in the Atmosphere

Given uncertainties in future carbon fuel use, fuel mix, biospheric contribution and ocean-atmosphere interaction, it is hazardous to predict future levels of carbon dioxide in the atmosphere. If the present

Digitized by Google

rate of increase (4.3% per year) of use of carbon based fuels continues indefinitely into the future, then the carbon dioxide content of the atmosphere would double by the year 2035. Table I-8 illustrates the dependence of the date of doubling of atmospheric carbon dioxide on the rate of energy use assuming the current mix of fuels, and that half of the carbon remains in the atmosphere. At conservative rates of increase of carbon fuel use (one to two percent per year), assuming that half of the fuel carbon remains airborne, the carbon dioxide levels would be expected to double current levels (332 ppm) in 60 to 80 years. The time would be reduced if future agricultural pressures lower the standing crop, or if coal use, particularly synthetic, increases at a greater rate than use of oil or gas.

Since large reserves of carbon-based fuels are known to exist, and much larger resources are suspected (see Tables I-9 and I-10), the burning of the fuels could increase the carbon content of the atmosphere five or ten fold over a time span of centuries if carbon-based fuels continue to be significant energy source.

F. Climate Change From Changing Carbon Dioxide

Attempts to calculate the effects of carbon dioxide on climate have focused on determining the change in the average surface temperature of the earth. Climate is much too complicated to be described by a

Digitized by Google

TABLE I-8

APPROXIMATE DATES FOR DOUBLING THE CARBON DIOXIDE CONTENT OF THE ATMOSPHERE

ASSUMED RATE OF INCREASE IN USE OF CARBON FUELS	DATE OF DOUBLING OF CARBON DIOXIDE CONTENT OF ATMOSPHERE
Constant 4.3%	2035
Constant 3%	2050
4.3% 1978 - 2000	
3% 2000-	2040
2% 2000-	2050
1% 2000-	2060

Digitized by Google

TABLE I-9

PROJECTED WORLD CARBON PRODUCTION
BY USE OF RECOVERABLE RESERVES[20]

FUEL	RECOVERABLE RESERVES (QUADS)	CARBON RELEASE (GTONS)
Oil	3,200 - 3,700	64 - 74
Gas	1,700 - 2,600	24 - 37
Coal	15,000	381
TOTAL	19,900 - 21,300	469 - 492

TABLE 1-10

PROJECTED WORLD CARBON PRODUCTION
BY USE OF RECOVERABLE RESOURCES[20]

FUEL	RECOVERABLE RESOURCES (Quads)	CARBON RELEASE (GTONS)
Oil	8,700 - 11,000	174 - 220
Gas	9,100 - 9,800	131 - 141
Coal	86,000 - 160,000	2,184 - 4,064
Sub-Total	103,800 - 180,800	2,489 - 4,425
Oil shales and Tar sand	14,000 - 100,000	280 - 2,000
Non-conventional Gas (U.S. only)	20,000 - 60,000	288 - 864
TOTAL	137,800 - 340,800	3,057 - 7,289

Digitized by Google

single parameter. Amounts and time distribution of precipitation, onset of freezing conditions, strength and patterns of wind are all parameters critical for understanding the impact of climatic change on man. However, present knowledge is such that surface temperature is universally used as a surrogate for climate in calculation on climatic change.

Three principal classes of assumptions have been employed to calculate the effects of carbon dioxide on surface temperature.

1) Assume the atmosphere is everywhere in radiative equilibrium with outgoing infrared radiation balancing incoming solar radiation at each point on the earth's surface. (Zeroth order model)

2) Assume that in addition to radiative processes, heat is transported meridionally from equator to pole in the oceans and atmosphere by eddy-diffusion. (First order model)

3) Assume that the basic hydrodynamical equations describing atmospheric motion can be solved numerically. (General circulation models, GCM)

G. Zeroth Order Calculations

The earth's thermal radiation is mainly confined to the 5 to 30 μm region. The water molecule is a strong absorber over much of this region, except for the important 8 to 18 μm interval where the earth's infrared emission peaks (for a surface temperature of 290°K, the peak is at a wavelength of 10 μm). Water is a principal contributor to the

Digitized by Google

greenhouse effect, even though it is not everywhere optically thick. Climate calculation usually assumes that the water vapor concentration remains constant even though carbon dioxide and temperature vary.

Current carbon dioxide abundances are enough to make the 15 μm region optically thick so that changes in carbon dioxide concentration will alter the greenhouse heating primarily by carbon dioxide absorption in the 10 μm band. The situation is further complicated in that a number of minor constituents such as nitrous oxide, methane, and a wide array of hydrocarbons are potentially important in enhancing the effect of carbon dioxide in closing off the 8 to 15 μm region. For example, a doubling of the methane concentration, currently 1.6 ppm would produce a temperature increase in excess of 1°C.

Chamberlain (§ III-A) has calculated on the basis of radiative theory, that if the carbon dioxide were doubled, then the average surface temperature would increase by 2.8°C using the assumption of a gray homogeneous atmosphere. Vesecky (§ III-B), using a nine-band model obtains a temperature increase of 3.8°C. As carbon dioxide is increased further, the temperature will continue to rise, although the 15 μm bands become more saturated, the 10 μm bands are effectively closing the 8-12 μm window. Chamberlain's and Vesecky's recent calculations are in general agreement with earlier radiative calculations.

Digitized by Google

H. First Order Models

In the first order models, the surface temperature is permitted to vary with latitude. Heat transport is modeled as a eddy-diffusive process and the oceans and atmosphere are considered to be a coupled system. The resulting equations are non-linear since the albedo is assumed to be a function of temperature. In the simplest case, the albedo is high where the temperature is low because of ice or snow cover. Carbon dioxide will affect the radiative components in the equation and thus influence both the average temperature and the temperature distribution with latitude.

Abarbanel (§ IV-B), using the First Order Model approach, finds that doubling the carbon dioxide content from 332 ppm to 664 ppm results in a temperature increase of 2.4°C. Interestingly, he finds that the temperature rise is much more marked in the polar regions with a temperature increase of 10°C at high latitudes, while in the equatorial regions it is less than the average.

I. Global Circulation Models

Manabe and Wetherald[20] have carried out the most detailed computing machine calculation using numerical simulations of the atmosphere but of necessity approximating very roughly cloud formation, air-sea interaction, and albedo change. They found that a doubling of the carbon

Digitized by Google

dioxide content raises the average temperature 2.9° and the calculations indicate a warming of 8 to 20°C in the high latitude regions with smaller than average increases in the equatorial regions.

A wide variety of models lead to similar numerical results with respect to the effect of doubling the carbon dioxide content, as has been noted by Schneider[21]. This observation is suggestive that the real control on surface temperature is due to the effects on the radiative energy balance by carbon dioxide and that the detailed dynamics of the atmosphere may not be crucial in determining average changes. A number of calculations are also in general agreement with the average warming being amplified at high latitudes.

J. Impacts of Climate Change

If civilization continues its heavy reliance on carbon based fuels, and if there are no major shifts in the current response of the oceans and biosphere to changing carbon dioxide content, then we should expect during the middle of the 21st Century a warming of 2 to 3°C accentuated by a factor of three or four at high polar regions. These average temperature changes are greater by at least a factor of two than those observed during abnormal historical weather conditions that prevailed for example during the "Little Ice Age" of the 16th and 17th Centuries. The changes, however, are smaller by about a factor of two than those experienced during the past million years in the glacial and interglacial periods.

Digitized by Google

The anticipated man-made changes by the year 2000 or even 2025 are likely to be small compared with historical variations though carbon dioxide, together with minor constituent pollutants, could either amplify a natural warming trend or dampen a natural cooling episide. At the present state of knowledge, we cannot predict whether the natural variation will be in the direction of warming or cooling.

Viewed in the longer perspective and noting past historical events, changes in climate would not lead to improved living conditions everywhere. Any change would produce stress and possibly disaster in some parts of the world since so many aspects of society have adapted, with very large investments in their infra-structures, to the climate of the past few decades.

Perhaps the most ominous feature of an average warming due to increased carbon dioxide, is the amplification of the warming in the polar regions. Generally, it is assumed that the polar ice sheets would respond to a warming trend over a time scale of thousands of years since the melting would proceed slowly at the surface exposed to the atmosphere. Mercer[22], however, has pointed out that the characteristics of the West Antarctic ice sheet are such that melting could proceed rapidly. The ice sheet is grounded below sea level with present summer surface temperatures of -4 to -5°C. The grounded portion is fringed by ice shelves which serve to buttress the grounded part of the ice sheet. The shelves are vulnerable to both oceanic and atmospheric

Digitized by Google

warming. An increase in summer temperature of 0 to 1°C could lead to rapid melting of the shelves and disintegration of the main ice sheet. The time scale for such a process is not known, but observed surges indicate that the West Antarctica ice sheet could discharge one-third to one-half of its volume in 100 years. The complete melting of the ice sheet would raise world-wide sea levels by 5m with consequent major disruptions of the world's coastal region. A warming of 5°C in Antarctica could take place in 50 to 75 years, depending on rates and kinds of carbon fuels burned.

A warmer climate will impact agriculture primarily through lengthening the growing season in higher latitudes and increasing summer temperatures provided precipitation patterns are not greatly altered. Higher summer temperatures will not necessarily increase productivity of all crops, since the increase of respiration could exceed the increases in photosynthesis. In high latitude regions, a northward movement of a viable growing season does not imply greater productivity, since the soils on formerly glaciated terrain are generally poor.

Some historical evidence suggest that warming could result in prolonged mid-continental drought[23]. "Dust Bowl" conditions could threaten range lands and semi-arid agriculture over large areas of North America, Asia and Africa.

Digitized by Google

Warming could also affect water availability both through altering, in unknown ways, precipitation patterns and enhancing evaporation from soils and plants. The latter effect, in decreasing soil moisture, reduces the amount of water available for groundwater reserves. Warmer climates will increase evaporation from lakes and reservoirs. Thus, one possibility is that climatic warming could alter the water balance over large regions.

The net energy impact of a warmer climate is not known. Demands on heating fuels will decrease, but these would be accompanied by increased use of air-conditioners. The net balance would be influenced by the demographic shift, induced by climatic change.

Shifts in coastlines, in agricultural patterns and water availability are sure to have major demographic effects. The social and political consequences of shifts in patterns of population are surely uncertain, but could be highly disruptive.

K. Conclusions

Despite the many uncertainties about the nature of the carbon cycle and of the effect on carbon dioxide on climate, it seems highly probable that continued increased in the world-wide use of carbon

Digitized by Google

based fuels at a rate of one to three percent per year, will lead to climatic changes in the second half of the 21st century. The changes will be amplified in high latitude regions and in these regions man-made changes may be larger than natural variations in the first half of the 21st Century. The impact of the projected changes on man is unknown but unlikely to be wholly favorable.

Means of ameliorating the effects of carbon dioxide increases are available, but application of these are unlikely to alter the above conclusion except for lengthening the time scale over which expected climatic changes would take place. The increased use of natural gas, if available, would lengthen the time available for a shift to non-carbon based fuels. Clearly a significant shift to a nuclear or solar energy economy would postpone carbon-induced climate shifts. Increasing the standing crop through massive reforestation could provide temporary storage for carbon, but land and water availability limit this measure. In principle, carbon dioxide in stack gas could be frozen into dry ice for deep ocean disposal or the stack gases could be used to accelerate the growth of certain plants in giant greenhouses. However, elementary considerations suggest that neither of the latter suggestions are economical in competition with alternative, nuclear or solar, energy systems.

Digitized by Google

The potential problems posed by a warming climate appear sufficiently serious to justify a comprehensive research effort designed to reduce the many uncertainties discussed above. Even though anticipated alteration would appear to be at least 50 years in the future, the world-wide nature of the changes and their possible adverse effects on man-kind warrant the continued attention of policy-makers to the carbon dioxide climate question.

Digitized by Google

Digitized by Google

REFERENCES FOR SECTION I

1. J. Tyndall, Philadelphia Magazine, Journal of Science, 22, 169-194, 273-285, 1861

2. S. Arrehnius, Philadelphia Magazine, Journal of Science, 41, 237-276, 1896

3. S. Arrehnius, Worlds in the Making, Harper and Row, New York, 1908

4. T. Chamberlain, Journal of Geology, 7, 545-584, 667-687, 751-787, 1899

5. C. Tolman, Journal of Geology, 7, 585-618, 1899

6. G. Callendar, Quarterly Journal of Royal Meteorological Society, 64, 223-237, 1938

7. R. Revelle and H. Suess, Tellus, 9, 18-27, 1957

8. C.D. Keeling, et al, Tellus, 28, 538-551, 1976

9. C.D. Keeling, et al, Tellus, 28, 552-564, 1976

10. Presidents Science Advisory Committee (PSAC), Restoring the Quality of Our Environment, The White House, Washington, 1965

11. J. Kelley, Journal Geophysical Research, 74, 1688-1693, 1969

12. B. Bolin and W. Bischof, Tellus, 22, 431-442, 1970

13. B. Bolin and C. Keeling, Journal of Geophysical Research, 68, 3899-3920, 1963

14. C. Keeling, Tellus, 25, 174-198, 1973

15. Central Intelligence Agency, U.S.S.R.: Development of the Gas Industry, 1978

16. C. Keeling in Chemistry of the Lower Atmosphere, S. Rasool (ed.) Plenum Press, New York, 251-329, 1973

Digitized by Google

17. J. Olson, H. Pfuderer and K. Chan, Changes in the Global Carbon Cycle and the Biosphere, Oak Ridge National Laboratory, ORNL/EIS-109, 1978

18. W. Broecker, personal communication, 1978

19. G. MacDonald, Long-Term Availability of Natural Resources, in Charles Neuman Symposium on Natural Resources, Clemson, South Carolina, 1977

20. S. Manabe and R. Weatherald, Journal of Atmospheric Sciences, 32, 3-15, 1975

21. S. Schneider, Journal of Atmospheric Sciences, 32, 2060-2066, 1975

22. J. Mercer, Nature, 271, 321-325, 1978

23. H. Lamb, Climate, Present, Past and Future, Vol. 2, Methuen, London, 1977

Digitized by Google

II THE OCEANS AS A SINK FOR CARBON DIOXIDE

The atmosphere interacts with the oceans through diffusive processes at the air-sea interface. Carbon dioxide mixes with the sea water and the carbon first resides as a dissolved gas or as a component of the carbonate or bicarbonate ion. The carbon can then be taken up by living matter to become organic carbon. The details of the many pathways by which carbon can move through the ocean is poorly understood since chemical, biological and physical processes are all involved.

Models of the ocean have been constructed in which the ocean is divided into boxes. The early models divided the ocean into two layers, an upper layer called the mixed layer, in which turbulent diffusive processes even out the carbon content which is in approximate equilibrium with the atmospheric carbon[1,2]. The deep layer exchanges carbon with the mixed layer, but the two layers are not at any one time in chemical equilibrium.

Studies of the Suess effect, radioactive C^{14} dilution by the burning of carbon based fuels, bomb injected C^{14} and other radioactive isotopes have led to box models of the oceans of increasing complexity.[3,4,5,6] These models are limited in the sense that data on the distribution of the isotopes must be used to determine the empirical transport

Digitized by Google

coefficients so that all one can hope for is a consistency between the observations and the model results. The box models by themselves cannot illuminate the physical, chemical and biological mechanisms by which carbon travels from the atmosphere through the oceans to sediments or back to the atmosphere. Because of the limitations of the box model, we explore in a preliminary way alternatives that use oceanographic data on the mass flow within the oceans.

A. Cold Ocean Sinks

The air-sea interface at which CO_2 is enchanged between the atmosphere and the oceans is adjoined to a well-mixed sea surface layer whose average thickness is conventionally taken as about 75 m. The total carbon in the layer (about 580 Gtons) is very comparable to that present as CO_2 in the atmosphere (702 Gtons); but only 1% of the mixed layer carbon is in the form of dissolved CO_2 - 90% is in the carbonation $CO_3^{=}$ and almost all of the rest is HCO_3^{-}. The relatively small mixed layer volume thus contains about 10^2 times the carbon density of the adjacent atmosphere by storing almost all the excess in carbonate and bicarbonate ions. But the layer is, at present, about 85% saturated and it is, consequently, difficult for it to absorb much more: almost all additional absorbed CO_2 must be accompanied by the disappearance of a carbonate ion effectively through the reaction $CO_3^{=} + CO_2 + H_2O - 2HCO_3^{-}$. Because of the large amount of CO_2

Digitized by Google

already absorbed, there is little $CO_3^{=}$ still available and further increases in atmospheric CO_2 would be accompanied by very much smaller increases in the carbon content of a mixed ocean layer with which it remained in equilibrium.

For small departures from equilibrium

$$\zeta \frac{\Delta[C]_A}{[C]_A} = \frac{\Delta[C]_{ML}}{[C]_{ML}}$$

where $[C]_A$ is the carbon density in the atmosphere, $[C]_{ML}$, that in the mixed layer, and $\zeta^{-1} \simeq 8\text{-}15$; ζ^{-1}, the so called "Revelle factor", reaches the larger value at 0°C and the lower value at 30°C. The time needed to establish approximate CO_2 equilibrium between the atmosphere and the mixed ocean layer is then a factor ζ less than the 7 years needed to attain equilibrium between their C^{14} contents; the latter essentially requires an exchange of the entire carbon reservoir of the mixed layer with that of the atmosphere. This time, 7ζ yrs $\simeq$ 8 months is not short enough to maintain atmosphere-mixed layer CO_2 equilibrium at all latitudes because horizontal surface motion exchanges water between hotter and colder regions in less than this time. However, it is short enough so that when averaged over the whole ocean mixed layer, CO_2 equilibrium with the atmosphere is re-established after an atmospheric perturbation in less than a year. This is so very much less than the time for doubling the atmospheric CO_2 burden from fossil fuel burning or the

Digitized by Google

residence time for a carbon atom in the mixed layer that we shall henceforth assume atmosphere-mixed layer CO_2 equilibrium is always achieved.

The ocean can absorb more than the fraction $\zeta \simeq 10^{-1}$ of any additional CO_2 injected into the atmosphere only because the rapidly responding mixed ocean layer is slowly replaced by fresher water which has not yet absorbed the added CO_2 burden. Models for this replacement involve either or both of two mechanisms:

i) The mixed layer exchanges water with layers directly below it, probably by the exchange of eddies -- a process represented phenomenologically by a diffusion equation (box models). The time scale depends sensitively on the spatial separation between the mixed layer and the depth of the most relevant fresher layers.

ii) Cold water from the mixed layer can, in certain regions, drop relatively rapidly to much lower depths then spread horizonally and be replaced by a continued upwelling in the rest of the ocean. The largest such removal of surface water appears to occur in the Antarctic region of the Pacific -- a downflow of about $20 \times 10^6\ m^3 s^{-1}$. This would be balanced by an average upwelling of 4.4 my/yr in the rest of the Pacific. In the Atlantic a similar upwelling might be expected from a downflow of $10 \times 10^6\ m^3 s^{-1}$ in the Norwegian Sea. The time scale for replacing the mixed layer of thickness $H = 75$ m by this mechanism is

Digitized by Google

$$\tau_{ML} = \frac{75 \text{ m}}{4.4 \text{ m/yr}} = 17 \text{ yrs} \tag{2}$$

We consider first only an estimate of the maximum consequences of mechanism ii) for ventilating the mixer layer.

We define the total carbon contents of the atmosphere, mixed layer, and the deeper rest of the ocean by C_A, C_{ML}, and C_D, respectively. Then, if CO_2 is injected into the atmosphere-ocean at the rate $F(t)$

$$f(t) = \dot{C}_A + \dot{C}_{ML} + \dot{C}_D \tag{3}$$

At present

$$\frac{\dot{C}_{ML}}{C_{ML}} = \zeta \frac{\dot{C}_A}{C_A} \tag{4}$$

with ζ of Equation (1). The factor ζ will decrease if very much more CO_2 enters the system because of the near saturation of the mixed layer and the ratio C_{ML}/C_A will decrease as C_A increases. We shall approximate the product

$$\zeta C_{ML}/C_A \equiv \zeta' \tag{5}$$

Digitized by Google

by a constant equal to the present value $\simeq 0.7\zeta \simeq 10^{-1}$. The direct coupling between $\dot{C}_{ML}$ and $\dot{C}_D$ is model dependent because $[C]_D$ can vary throughout the deeper layers. Therefore, the negative contribution to $\dot{C}_D$ carried by the general upwelling accompanying the local downflow into it from the mixed layer is not simply related to C_D . We maximize the effect of the upwelling from the cold water sinks by assuming

$$\dot{C}_D = \frac{C_{ML} - C_{ML}(-\infty)}{\tau_{ML}} \tag{6}$$

The reference time $t = -\infty$ refers to the steady state which existed before fossil fuel burning significantly changed C_A and thus C_{ML} , when $\dot{C}_D(-\infty) = 0$. This assumption that the upwelling water into the mixed layer is so old that its carbon content is independent of recent increases from terrestrial surface activity during the past 150 yrs will, of course, exaggerate the effect of this mechanism in supplying surface water capable of maximally absorbing increasing atmospheric CO_2. Because $\left[C_{ML} - C_{ML}(-\infty)\right]\left[C_{ML}^{-1}\right]$ is very small, we can use Equations (4) and (5) in Equations (3) and (6) to obtain

$$\dot{C}_D = \frac{C_A - C_A(-\infty)}{\tau_{ML}}\zeta' \tag{7}$$

and

$$f(t) = (1 + \zeta')\dot{C}_A + \frac{C_A - C_A(-\infty)}{\tau_{ML}}\zeta' \tag{8}$$

Digitized by Google

For the present exponentially increasing CO_2 injection

$$f = f_o \exp (t/\tau_f) \tag{9}$$

and the solution of Equation (8) is

$$C_A - C_A(-\infty) = \frac{\tau_f f_o \exp (t/\tau_f)}{1 + \zeta'} \left[1 + \frac{\zeta'\tau_f}{(1 + \zeta')\tau_{ML}}\right]^{-1} \tag{10}$$

With $\tau_f = 23$ yrs corresponding to a 4.3% increase per year in CO_2 injection into the ocean-atmosphere reservoir, $\tau_{ML} = 17$ yrs , and $\zeta' = 0.1$, Equation (10) gives 0.8 for the total fraction of injected CO_2 which should still reside in the atmosphere. Because of the small ζ', a τ_{ML} very much less than τ_f is needed before $C_A - C_A(-\infty)$ would depart greatly from the value it would have when in equilibrium with a non-ventilated mixed layer, represented by the first term on the RHS of Equation (10). This is particularly true in that the use of Equation (6) makes the whole discussion an overestimate of the cold water sinks. Thus, it is very unlikely that cold water sinks of presently estimated magnitude could by themselves account for the observations which show only about half of the CO_2 from fossil fuel burning still airborne. When, however, the continually accelerated rate of fossil fuel burning begins to diminish, τ_f will grow and the corrective factor $\left[1 + \zeta'\tau_f(1 + \zeta')^{-1}\tau_{ML}^{-1}\right]^{-1}$ can be important; but, if atmospheric CO_2 has increased greatly by that time, the accompanying decrease in ζ' may no longer be small.

Digitized by Google

B. A Pipe Model of the Oceans

It is a sad commentary on the state of oceanography that we do not know of the applicability (if any) of two extreme models:

(i) oceanwide diffusive and convective exchange processes adjoining vertical layers, and

(ii) Processes at the ocean boundaries which alter the temperature and salinity (and hence density), with the newly formed water masses spreading into the ocean interior along isopycnal surfaces.

The question enters the CO_2 problem in a vital manner. The ocean sink associated with the formation of water penetrating to intermediate depths has a time constant of only 100 years; for bottom water this is 1000 years. Since we are trying to make predictions for a century, this might be a vital difference.

One-d models are rightfully in disrepute and we do not need to join the chorus of disclaimers (all of whom use such models). In fact, one of us (WM) is the originator of a particularly naive one-d model[7], but in limiting this model to Antarctic bottom water and the resulting constant rate of upwelling by 1 cm day^{-1}, and ignoring the large intermediate sources, he now suspects that he has thrown out the baby with the bottom water.

Digitized by Google

1. A Pipe Model

The ocean is modeled by a series of i pipes, from $1 = 1$ at the bottom to $i = n$ representing the mixed layer at top. The temperatures, salinity, density and some other stuff (deuterium, CO_2) in pipe i are designated T_i, S_i, ρ_i, x_i. These are averages formed throughout the length of the pipe. Neighboring pipes are connected, with q_i designated the volume flux from pipe i into $i + 1$. $q_o = 0$ (the bottom is taken as impermeable), and $q_n = 0$ (ignoring for the present evaporation and precipitation).

Pipes are connected by conducting wires (Fig. II-1), permitting the diffusion of heat (and salt and stuff), with the flux proportional to the temperature difference. This is to model turbulent diffusion in the ocean. Accordingly, the eddy coefficients are the same for heat, salt and stuff.

Finally, there is an import by Q_i m^3/sec of water with the properties T_i', S_i', ρ_i', x_i'. In general, $T_i' \neq T_i$ and $S_i' \neq S_i$, $x_i' \neq x_i$; but $\rho_i' = \rho_i$, for if it were otherwise, the inflowing water would be too heavy or too light and would sink to the appropriate depth in a few Väisälä periods.

2. The Water Mass Makers

In the present picture we take the view that the water is drawn from the few uppermost pipes (Q_i is negative for i near n) and then converted by "Water Mass Makers" and fed into the various lower pipes. What we are trying to model are some of the following processes:

Digitized by Google

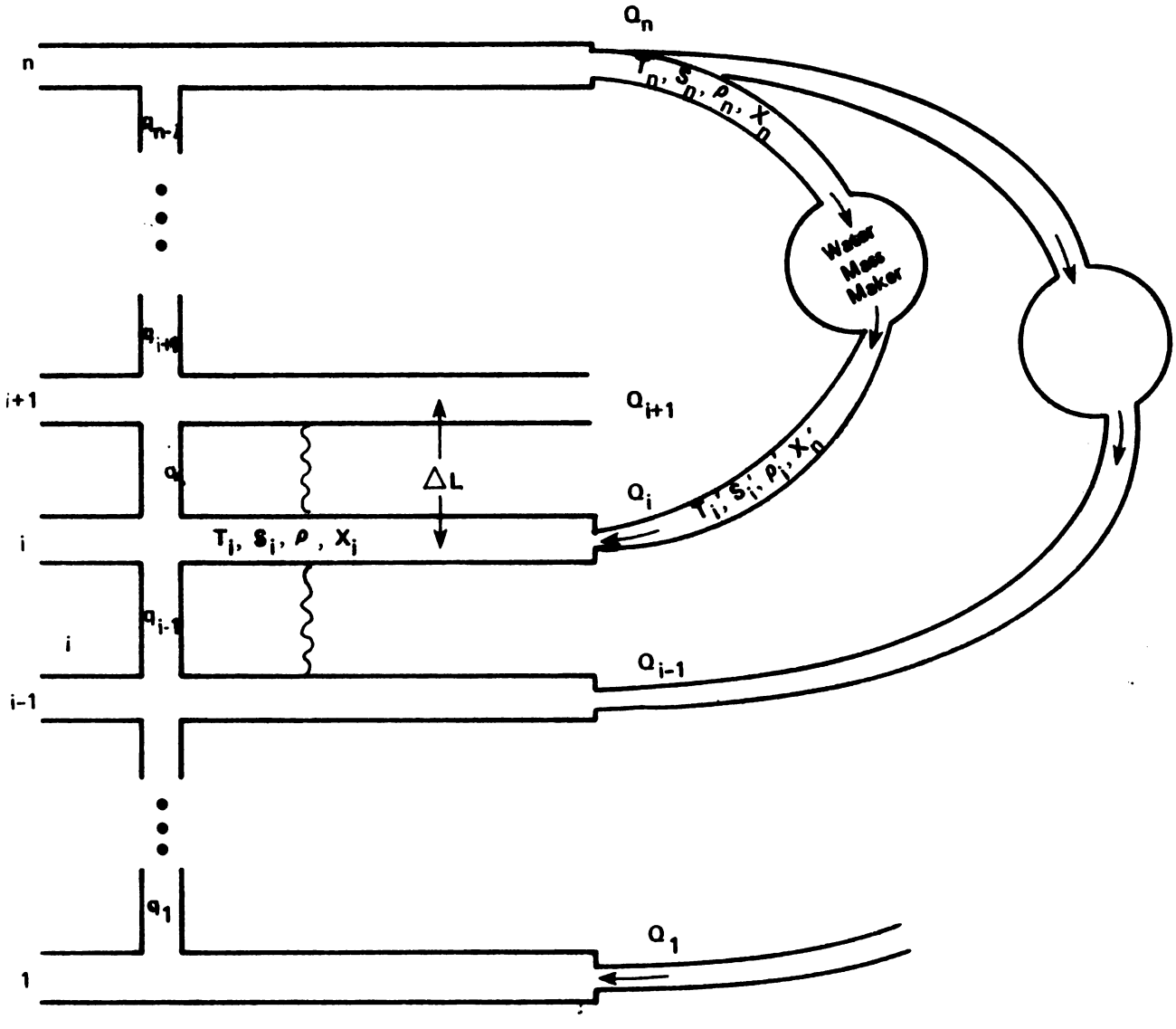

Figure II-1

AN OCEAN PIPE MODEL

Digitized by Google

a) The Norwegian Sea is filled with shallow Atlantic water, in winter the surface water is cooled by contact with the atmosphere, eventually the water column turns over forming a fairly homogeneous cold and moderately salty water mass which flows over a fill into a depth appropriate to its density;

b) In the process of freezing at high latitudes, the newly formed sea ice is fresh, and the residual water is salty and cold. Some form of this process in the Weddell Sea is probably responsible for the formation of Antarctic Bottom Water;

c) Extensive evaporation from the Mediterranean Sea results in increased salinity that leads to the formation of the densest waters in the world's ocean. In this discussion we use the oceanographic unit

$$1 \text{ Sverdrup} = 10^6 m^3/\text{sec} = 3 \times 10^{19} \text{ cm}^3/\text{year}$$

3. <u>Dilution</u>

Suppose that on the average Q m^3/cm of Mediterranean water flows through Gibralter and down the continental slope into the Atlantic. In the process it mixes with the local water with the consequence that by the time it arrives at equilibrium depth, the flow consists of Q' m^3/sec of diluted Mediterranean water, with $Q' > Q$. We will want, somehow, to include this dilution as part of the process of water mass formation.

Digitized by Google

4. Conservation

We now get the following equation for various conservations:

Mass: $q_{i-1} + Q_i = q_i$

Heat: $q_{i-1}T_{i-1} + Q_iT_i' + K\,(T_{i-1} - T_i) = q_iT_i + K\,(T_i - T_{i+1})$

Salt: $q_{i-1}S_{i-1} + Q_iS_i' + K\,(S_{i-1} - S_i) = q_iS_i + K\,(S_i - S_{i+1})$

To this we add the equation of state:

$$\rho_i = f(S_i, T_i) \quad \rho_i' = f(S_i', T_i')$$

so that there are 4n equations in the 4n unknown q_i, T_i, S_i, ρ_i.

In general, if we start by specifying T_i' and S_i', and hence ρ_i', and then calculate the steady state T_i, S_i, and hence, ρ_i, we will find that $\rho_i' \neq \rho_i$. We will need some procedures for satisfying the restraint $\rho_i' = \rho_i$.

5. Continuum

We now divide the conservation equations by $A = 3 \times 10^{14} m^2$, the surface area of the world's oceans. (We should use $A(z)$. Use the notation $q_i/A = w_i$ (the velocity of upwelling). Set $p = Q/A$, the specific source function. Further, write

Digitized by Google

$$\kappa = \frac{K\Delta L}{A} \, m^2 \, sec^{-1}$$

so that κ has the dimensions of a diffusivity. We then write the differential equation

$$-\kappa \frac{d^2T}{dz^2} + \frac{d}{dz}(WT) = S \tag{11}$$

for temperature, and similarly for salinity. Here

$$\Delta W_i = W_{i+1} - W_i = Q_i/A \tag{12}$$

is the increment of upwelling velocity at depth z_i due to a source Q_i. The source function

$$S = \sum_i^{n-1} \Delta W_i \, T_i^{input} \, \delta(z-z_i) + W_1 T_B \delta(z) - W_n T_S \delta(z-z_s)$$

and

$$W = \theta(z) W_1 + \sum_i^{n-1} \Delta W_i \, \theta(z-z_i) - W_n \theta(z-z_s) \tag{13}$$

where $\theta(z)$ is the step function, and $z_o = 0$ is the sea bottom, $z_n = z_s$ is the sea surface.

Digitized by Google

The foregoing equation then becomes

$$-\kappa \frac{d^2T}{dz^2} + W \frac{dT}{dz} = S - T \frac{dW}{dz} = \sum_{i=1}^{n-1} \Delta W_i \, (T_i^{input} - T(z_i))\delta(z-z_i). \tag{14}$$

We expect that the ocean can be modelled by a relatively small number of source depths, corresponding perhaps to the Antarctic Bottom Water, North Atlantic Deep Water and Mediterranean Water. Within any layer between two source depths we have simply

$$-\kappa \frac{d^2T}{dz^2} + W \frac{dT}{dz} = 0 \tag{15}$$

with simple analytical solution.

The problem is to come up with reasonable source functions that lead to acceptable distribution $T(z)$, $S(z)$. The problem is mathematically trivial, but oceanographically very touchy.

Digitized by Google

C. Solutions to the Pipe Models

Mathematically, the model described above may be set up as follows: we consider a single quantity, such as CO_2 concentration, $C(z,t)$, which we take to be horizontally uniform and a function only of depth and time, in accord with our previous discussion. At the surface, z_s, we assume $C(z_s,t) = C_s(t)$, a given CO_2 concentration in the mixed layer. At the bottom, z_B, we take $C(z_B,t) = C_B$, a constant. In between the surface and the bottom are N sources of CO_2, at depths $z_1 \ldots z_N$, injecting CO_2 with concentrations $\bar{C}_i(t)$ at rates ΔW_i. (ΔW_i has the dimensions of a velocity rather than volume per second because we normalize everything per unit horizontal area; ΔW_i is just the rate at which water is injected by the ith "pipe". That is, $\Delta W_i = Q_i$/unit area. Thus between the ith and $(i+1)^{st}$ "pipe" there is an upwelling of water with velocity W_{i+i}, where $\Delta W_i = W_i - W_{i+i}$. To conserve water, these must then be an outflow of water at a rate $\Delta W_o = W_1$ immediately below the surface z_s. This removes CO_2 with concentration $C_s(t)$. The geometry is illustrated in Fig. II-2.) CO_2 is thus distributed through the water column both by diffusion and by being pumped from the surface to various depths z_i at known rates, ΔW_i. The CO_2 concentration then satisfies the diffusion equation

$$-\kappa \frac{\partial^2 C}{\partial z^2} + \frac{\partial}{\partial z}(WC) = -\frac{\partial C}{\partial t} + \sum_{i=1}^{n} \Delta W_i \bar{C}_i \delta(z-z_i) - W_1 C_s \delta(z-z_s) \qquad (16)$$

with the Boundary condition

$$C(z_s,t) = C_s(t) \qquad (17a)$$

$$C(z_B,t) = C_B \qquad (17b)$$

Digitized by Google

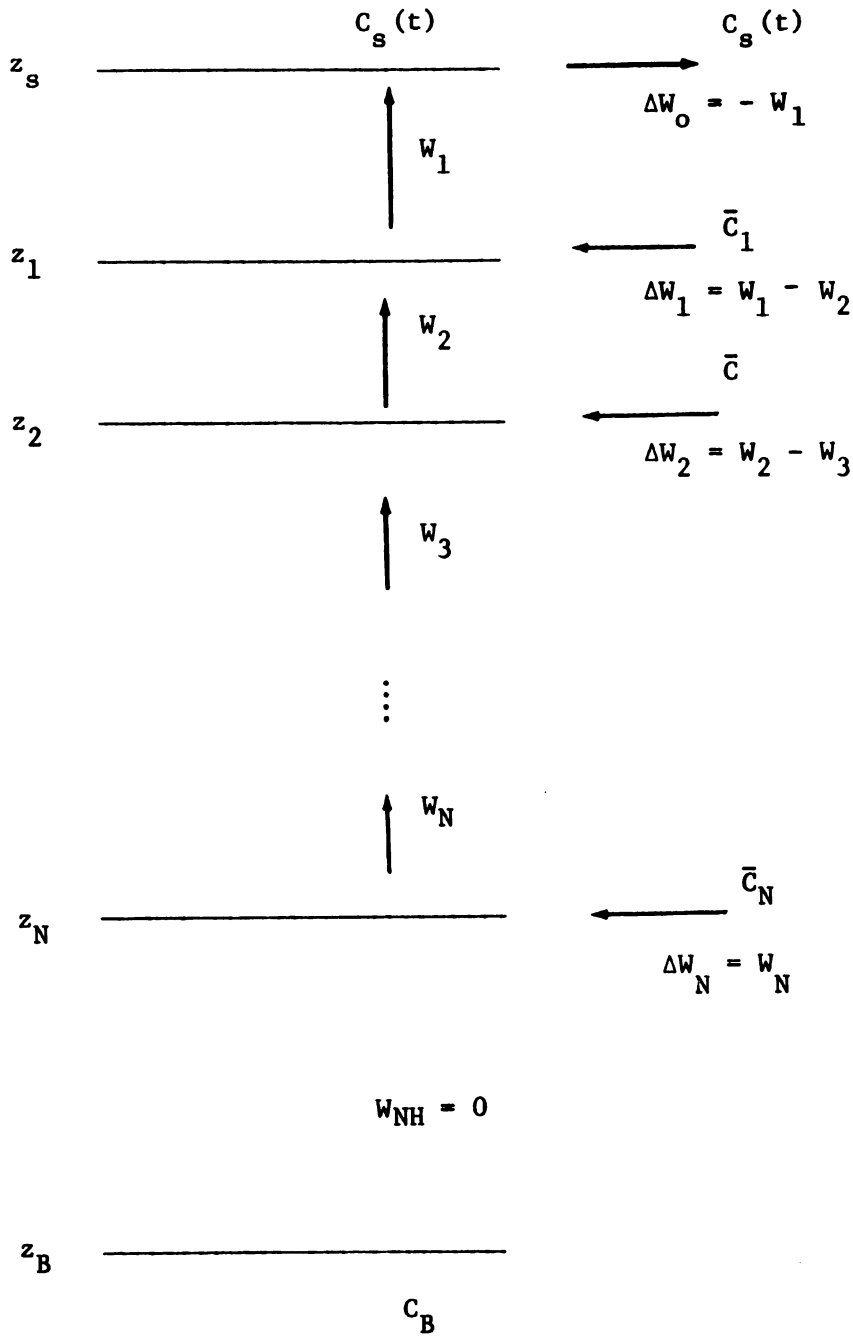

Figure II-2

THE GEOMETRY ILLUSTRATING THE USE OF THE PIPE MODEL

Digitized by Google

For the case we are dealing with here, all the $\bar{C}_i = C_s(t)$ since the pumping mechanism simply redistributes the surface CO_2 concentration. We write (16) in a more general form since we will later apply it to temperature and salinity, where, as described before, the pumping mechanism injects water with different temperature and salinity from the surface water.

We note that $C(z,t)$ is continuous across the layer boundaries, and the vertical derivative $\partial C/\partial z$ is not. In fact, from (16) we see that

$$\lim_{\varepsilon \to 0} \kappa\left(\left.\frac{\partial C}{\partial z}\right|_{z=z_i+\varepsilon} - \left.\frac{\partial C}{\partial z}\right|_{z=z_i-\varepsilon}\right) = \left(W_i - W_{i+1}\right)\left(C(z_i,t) - C_i(t)\right) \quad .$$

Thus we can also formulate the problem by writing

$$C(z,t) = C_i(t) \qquad z_{i-1} > z > z_i$$

where

$$-\kappa \frac{\partial^2 C_i}{\partial z^2} + W_i \frac{\partial C_i}{\partial z} = \frac{-\partial C_i}{\partial t} \tag{18}$$

with the Boundary conditions

(i) $$C_1(z_s,t) = C_s(t) \tag{19a}$$

(ii) $$C_{N+1}(z_B,t) = C_B \tag{19b}$$

(iii) $$C_i(z_i,t) = C_{i+1}(z_i,t) \qquad i = 1 \ldots N \tag{19c}$$

(iv) $$\kappa\left(\frac{\partial C_i}{\partial z} - \frac{\partial C_{i+1}}{\partial z}\right)\Bigg|_{z=z_i} = \left(W_i - W_{i+1}\right)\left(C_i\Big|_{z=z_i} - \bar{C}_i\right) \qquad i = 1 \ldots N \tag{19d}$$

Digitized by Google

Equation (16) leads to a simple conservation law. By integrating from z_B to z_s we find

$$\frac{\partial}{\partial t}\int_{z_B}^{z_s} C(z,t)\,dz = \kappa\left(\left.\frac{\partial C}{\partial z}\right|_{z_s} - \left.\frac{\partial C}{\partial z}\right|_{z_B}\right) + \left(-W_i C_s + \sum_{i=1}^{n} \Delta W_i \bar{C}_i\right) \tag{20}$$

If we have $\bar{C}_i = C_s$, $i = 1 \ldots N$, then the second term on the RHS of (20) disappears. This simply expresses the obvious fact that the rate of change of that CO_2 in the water column equals the rate at which it diffuses in through the surface minus the rate at which it diffuses out into the bottom.

Temperature, $T(z,t)$, and salinity, $S(z,t)$, satisfy the same equation with two modifications. First, we take the surface boundary conditions to be time independent so that $T = T(z)$ and $S = S(z)$ only; thus $\partial T/\partial t$ and $\partial S/\partial t$ disappear. Secondly, we assume that the pumping mechanism changes the surface temperature and salinity so that $\bar{T}_i \neq \bar{T}_s$ and $S_i \neq \bar{S}_s$. Instead we invoke the equation of state and require the density $\rho(T_i,S_i)$ of the injected water to equal the density $\left(\rho[T(z_i), S(z_i)]\right)$ of the ambient water. For given ΔW_i, T_i and $\bar{S}_i$ these conditions are used to determine the injection depths z_i

The first step in solving an equation like (16) is to Fourier transform in time. We define

$$C(z,\omega) = \int_{-\infty}^{\infty} dt e^{i\omega t}\, C(z,t) \tag{21}$$

Digitized by Google

with inverse

$$C(z,t) = \int_{-\infty}^{\infty} \frac{d\omega}{2\pi i} e^{-i\omega t} C(z,\omega) \quad . \tag{22}$$

Corresponding definitions obtain for $C_s(t)$. Then (16) becomes, for the Fourier transforms,

$$-\kappa \frac{\partial^2 C}{\partial z^2} + \frac{\partial}{\partial z}(WC) - i\omega C = -W_1 C_s \delta(z-z_s) + \sum_{i=1}^{N} \Delta W_i \bar{C}_i \delta(z-z_1) \ . \tag{23}$$

Equivalently, (18) becomes

$$-\kappa \frac{\partial^2 C_i}{\partial z^2} + W \frac{\partial C_i}{\partial W} - i\omega C_i = 0 \tag{24}$$

and the boundary conditions in (19) also hold for the Fourier transforms. The solution to (24) is

$$C_i(z,\omega) = A_i^+(\omega)\, e^{\alpha_+(\omega)z} + A_i^-(\omega)\, e^{\alpha_-(\omega)z} \qquad i = 1 \ldots N+1 \tag{25}$$

where

$$\alpha_\pm(\omega) = \frac{W}{2\kappa} \pm \sqrt{\frac{W^2}{4\kappa^2} - i\frac{\omega}{\kappa}} \tag{26}$$

The boundary conditions in (19) then form a set of $2N + 2$ linear equations which determine the $A_i^\pm(\omega)$ in terms of $C_s(\omega)$ and C_B . The solution is then obtained by evaluating Eq. (22). For a large value of N , this is in practice a messy procedure, and we shall therefore, for purposes of orientation, first look at the case of a single source.

Digitized by Google

The model is shown below in Figure II-3.

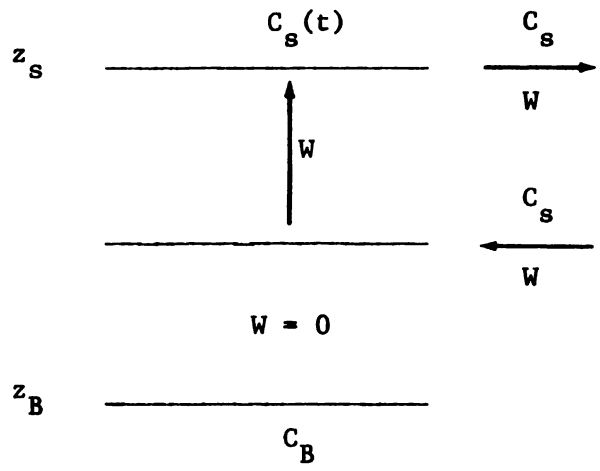

Figure II-3

For simplicity we chose $z_B = -\infty$ and $C_B = 0$. We also chose $z_1 = 0$. In the two layers we then have

$$-\kappa C_1'' + WC_1' - i\omega C_1 = 0 \quad . \tag{27a}$$

$$-\kappa C_2'' \qquad - i\omega C_2 = 0 \quad . \tag{27b}$$

Thus

$$C_1 = \left(A_+ e^{\alpha z} + A_- e^{-\alpha z}\right) e^{\frac{W}{2\kappa} z} \tag{28a}$$

$$C_2 = \left(B_+ C^{\beta z} + B_- e^{-\beta z}\right) \tag{28b}$$

with

$$\alpha = \sqrt{\frac{W^2}{4\kappa^2} - i\,\frac{\omega}{\kappa}} \tag{29a}$$

$$\beta = \sqrt{-i\,\frac{\omega}{\kappa}} \quad . \tag{29b}$$

Digitized by Google

Since C_2 must vanish as $z \to -\infty$, we see $B_- = 0$. (Note that $\sqrt{-i\omega/\kappa}$ has a positive real part for ω in the upper half plane.) The remaining boundary conditions are

$$\left(A_+ e^{\alpha z_s} + A_- e^{-\alpha z_s}\right) e^{\frac{W}{2\kappa} z_s} = C_s(\omega) \tag{30a}$$

$$A_+ + A_- = B_+ \tag{30b}$$

$$\kappa\alpha(A_+ - A_-) = \left(\frac{W}{2} + \kappa/\beta\right) B_+ - WC_s(\omega) \ . \tag{30c}$$

These three equations can be solved for A_+, A_- and B_+.

$$C_1(z,\omega) = e^{\frac{Wz}{2\kappa}} C_s(\omega) \frac{\left[W \sinh\alpha(z_s - z) + \left(\kappa\alpha \cosh\alpha z + \left(\frac{W}{2} + \kappa\beta\right) \sinh\alpha z\right) e^{-\frac{Wz_s}{2\kappa}}\right]}{\left[\left(\frac{W}{2} + \kappa\beta\right) \sinh\alpha z_s + \kappa\alpha \cosh\alpha z_s\right]} \tag{31a}$$

$$C_s(z,\omega) = \frac{e^{\beta z} C_s(\omega)}{\left[\left(\frac{W}{2} + \kappa\beta\right) \sinh\alpha z_s + \kappa\alpha \cosh\alpha z_s\right]} \ . \tag{31b}$$

We also write the solution for the quantity $\kappa\, \partial C/\partial z|_{z=z_s}$, which is relevant for the conservation law in Eq. (20). (Note that $\kappa\, \partial C/\partial z|_{z=-\infty}$ vanishes.)

$$\kappa \left.\frac{\partial C}{\partial z}\right|_{z=z_s} = \frac{W}{2} C_s(\omega) + \kappa\alpha e^{\frac{Wz_s}{2\kappa}} C_s(\omega) \ \cdot$$

$$\frac{\left[\left(\kappa\alpha \sinh\alpha z_s + \left(\frac{W}{2} + \kappa\beta\right) \cosh\alpha z_s\right) e^{-\frac{Wz_s}{2\kappa}} - W\right]}{\left[\left(\frac{W}{2} + \kappa\beta\right) \sinh\alpha z_s + \kappa\alpha \cosh\kappa z_s\right]} \ . \tag{32}$$

Digitized by Google

To make those somewhat formidable looking expressions more transparent, let us choose

$$C_s(t) = \begin{cases} C_s e^{t/\tau} , & t < T \\ 0 , & t > T . \end{cases}$$

Then

$$C_s(\omega) = C_s \frac{e^{(i\omega + 1/\tau)T}}{(i\omega + 1/\tau)}$$

Since the solution $C_1(z,\omega)$ and $C_2(z,\omega)$ are proportional to $C_s(\omega)$, they both have a pole in the upper half ω plane at $\omega = i/\tau$. This pole produces, on inverting the Fourier transforms through Eq. (22), the "steady state" contributions to $C_1(z,t)$ and $C_2(z,t)$; that is, the part proportional to $e^{t/\tau}$. The coefficients of $e^{t/\tau}$ are simply residues of this pole. These residues are easy to compute, particularly in various limits.

We can identify three times in the problem: (i) τ, the growth rate of the mixed layer concentration; (ii) z_s/W, the time for transport of water through the "pipe"; and, (iii) κ/W^2, a diffusion time.

In the limit where the diffusion time is very short -- i.e., $\tau \gg \kappa/W^2$ and $z_s/W \gg \kappa/W^2$ -- it is easy to see that the "steady state" solution is simply

Digitized by Google

$$C_1(z,t) = C_s e^{t/\tau} \tag{33a}$$

$$C_2(z,t) = C_s e^{t/\tau} e^{z/\sqrt{\kappa\tau}} \ . \tag{33b}$$

The solution is simply constant in depth down to the source, and below that dies off exponentially. This is because in the upper layer the CO_2 is uniformly mixed by the "pipe", while in the lower it spreads only by diffusion.

The opposite limit, in which $W \to 0$, of course yields simply

$$C_1(z,t) = C_2(z,t) = C_s e^{t/\tau} e^{\frac{z-z_s}{\sqrt{\kappa\tau}}} \quad ; \tag{34}$$

now, the only spreading is by diffusion everywhere.

These steady state solutions, however, are relevant physically only if the time for water transfer through the "pipe" is short compared to the growth time τ of the mixed layer concentration; i.e., if $z_s/W \ll \tau$. For the real ocean, however, we have $z_s \sim$ kilometers, $W \sim$ a few meters per year, so $z_s/W \sim$ hundreds of years, while the characteristic time for CO_2 growth is only about 20 years. Thus the pumping mechanism cannot in fact keep up with the CO_2 growth, and hence the steady state situation is irrelevant; we must look for transients. This means we cannot confine our attention only to the pole as $W = i/\tau$; we must look more widely at the ω dependence.

Digitized by Google

This is not difficult to do if we are willing to assume that the "pipe" transport dominates diffusion -- that is, if κ is very small. It is easier to look directly at Eq. (32). When $\kappa \to 0$, we find from (32) that

$$\kappa \left.\frac{\partial C}{\partial z}\right|_{z=z_s} \to WC_s(\omega)\left(1 - e^{i\omega z_s/W}\right) \tag{35}$$

$$+ \text{ terms which vanish with } \kappa \quad .$$

Upon inverting the Fourier transform, and invoking the conservation law (20), we find

$$\frac{\partial}{\partial t}\int_{-\infty}^{z_s} C(z,t)\, dz = W\left(C_s(t) - C_s(t-s/w)\right) \quad . \tag{36}$$

Thus, if $S/W \ll \tau$, the right hand side is just

$$S\frac{\partial}{\partial t} C_s(t)$$

in conformity with the steady state solution in which $C(z,t)$ is constant in z in the upper layer of the ocean. But if $S/W \gg \tau$, then the right hand side is

$$WC_s(t) \quad .$$

Thus, in the physically relevant case we find, if diffusion is small,

$$\frac{\partial}{\partial t}\int_{-\infty}^{z_s} C_s(z,t)\, dz \simeq WC_s(t) \quad . \tag{37}$$

Digitized by Google

This case has been analyzed by Ruderman (see § II-A of this report -- Eq. (37) above is Ruderman"s Eq. (6)), so we do not need to study it further here. Numerically, for this case, the effect of the "pipe" is not large. For it to be large, one would have to be in the regime where $z_s/W << \tau$ instead.

Discussion

A full exploration of the "pipe mode" for ocean circulation will require detailed oceanographic data on the movement of water masses, particularly those generated in the cold regimes. Estimates of a downflow of 20×10^6 m^3 s^{-1} in the Antarctic region of the Pacific and 10×10^6 m^3 s^{-1} from the Norwegian Sea lead to the conclusion that the cold water sinks cannot account for the observation that only half of the carbon introduced into the atmosphere by burning carbon based fuels remains in the atmosphere. If mass flow from the surface downward to substantial depths is to provide a significant sink, then either the Antarctic and Norwegian flows are underestimated or other areas of the oceans not yet identified contributed to the removal of carbon from the atmosphere.

Within the uncertainties of the "pipe model", type calculations, it appears that the conclusion that the ocean is a limited sink for carbon, as derived from one dimensional turbulent diffusion calculation is supported. It is difficult to understand how the oceans take up one half

Digitized by Google

of the fuel generated carbon. A requirement that oceans provide a sink for additional carbon derived from the biosphere would raise further difficulties in understanding both models of ocean processes and the oceanographic data that have been used in constructing these models.

Digitized by Google

REFERENCES FOR SECTION II

1. R. Revelle and H. Suess, Tellus 9, 18-27, 1957

2. H. Craig, Tellus 9, 1-17, 1957

3. C. Keeling, in Chemistry of the Lower Atmosphere, S. Rasoul ed. Plenum Press, 251-329, 1973

4. M. Stuiver, Science 199, 253-258, 1978

5. P. Tans, Carbon 13 and Carbon 14 in Tree and the Atmospheric CO_2 Increase, Thesis, Groningen, 1978

6. U. Siegenthaler and H. Oeschager, Science, 199, 388-395, 1978

7. Abyssal recipes. Deep-Sea Research 13, p. 707-730, 1966.

Digitized by Google

Digitized by Google

III RADIATIVE LIMITS ON CLIMATE

The sun's radiation in the visible part of the spectrum, except for that fraction which is directly reflected back out into space, warms the earth. For an earth in radiative equilibrium, the solar radiation which interacts with the atmosphere and the earth's surface must be balanced by an equal amount of outgoing infrared radiation. The temperature of the earth as observed from space, the "effective temperature", is determined by the amount of energy which the earth must lose to remain in radiative equilibrium. The effective temperature is lower than the surface temperature since all parts of the atmosphere radiate into space as well as the land and oceans. The actual surface temperature and the temperature profile of the atmosphere are determined by the interplay of radiative processes, convective transfer of heat and the heat released in the phase transitions of water. Altering the radiative properties through changing the concentrations of infrared absorbers will change climate.

In this section, we explore two models of the atmosphere is which only the radiative processes are taken into account. These models are a first step in a hierarchy of atmospheric models of increasing complexity.

The study of the effect of carbon dioxide of the radiative properties of the atmosphere has a long history tracing back to the work of Tyndale

Digitized by Google

in 1861. More recently a number of studies have explored the impact of changing carbon dioxide content on climate but the emphasis has been on the 15 μm absorption band of CO_2 (see for example Plass[1]). In this report we emphasize that the 16 μm region is almost opaque at current concentrations of CO_2 and that the bands in the 10 μm region are of greatest interest. Furthermore, other minor constituents of the atmosphere enhance the warming effect of CO_2 by blocking outgoing infrared radiations.

A. Gray Homogeneous Model of the Atmosphere

The troposphere is not in radiative equilibrium nor is it even approximately gray (meaning that the absorption coefficient is independent of frequency). Further, it is not vertically homogeneous, since H_2O is distributed with a scale height of about 2 km, CO_2 with 8 km, and O_3 existing mainly in the stratosphere. Hence it is surprising that a gray, radiating homogeneous model has any value at all. Certainly this kind of model would not yield a very useful temperature-height profile.

Such a simplified model can be useful, however, for exploring the importance of changes in the greenhouse effect caused by changes in the composition in global heat balance models of climate.

Digitized by Google

1. The Gray Model

In the gray model only two temperatures are important: The effective emission temperature, T_e, of the planet is fixed by a balance between the incident solar flux and the planetary thermal emission. For a rotating planet of radius R.

$$4\pi R^2 \sigma T_e^{\ 4} = (1-\Lambda)\pi R^2 \ (\pi F_\Theta) \tag{1}$$

where Λ is the omnidirectional albedo and πF_Θ is the solar flux outside the atmosphere. The surface temperature, T_s, which is assumed to be the immediate source of radiation as far as atmospheric heating is concerned, is related to T_e in a gray model by (Chamberlain, 1978, p. 11)[2]

$$T_s^4 = T_e^4 \left(1 + \frac{3}{4}\tau_g\right) , \tag{2}$$

where τ_g is the vertical opacity of the atmosphere.

If the ground emits isotropically with intensity $B_\lambda (T_s)$, the flux transmission directly to cold space is

$$\begin{aligned} \sigma T_s^4 \ Q(\tau) &= \int_0^\infty d\lambda \ B_\lambda (T_s) \int_0^{2\pi} d\phi \int_0^1 e^{-\tau/\mu} \ \mu d\mu \\ &= \sigma T_s^4 \ 2E_3(\tau) \approx \sigma T_s^4 \ e^{-\beta\tau} \end{aligned} \tag{3}$$

Digitized by Google

where $E_3(\tau)$ is the exponential integral, which we approximate with a simple exponential. As τ varies from ∞ to 0 and the transmission function $Q = 2E_3(\tau)$ varies from 0 to 1, the coefficient β varies from 1.2 to 2.0. For H_2O and O_3 we choose $\beta = 1.66$, which gives the exact value of E_3 when $Q = 1/2$; for CO_2 at 15 μm, we take $\beta = 1.2$.

For a realistic atmosphere the same kind of considerations hold except that τ is a function of λ, and

$$Q \approx \sum_{j=1}^{n} p_i \, e^{-\beta\tau} \tag{4}$$

where the summation is over narrow wavelength intervals and p_i is the fractional flux in the i th interval,

$$p_i = \frac{\pi B_{\lambda i}(T_s)\Delta\lambda_i}{\sigma T_s^4} \tag{5}$$

2. Earth's Infrared Absorption

Between 0.54 and 8 μm H_2O has strong vibration-rotation bands and longward of 15 μm occur rotational lines from the ground vibrational state. The Earth's thermal radiation is mainly confined to the 5 to

Digitized by Google

30 μm region. The H_2O molecule is thus a strong absorber over the thermal spectrum, except for the important 8 to 18 μm interval, where the Earth's emmision peaks (at 290°K, λ_{max} = 10 μm). The 12 to 18 μm region is dominated by the CO_2 ν_2-(bending) mode fundamental, leaving an 8 to 12 μm transparency window. A portion of this window is blocked by the 9.6 μm band of $O_2 \rightarrow O_3$. Greenhouse heating of the atmosphere is thus dependent on composition in several distinct ways.

First, water vapor is dominant over a wide wavelength interval, although in much of this region it is not optically thick. Hence atmospheric cooling to space is critically dependent on H_2O abundance and even the vapor in the stratosphere is significant. (The latitudinal variation of H_2O is the main cause of the difference in temperature profiles between polar and tropical zones).

Second, CO_2 fills a large part of the H_2O window, and current CO_2 abundances are enough to make the 15 μm region optically thick. Major CO_2 abundance changes will alter the greenhouse heating mainly by CO_2 absorption in the 10 μm bands.

Finally, minor constituents that absorb strongly in the 8 - 12 μm region can be critically important. Nitrous oxide (N_2O) and a wide array of hydrocarbons are potentially important, and the gray model can be used to estimate their effects.

Digitized by Google

The abundance of water vapor typically varies from 0.2 to $2 gm/cm^2$ (or cm of precipitable water). We adopt a global average of $1 gm/cm^2$. With sufficient accuracy H_2O may be regarded as completely opaque except in the near infrared and visual (P_i - .03) ; and 8.5 to 12.5 where $\tau = 0.10$ and $p = 0.29$; and 12.5 - 15 μm where $\tau < 1$ and $p = 0.14$. However, in the latter region H_2O does not contribute to atmospheric heating since it is dominated by CO_2, and the H_2O therefore can be neglected from 12.5 to 18 μm with $p = 0.26$ (Kondratyev, 1969, p. 119). Thus Eq. (4) gives the absorption function due to water alone as

$$A(H_2O) = 1 - Q(H_2O) = 0.45 \tag{6}$$

As CO_2 increases the mean opacity within a fixed wavelength interval increases, but also the band effectively widens as weaker absorptions become stronger. Here we will not consider the broadening of the 15 μm band because a more important optically thin effect is the emission by the 10 μm bands. Thus the treatment of 15 μm + 10 μm together should give a good representation of CO_2.

For CO_2 a volume mixing ratio of $f = 333$ ppm corresponds to an equivalent thickness at STP conditions of

$$\xi(CO_2) = 266 \text{ atm-cm} \tag{7}$$

Digitized by Google

An empirical formula for the mean transmission in the nearly saturated 15 μm band is (Kondratyev, 1969, p 126)[3]

$$\left\langle Q(15\mu) \right\rangle = \exp(-\beta' a \xi^b) \tag{8}$$

where the absorption data near $\xi = 300$ atm-cm yield, where $\beta' = 1.2$, $a = 0.361$, and $b = 0.23$. Then the total absorption due to CO_2 at 15 μm (or more precisely between 12.5 and 18.2 μm) is

$$A(CO_2) = 1-Q(CO_2) = p(15\mu)\ [1-\exp(-\beta'\ a\xi^b)] = 0.27(0.791) = 0.214 \tag{9}$$

For the weak CO_2 band absorption we use the treatment in Section V, below, for minor constituents. The properties of the two intercombination bands at 10 μm are listed in Table III-1 and from Eq. (32), we have $A(10\mu) = 0.025$.

For $\xi = 0.3$ atm-cm of ozone in the stratosphere we find (Kondratyev, 1969, p 137)[3] over the band (9.4 to 9.9 μ) a mean transmission of

$$\left\langle Q(9.6\mu) \right\rangle = \exp(-2.8\xi) \tag{10}$$

or

$$A(O_3) = 1 - Q(O_3) = p(9.6\mu)(1 - e^{-2.8\xi}) = 0.035(.57) = 0.020 \tag{11}$$

Digitized by Google

Table III-1

ABSORBERS IN 8 - 12 μm WINDOW

Species	Band, λ(μm)	f(ppm)	S(cm)	$\mathcal{N}S(cm^{-1})$
N_2O Nitrous oxide	ν_1 7.8	0.28	10^{-17}	60.
CH_4 Methane	ν_4 7.66	1.6	7×10^{-18}	240.
NH_3 Ammonia	ν_2 10.5	6×10^{-3}	$\sim10^{-20}$(?)	~1.
$CF_2C\ell_2$ F-12	ν_1 9.1	1×10^{-4}	5×10^{-17}	0.1
	ν_6 8.7		3×10^{-17}	0.06
	ν_8 10.9		5×10^{-17}	0.1
$CFC\ell_3$ F-11	ν_1 9.2	1×10^{-4}	3×10^{-17}	0.06
	ν_4 11.8		6×10^{-17}	0.1
Hydrocarbons	--	$\lesssim 4\times10^{-3}$	$\lesssim5\times10^{-17}$	$\lesssim$4·
CO_2	$2\nu_2-\nu_3$ 9.4	333	8.6×10^{-22}	6.
	$\nu_1-\nu_3$ 10.4		2.7×10^{-21}	19.

Note: For uniform mixing the integrated abundance is $\mathcal{N} = f\mathcal{N}_{atm} = f \times 2.15 \times 10^{25} cm^{-2}$. Since $f \equiv N/N_o = N/2.69 \times 10^{19}$ and S.T.P. thickness is $\xi = \mathcal{N}/N_o = f\mathcal{N}_{atm}/N_o$, we have

$$f(ppm) = 1.25\ \xi(atm\text{-}cm)\ .$$

If number in last column exceeds 10, a doubling of present abundance would produce $\Delta T > 1°C$.

Digitized by Google

If the various substances do not overlap seriously in their spectral regions of absorption, the A's can be added. Thus from Eqs. (4), (6), (9), and (11), we have (with $\beta = 1.66$)

$$Q_{net} = e^{-\beta\tau_g} = 1 - [A(H_2O) + A(CO_2, 15\mu) + A(CO_2, 10\mu) + A(O_3)] = 0.29 \tag{12}$$

giving

$$\tau_g = 0.748 \quad . \tag{13}$$

3. <u>Earth's Emission and Surface Temperatures</u>

With an albedo $\Lambda = 29\%$, Eq. (1) gives $T_e = 257°K$. Then Eqs. (2) and (13) yield

$$T_s = 287.2 \tag{14}$$

which is close to the world average (~290°K). It is probably fortuitous that the agreement is so good, although it does suggest that the gray model may provide some insight into climate changes due to changes in τ_g .

Digitized by Google

4. <u>Variation of Ground Temperature with CO_2 Abundance</u>

Differentiating Eq. (12) gives, with Eqs. (9) and (32), below,

$$\beta e^{-\beta\tau} = \frac{dA(CO_2)}{d\tau} = p(15\mu)\ \exp(-\beta' a\xi^b)\ \beta' ab\xi^b \left(\frac{1}{\xi}\frac{d\xi}{d\tau}\right)$$

$$+ 1.08 \times 10^{-3}\ S_{\tilde{\nu}} N_o \frac{d\xi}{d\tau} \quad . \tag{15}$$

In terms of the mixing ratio or volume concentration

$$f\frac{d\tau}{df} = [CO_2]\frac{d\tau}{d[CO_2]} = \frac{p(15\mu)\beta' ab\ \exp(-\beta' a\xi^b)\xi^b}{\beta e^{-\beta\tau}} + \frac{1.08\times 10^{-3}\ S_{\tilde{\nu}} N_o \xi}{\beta e^{-\beta\tau}}$$

$$= 4.21 \times 10^{-2} + 7.5 \times 10^{-2} = 0.117 \quad . \tag{16}$$

Similarly from Eq. (2) we obtain

$$\frac{dT_s}{d\tau} = \frac{3T_e}{16(1 + .75\tau)^{3/4}} = \frac{3T_s}{16(1 + .75\tau)} = 34.5 \tag{17}$$

and therefore

$$f\frac{dT_s}{df} = 4.0°K \quad . \tag{18}$$

Digitized by Google

If the CO_2 content were doubled, the gray model would give $T_s = 290.0$ or $\Delta T_s = 2.8°K$. This value compares nicely to values obtained from more elaborate models. In reviewing a number of recent studies, Schneider (1975)[4] concluded that a doubling of CO_2 would produce a ΔT_s of 1.5 to 3°K . As CO_2 is increased further, the temperature will continue to rise; although the 15 μm bands become more saturated, the 10 μm bands are effectively closing the 8 - 12 μm window, as is illustrated in Fig. III-A.

The energy-budget climate model (§ IVA) relates the infrared radiation to surface temperature, $T_s(x)$, by an empirical relation

$$I \equiv \sigma T_e^4(x,f) = A + B[T_s(x,f) - 273] \tag{19}$$

where x is the sine of the latitude. If the solar constant is indeed constant but f is allowed to vary, then $\langle T_e \rangle$ (averaged over the planet) remains constant with f . Representing the latitudinal variation of surface temperature by

$$T_s(x,f) = T_o(f) + T_2(f)P_2(x) \tag{20}$$

we have

$$\langle T_s(f) \rangle = T_o(f) \tag{21}$$

Even though A and B are each independent of local surface temperature in accord with Eq. (29), they must nevertheless vary with the global mean $\langle T_s(x,f) \rangle$ in order to preserve a constant $\langle T_e \rangle$. Thus

Digitized by Google

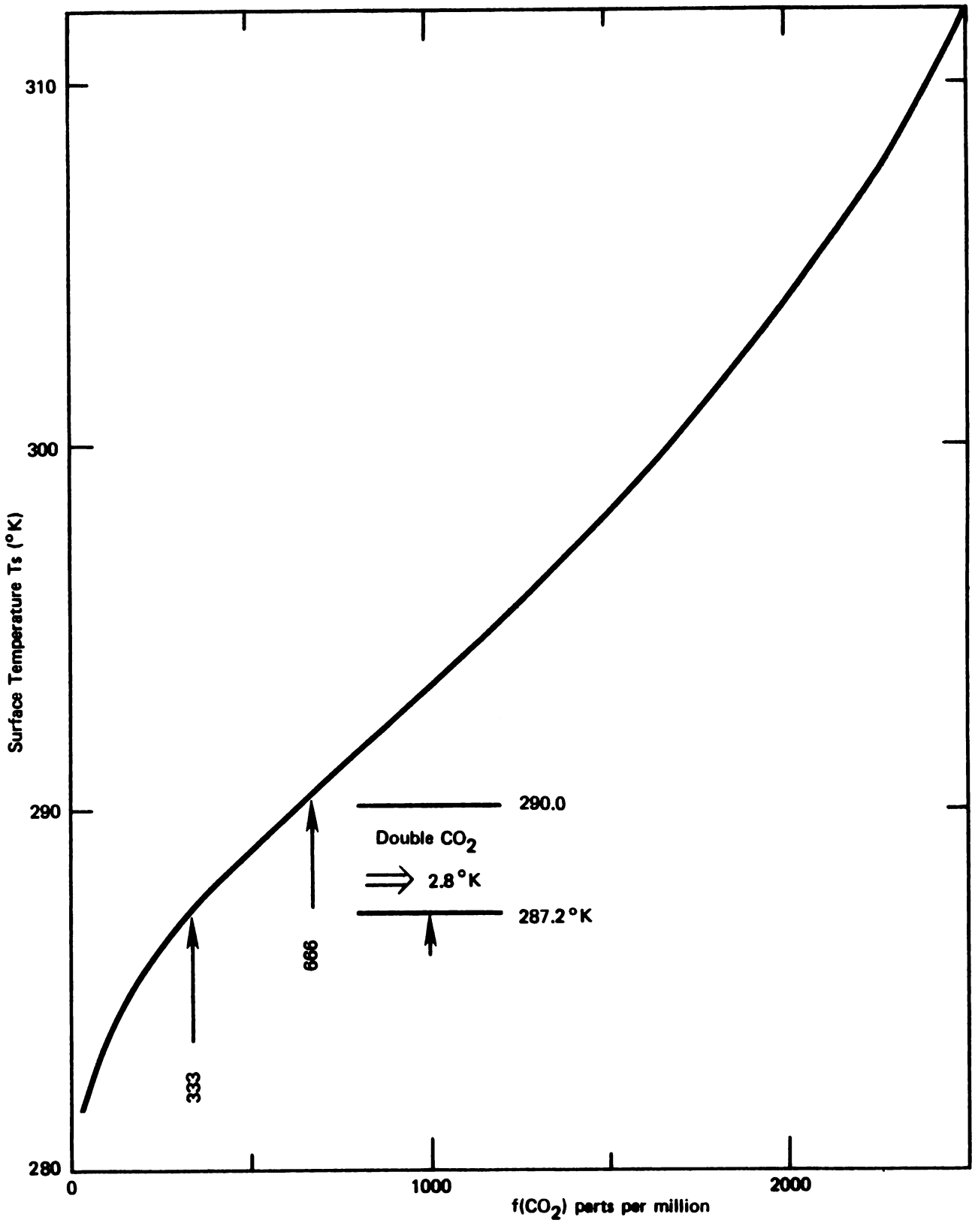

Figure III-A

TEMPERATURE VERSUS CO_2 ABUNDANCE IN A GRAY MODEL IS IN GLOBAL RADIATIVE EQUILIBRIUM

The inflection point around 750 - 1000 ppm develops because the 15 μm band is becoming saturated but the 10 μm bands are not yet strong enough to produce appreciable heating.

Digitized by Google

$$A(f) + B(f)\ [T_o(f) - 273] = \text{const.} \tag{22}$$

As a practical method of computing a global model with a modified f, we note from Eq. (2) that a gray radiative model valid at every latitude would yield a latitudinal dependence of flux of

$$I[f,T_s(x)] = I\left(f,T_s^{(o)}\right) + \frac{dI\left(f,T_s^{(o)}\right)}{dT_s}\left(T_s-T_s^{(o)}\right) + \ldots$$

$$= \frac{\sigma T_s^{(o)4}}{1+.75\ \tau_g} + \frac{4\sigma T_s^{(o)3}}{1+.75\ \tau_g}\left(T_s-T_s^{(o)}\right) \tag{23}$$

where $T_s^{(o)}$ is a convenient reference temperature. For $T_s = 273$, Eq. (23) can be compared with Eq. (19) to obtain the A and B dependence on τ_g or f. This result suggests that A and B are scaled by

$$A(f) = \frac{A(f_o)(1+.75\ \tau_{g,o})}{1+.75\ \tau_g} \tag{24}$$

and

$$B(f) = \frac{B(f_o)(1+.75\ \tau_{g,o})}{1+.75\ \tau_g} \tag{25}$$

where $\tau_{g,o}$ corresponds to abundance f_o.

Digitized by Google

The mean surface temperature of the planet T_o, when the infrared flux is a specified function of latitude, Eq. (19), will not be the same as the simpler radiative mean, Eq. (2). If the optical thickness is modified by $\Delta\tau_g$, the radiative change is given by Eq. (17), whereas the latitude dependence gives, by Eqs. (22), (24), and (25),

$$\frac{\Delta T_o}{\Delta\tau_g} = \frac{3}{4}\left(\frac{A/B + T_o - 273}{1 + .75\,\tau_g}\right) \tag{26}$$

With $A = 211.2\ W/m^2$ and $B = 1.55\ W/m^2{}^\circ C$, Eq. (25) is about twice the rate of Eq. (17).

5. Radiative Effects of Minor Constituents

The addition to the atmosphere of a minor constituent that absorbs in the 8 to 12 μm window could be important. In this region $\pi B_\lambda/\sigma T_s^4 \approx .060 - .070/\mu$ and hence Eq. (5) is

$$p_i \approx 0.065\ \Delta\lambda_\mu \quad , \tag{27}$$

where $\Delta\lambda_\mu$ is the width of the absorption in microns. We will estimate the minimum amount of a trace gas that could produce a 1°K change in global temperature.

For an optically thin amount of absorber, we have simply

$$A_i = p_i\left[1 - e^{-\beta\tau_i}\right] \approx \beta p_i \langle\tau_i\rangle \ , \tag{28}$$

Digitized by Google

where $\langle\tau\rangle$ is the mean value in the band, or

$$\langle\tau\rangle = \frac{N}{\Delta\lambda} \int \alpha \quad d\lambda \tag{29}$$

which gives

$$A = \beta(.065)\ N \int \alpha \quad d\lambda$$

$$= .108\ N\ S_\lambda \tag{30}$$

where N is the integrated column density (molecule/cm^2) and S_λ the integrated absorption coefficient or strength (in units of cm^2 micron). The more common units for strengths are cm (cross section in cm; spectrum in cm^{-1}):

$$S_{\tilde{\nu}} = \int \alpha \quad d\tilde{\nu} \tag{31}$$

Hence at 10 μm ,

$$A = 0.108\ N\ S_{\tilde{\nu}}\ \lambda_\mu^{\ 2}\ 10^{-4}$$

$$= 1.08 \times 10^{-3}\ N\ S_{\tilde{\nu}} \tag{32}$$

The maximum band strengths are not likely to exceed 5×10^{-17} cm (see Appendix A, Ruderman).

Digitized by Google

From Eq. (12) we have

$$\frac{dA}{d\tau_g} = \beta e^{-\beta\tau_g} = 1.66\ (0.15)$$

$$= 0.25 \tag{33}$$

and with Eq. (17) the T_s - A relation becomes

$$\frac{dT_s}{dA} = \frac{dT_s/d\tau_g}{dA/d\tau_g} = 138 \quad . \tag{34}$$

Thus for 1°K changes in T_s, we are searching for increments in A the order of 7×10^{-3}, or from Eq. (32),

$$\Delta N \gtrsim \frac{7 \times 10^{-3}}{1.08 \times 10^{-3} \times 5 \times 10^{-17}} = 1.3 \times 10^{17}\ \mathrm{cm}^{-2} \tag{35}$$

The integrated column density of the atmosphere is $2.15 \times 10^{25}\ \mathrm{cm}^{-2}$ so we are concerned with mixing ratios of minor constituents greater than

$$\Delta f \sim 5 \times 10^{-9} \tag{36}$$

or a few parts per billion (ppb) for substances that have a single strong absorbing band in the 8 to 12 μm window.

The halogenated methanes (Freons) have been cited as a striking example of the effect we are examining here (Ramanathan 1975).[5] The two Freons F-11 and F-12 together have five bands with strengths

Digitized by Google

$S_s \sim 3 \times 10^{-17}$ cm . The 1975 abundance was 0.1 ppb; an increase of 10 times would place these substances in the climate critical category.

Most substances will not have bands in the window with strengths close to the maximum. From Eq. (35) the pertinent quantity for bands in the window is

$$\Delta N \cdot S \gtrsim 10 \qquad (37)$$

if an absorber is to produce a $1^{o}C$ change on future climate (see Table III-1). Both N_2O and CH_4 sit in regions where there is already strong absorption and they have to be analyzed (as we did CO_2) allowing for the present near-saturation.

All of the substances in the Table except the hydrocarbons have been examined with a more elaborate radiative model (Wang, et al, 1976)[6] and found to be marginally important, if their abundances increase. For N_2O, CH_4, and NH_3, factors of two are important.

More attention needs to be directed toward the global abundance and long term growth rate of hydrocarbons, which are among the primary urban pollutants, and whose emission is largely uncontrolled. The abundance in Table III-1 applies to the total hydrocarbon population; the strength listed is the maximum from Appendix A and probably is much smaller. Aldehydes (a hydrocarbon family) are partly destroyed near their urban

Digitized by Google

source, where they participate in the production of oxidants. Away from high concentrations of NO_x, the aldehydes disappear by photodissociation and attachment to aerosols.

6. Destruction of Trace I.R. Absorbers

Many of the hydrocarbons are not only being emitted at increasing rates, but their natural sinks are becoming saturated. The principal sink for methane is hydroxyl:

$$CH_4 + OH \rightarrow CH_3 + H_2O \quad . \tag{38}$$

Indeed, OH plays a crucial role in scavenging a number of the less soluable trace gases, such as CO, H_2S, SO_2, and the partially halogenated methanes, $CH_x C\ell_y F_z$ and $CH_x Br_y$. A depletion of OH may thus aggravate a build up of infrared absorbing pollutants and their inpact on the climate. At present there is a danger of such a depletion occurring because of the increasing production of CO, which is removed mainly by

$$OH + CO \rightarrow CO_2 + H \tag{39}$$

The present CO production from fossil fuel burning is 0.4×10^9 ton/year whereas the natural production is 1 to 3×10^9 ton/year. The problem is amplified by the fact that the main natural source of CO is the oxidation of CH_4. Following reaction (38), oxidation proceeds by

Digitized by Google

$$CH_3 + O_2 + M \rightarrow CH_3O_2 + M \quad (40)$$

$$CH_3O_2 + NO \rightarrow CH_3O + NO_2 \quad (41)$$

$$CH_3O + O_2 \rightarrow HO_2 + CH_2O \quad . \quad (42)$$

Finally, formaldehyde is dissociated into H_2 + CO, or it may condense onto aerosols and ultimately rain out.

The principal source of tropospheric OH is photodissociation of tropospheric ozone:

$$O_3 + h\nu(\lambda < 4110A) \rightarrow O(^1D) + O_2 \quad (43)$$

followed by

$$H_2O + O(^1D) \rightarrow 2\ OH \quad (44)$$

Thus present levels of man-made CO emission are large enough to perturb the CO-OH-CH_4 cycle. Reactions that recycle OH, such as HO_2 + NO — OH + NO_2, may account for some 30 per cent of the present OH.

7. Feedbacks: Comments on Water and the Stratosphere

Earth is the water planet and water affects climate differently in its different manifestations: vapor, clouds, sea, sea-ice, land-ice and

Digitized by Google

snow, and foliage. Common to all models is the acknowledgement of the effect and inability to do anything useful about it. It is not unlikely that the response of water to a change in CO_2 is the dominant factor in climate change. If so, we do not even know the algebraic sign of the change.

Also physical processes in the stratosphere can feed back on surface temperatures. The water abundance in the stratosphere is only several parts per million and is probably fixed by the vapor pressure at the tropical tropopause [although H_2O can be made in the stratosphere by reaction (38)]. A change in the content of water due to a change in stratospheric temperature will affect the earth's greenhouse. An alteration of the ozone abundance will change the absorption at 9.6 μm, which is the main absorber in the 8 - 12 μm window. Thus an increase in tropospheric CH_4 could affect stratospheric HO_x chemistry, the ozone abundance, and thence the climate.

B. A Simple Band Model for Infrared Emission from the Terrestrial Atmosphere

The energy budget climate model described elsewhere in this report requires knowledge of the infrared flux (I) radiated to space by which the Earth balances incoming solar radiation. The flux I must be given as a function of the local surface temperature (T_s) and a few other atmospheric parameters such as the CO_2 concentration, lapse rate, etc.

Digitized by Google

A proper treatment of infrared emission from the Earth's atmosphere involves a multitude of complex factors, viz. Paltridge and Plott (1976) or Kondratyev (1969). Our hope here is to develop a model simple enough to be tractable yet incorporating enough observational and theoretical knowledge of the atmosphere so as to be responsive to changes in the atmosphere such as a changing CO_2 content. While this effort is intended primarily as an input to the aforementioned climate model, several interesting features are revealed by exercising the model.

Rather than letting radiative transfer determine the temperature structure of the atmosphere we will assume that the atmospheric structure is known and simply let this assumed structure radiate to space. Our assumed structure is based on the U.S. Standard Atmosphere, 1976. In this sense the model can be seen as a perturbation on this Standard Atmosphere.

Although we compare model results, i.e. values of the infrared (IR) flux radiated to space, with satellite observations and other empirical data, the model has not been "turned" to observational data except by the introduction of a normalizing constant for the total infrared flux and the use of empirical values of atmospheric parameters, e.g., lapse rates, scale heights, surface densities, etc. Where possible, these parameters are taken from the U.S. Standard Atmosphere (1976).

Digitized by Google

The model is briefly summarized in terms of three assumptions:

- The atmosphere is locally plane parallel with a temperature profile $T(z)$ given by a piecewise linear curve consistent with the U.S. Standard Atmosphere (1976). For surface temperatures T_s other than 288°K, the lapse rate is held constant and the tropopause temperature held constant at 217°K (see Fig. III-1). Structure above the tropopause is also held constant.

- The atmosphere radiates IR emission only in the 8-100μ (100 - 1250 cm^{-1}). This spectral range is divided into nine bands chosen so as to reflect salient features of the terrestrial IR spectrum and their changes over different parts of the Earth. The bands correspond to the atmospheric window and the absorption bands of H_2O, CO_2 and O_3 (see Table III-2 and Fig. III-2).

- The IR emission of the Earth's surface arises from a black body at the surface temperature (T_s). Emission in the optically thick CO_2 and H_2O absorption bands arises from an atmospheric layer whose temperature is appropriate to an optical depth of 2/3 measured vertically downward from the top of the atmosphere (Chamberlain, 1978). The O_3 band and optically thin

Digitized by Google

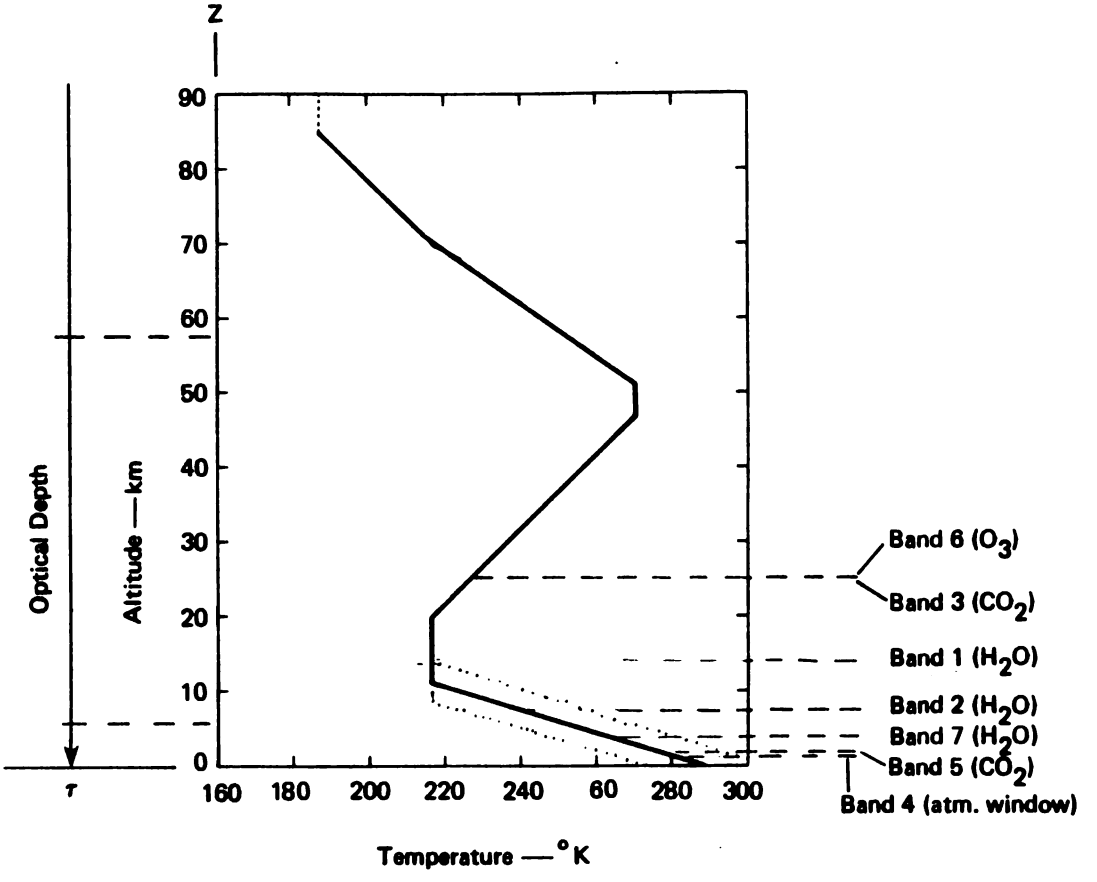

Figure III-1

SCHEMATIC DIAGRAM OF TEMPERATURE PROFILE USED IN NINE-BAND IR EMISSION MODEL FOR THE TERRESTRIAL ATMOSPHERE

The ordinates are height (z) or optical depth (τ). Optical depth τ is measured downward from the top of the atmosphere. The plot of T(z) is taken from the U.S. Standard Atmosphere, 1976. The dotted lines indicate perturbations for surface temperatures above and below 288° K. The τ=2/3 levels for various bands are indicated for the case of T_s=288° K, relative humidity = 50%, CO_2 content = 332 ppm.

Digitized by Google

Table III-2

BAND CHARACTERISTICS

Band i=	Major Absorber	Spectral Range (cm^{-1})	Band Center $\tilde{\nu}_i(cm^{-1})$, $\lambda(\mu)$	Bandwidth $\Delta\tilde{\nu}(cm^{-1})$	Spectral Information*	Effective Height** z_i(km)	Effective Temperature* T_i(K)	Power Flux** $P_i(Wm^{-2})$
1	H_2O	100-400	250, 40.0	300	R_1 = 1000	10.9	217	41.4
2	H_2O	400-550	475, 21.1	150	R_2 = 59.3	4.0	262	47.8
3	CO_2	550-600	575, 17.4	50	R_3 = 14.6	2.3	273	18.0
4	CO_2	600-750	675, 14.8	150	R_4 = 438	18.3	217	19.9
5	CO_2	750-800	775, 12.9	50	R_5 = 7.39	2.4	272	14.7
6	None	800-925	862, 11.6	125	—	0	288	40.9
7	CO_2	925-1000	962, 10.4	75	S_7 = 0.87	0***	288***	19.3
8	O_3/CO_2	1000-1100	1050, 9.5	100	R_8 = 1733 S_8 = 1.2	0***	288***	14.1
9	H_2O	1100-1250	1175, 8.5	150	R_9 = 6.2	0	288	25.7

* R_i and S_i were calculated from the tables given by Houghton (1977, Appendix 10) with units converted to $cm^{-1}(kgm^{-2})^{-1}$.

** These quantities are obtained by applying the model to the case where T_s = 288K, $v_{CO_2} = 333 \times 10^{-6}$, relative humidity = 50% and a = 1 (see text below).

*** Band treated as transmission through an optically thin layer.

Digitized by Google

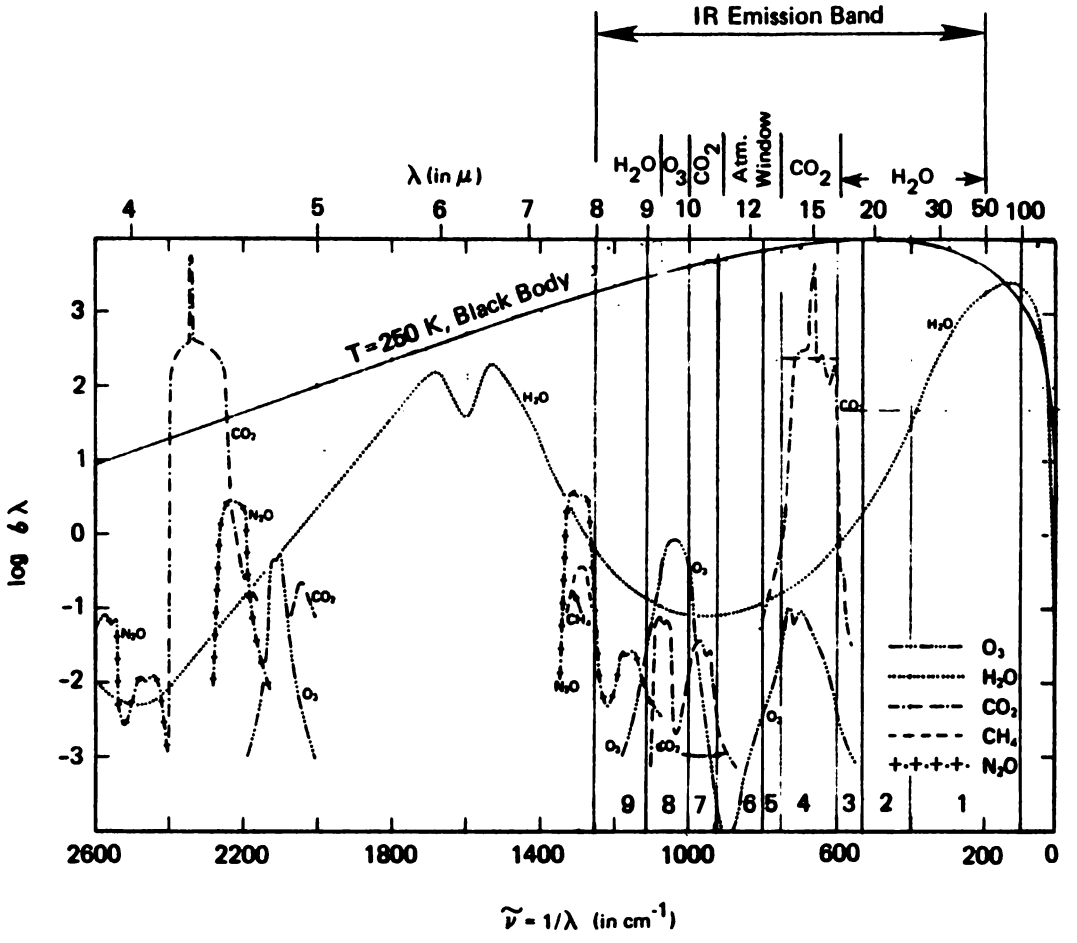

Figure III-2

INFRARED BAND ABSORPTION OF ATMOSPHERIC GASES

The IR emission band ($\tilde{\nu}$ = 200-1000cm^{-1}) in which the model is allowed to radiate is shown as being composed of nine bands: atmospheric window (6), O_3 (8), CO_2 (3, 4, 5, 7, 8) and H_2O (1, 2, 9). A black body curve for 250° K is shown normalized to the upper boundary of the graph. The plot is modified from that given by Allen (1976).

Digitized by Google

CO_2 bands are handled as thin absorbing layers over the surface which radiates as a black body at T_s .

1. Model Description

a. Division into Bands

We divide the terrestrial IR radiation spectrum into nine bands as shown in Figure III-2. This appears to be about the minimum number one can use and still hope to include the major effects of the absorbing gases. In Table III-2 we have summarized the characteristics of these bands. In band 1 we include the strong (50μ) absorption band of water vapor. Band 2 also contains water vapor absorption, but considerably less strong than band 1. The strong CO_2, ν_2 bending mode band at 15μ is accounted for in bands 3, 4 and 5.

The 8-12μ atmospheric window is divided into four bands. Band 6 is completely transparent and thus radiates at an effective temperature equal to the surface temperature T_s . One can consider radiation in this band to be from a grey body with emissivity ε . Since $\varepsilon \sim 0.95$, we shall simply take it as unity in our calculations here. Band 7 presently contains only weak water vapor and CO_2 absorption. We have added this band in anticipation of a major rise in atmospheric CO_2 content. As noted by Chamberlain elsewhere in this report, the major effect of increases in CO_2 content, so far as the greenhouse effect is concerned, will probably lie in making currently transparent portions of the atmospheric window more opaque, rather than making the 15μ CO_2 band even more opaque. Band 8

Digitized by Google

contains the 9.6μ ozone and 9.4μ CO_2 absorption bands. Band 9 contains relatively weak water vapor absorption.

b. Total IR Radiation to Space

The total IR radiation to space is given by a summation over 9 terms:

$$F = a\sum_{i=1}^{9} \Pi B_{\tilde{\nu}}[\tilde{\nu}_i, T_i(T_s,\ldots)]\Delta\tilde{\nu}_i \tag{45}$$

where the Planck function for $\tilde{\nu}$ in cm^{-1}, T in K is

$$B_{\tilde{\nu}}(\tilde{\nu},T) = c_1\tilde{\nu}^3/[\exp(c_2\tilde{\nu}/T) - 1]\ Wm^{-2}sr^{-1}(cm^{-1})^{-1}$$

$$c_1 = 1.911 \times 10^{-8}$$

$$c_2 = 1.439$$

and

$$\tilde{\nu}_i = \text{band center wavenumber } cm^{-1}$$

$$\Delta\tilde{\nu}_i = \text{bandwidth in } cm^{-1}$$

The factor π arises when converting the radiance or specific intensity $B_{\tilde{\nu}}$ to a flux through a plane parallel atmosphere. The constant a, of order unity, is used, as discussed below, to normalize the value of I to some desired value for a specified set of conditions. For example, it

Digitized by Google

could account for IR outside the 100-1250 cm^{-1} band. The effective temperatures T_i are determined for each band as discussed below. Each $T_i(T_s,\ldots)$ is a function of the surface temperature T_s as well as other atmospheric parameters, e.q. CO_2 content, relative humidity, etc.

2. Effective Temperature Calculations

The effective temperatures for optically thick bands are determined by noting the altitude (or equivalent pressure level) at which the mean optical depth measured vertical downward from the top of the atmosphere in band i is 2/3. The temperature T_i at this level is then the effective temperature at which the ith band radiates. The value 2/3 for the optical depth of the effective radiating level is derived by Chamberlain (1978).

a. Transparent Atmospheric Window (800-925 cm^{-1}, Band 6)

In this completely transparent portion of the atmospheric window the effective radiating level is at the surface $(z_i = 0)$ and the effective temperature simply the surface temperature $T_i = T_s$.

b. Water Vapor Bands (1, 2 and 9)

For altitudes below about 30 km the lines in the water vapor bands of interest here are not well separated and overlap considerably. Goody (1964) has developed a random model to account for this overlap in which the mean transmission $\bar{\tau}$ in a spectral range $\Delta\tilde{\nu}$ is given by

Digitized by Google

$$\bar{\tau} = \exp\,(-\,W_i/\Delta\tilde{\nu}) \tag{46}$$

where W_i is the total equivalent width of the lines in the range $\Delta\tilde{\nu}$. A mean vertical optical depth of 2/3 implies a mean transmission $\bar{\tau} = 1 - \exp(-2/3) = 0.487$ above the effective radiating level, z_i . Thus z_i is defined by making W_i such that

$$W_i/\Delta\tilde{\nu} = -\ln\,(\bar{\tau} = 0.487) = 0.72 \tag{47}$$

W_i is calculated differently depending on whether or not the lines in the interval $\Delta\nu_i$ are weak (unsaturated) or strong (saturated such that additional absorption can only occur in the wings of a line) - see Houghton (1977) for reference.

Following Houghton (1977, Ch. 4) the equivalent width for <u>weak lines</u> over the ith band is given by

$$W_i = \sum_j W_j = \sum_j \int_{path} s_j c\rho dz \approx S_i \int_{path} c\rho dz \tag{48}$$

where W_j is the equivalent width over the jth subinterval inside the interval $\Delta\tilde{\nu}$, ℓ is the path length, c the mass mixing ratio of the absorber and ρ the atmospheric mass density. Here we have assumed s_j constant along the path. The quantity s_j is the line strength for lines in the jth subinterval. $S_i = \sum_j s_j$ in units of $cm^{-1}(kg\ m^{-2})^{-1}$.

Digitized by Google

For strong lines, the equivalent width is

$$W_i = \sum_j W_j = 2\sum_j \left[\int_{path} (s_j\gamma_j) \quad c\rho dz\right]^{1/2} \approx 2\sum_j (s_j\gamma_j)^{1/2} \left[\int_{path} c\rho dz\right]^{1/2}$$

where we assume $s_j\gamma_j$ is constant along the path.

Taking account of pressure broadening by letting the half width $\gamma_j = p\gamma_{oj}/p_o$ we have

$$W_i = 2\sum_j \left[\int_{path} (s_i\gamma_{oj})(c\rho p/p_o)dz\right]^{1/2} \approx 2\, R_i \left[\int_{path} (c\rho p/p_o)dz\right]^{1/2} \qquad (49)$$

where p is the local pressure, p_o the standard pressure (1.013×10^5 Pa), $R_i = \sum_j (s_j\gamma_{oj})^{1/2}$ in units of $cm^{-1}(kg\ m^{-2})^{-1}$, and γ_{oj} is the half width over the jth subinterval at STP. The quantities S and R are conveniently tabulated (in cgs, not mks units!) by Houghton (1977, Appendix 10) for water vapor, carbon dioxide and ozone. The values of S or R, appropriate to the effective temperature and summed over bands of interest, are shown in Table 1. S and R are temperature dependent and especially for weak lines this dependence can be important. To include the temperature variation we have used linear interpolation between the S and R values given for 220, 260 and 300 K by Houghton. This linear interpolation when combined with a simple iterative computational scheme yields values of R and S which are consistent with the effective temperatures determined.

Digitized by Google

It now remains to calculate the integral quantities in Eqs. (48) and (49) for both weak and strong lines. In the case of water vapour we let $c\rho = \rho_w = \rho_{wo} \exp(-z/H_w)$ with a scale height H_w of about 2 km. The surface mass density of water vapour ρ_{wo} is discussed below. For <u>weak lines</u> from Eq. (48) we have

$$W_i \approx S_i \rho_{wo} \int_{path} e^{-z/H_w} dz = S_i \rho_{wo} \int_{z_i}^{\infty} e^{-z/H_w} dz = S_i \rho_{wo} H_w e^{-z_i/H_w} \tag{50}$$

where the path is from the effective radiating level z_i vertically upward to infinity.

For strong lines from Eq. (49), letting $c\rho = \rho_w$, as above, and $(p/p_o) = \exp(-z/H)$ where H is the scale height for the atmosphere as a whole, we have:

$$W_i \approx 2R_i \left[\int_{path} \rho_{wo} e^{-z/H_w} e^{-z/H} dz \right]^{1/2} =$$

$$2R_i \rho_{wo}^{1/2} \left(\frac{H_w H}{H_w + H} \right)^{1/2} \exp\left[\frac{-z_i (H_w + H)}{2 H_w H} \right] \tag{51}$$

Using $H_w = 2\text{x}10^3$ and $H = 8.5\text{x}10^3$m we have $H_w H/(H_w+H) = 1619$ and (51) becomes

$$W_i \approx 80.5\ R_i \rho_{wo}^{1/2} \exp(-z_i/3238) \tag{52}$$

Digitized by Google

We must now estimate the surface mass density of water vapour ρ_{wo}. A number of workers (e.g. Manabe and Wetherald, 1975) have used a constant relative humidity formulation. Following this suggestion we shall calculate ρ_{wo} so as to maintain a constant relative humidity r ($r = 0.5$ for 50% relative humidity). One can fit the saturation vapour pressure of water vapour over pure liquid water (mb) in the range -30 to +40C reasonably well by a law of the form $P_{sv}(T_s) = 23.4 \exp[0.076\ (T_s - 293)]$. The surface mass density then becomes

$$\rho_{wo}(T_s) = r(0.0177) \exp[0.076(T_s - 293)] \text{ kg m}^{-3} \qquad (53)$$

For 50% relative humidity and $T_s = 288$, Eq. (53) gives 6.05×10^{-3} kg m^{-3} which is comparable to the midlatitude mean water vapour mass density given by the U.S. Standard Atmosphere, 1976.

Using Eqs. (52 and 53) the effective heights z_i and temperatures T_i can be calculated for the water vapour bands 1, 2 and 9. Letting $r = 0.5$ and $T_s = 288°K$ we find, using the data of Table III-2, the heights also given in Table III-2. In all cases we have assumed strong lines. The heights imply temperatures via an atmospheric temperature - height profile. For $T_s = 288°K$ we go directly to the U.S. Standard Atmosphere. The temperatures T_i corresponding to the heights z_i are shown in Table III-2. We will discuss below the temperature profile to be used when $T_s \neq 288°K$.

Digitized by Google

c. Carbon Dioxide Bands (3, 4, 5, 7 and 8)

The expressions for required equivalent width, Eq. (47), holds equally well for CO_2 as do the expressions for equivalent width Eqs. (48 and 49), provided z_i is relatively close to the surface, i.e., within about a scale height or two. Since CO_2 is well mixed in the atmosphere up to stratospheric heights, it has the same scale height as the atmosphere as a whole. Thus for weak lines we have from Eq. (48):

$$W_i \approx S_i m_{CO_2} \rho_o \int_{z_i}^{\infty} e^{-z/H} dz = 1.86 \, v_{CO_2} S_i H e^{-z_i/H} \tag{54}$$

where m_{CO_2} (v_{CO_2}) is the mass (volume) mixing ratio of CO_2, ρ_o is the surface mass density of the atmosphere = 1.225 kg m^{-3} and H is the scale height of the atmosphere. For strong lines equation (49) becomes

$$W_i \approx 2R_i \left[\int_{path} m_{CO_2} \rho_o e^{-2z/H} \right]^{1/2} = 2R_i \, (1.86 \, v_{CO_2} H/2)^{1/2} e^{-z_i/H}$$

$$= 1.93 \, R_i \, (v_{CO_2} H)^{1/2} e^{-z_i/H} \tag{55}$$

In band 4 where the CO_2 absorption is very strong Eq. (55) with $H = 8{,}500$ m yields an effective radiating level which is on the order of 18 km. At 18 km the scale height is appreciably different from its surface value. Hence it is appropriate to let $H \to H'$ where H' is a value more appropriate to the expected effective radiating level z_i. Here we choose $H' \sim 7{,}300$ m

Digitized by Google

which is appropriate to the density change between the surface and about 18 km.

In band 4 using $H' = 7{,}300$ m , $T_s = 288°K$, $v_{CO_2} = 333$ ppm and R_3 from Table III-2 we find that $z_3 = 18.2$ km . Using the 1976 U.S. Standard Atmosphere this leads to an effective temperature $T \approx 217°K$.

Bands 3 and 5 contain the wings of the strong 15μ CO_2 absorption band. These two bands have been included as separate bands because it is here rather than in band 4 (which is already very strongly absorbed) that <u>changes</u> in CO_2 concentration will be important so far as radiation balance is concerned. Although water vapour is also an important absorber in bands 3 and 5, we have neglected it here in the interest of simplicity. We believe the errors introduced to be minor ones since the scale height of water vapour is so much smaller than that of CO_2. Most probably the errors introduced lead to an overestimate of the temperature increase for CO_2 doubling.

In bands 7 and 8, CO_2 absorption is presently very weak and could well be neglected. However, as discussed in Sec. IIIA of this report, future increases in atmospheric CO_2 content should make a greater impact in bands 7 and 8 than in band 4. This is because band 7 (at 10.4μ) is presently a nearly transparent part of the atmospheric window. Similarly in band 8, CO_2 absorption near 9.4μ will add to the

Digitized by Google

ozone absorption present there. In bands 7 and 8 the CO_2 absorption is presently weak and hence will grow linearly with increases in atmospheric CO_2 content; whereas in band 4 the CO_2 absorption is strong and will grow only as the square root of the CO_2 concentration. In addition band 4 is nearly completely opaque already. Using (54) for weak lines with $z = 0$ and the parameters of Table III-2, we find a mean transmission of $\bar{\tau} = 0.95$ for band 7.

d. Ozone and CO_2 Band (8)

The ozone layer near 25 km altitude is a strong absorber at 9.6μ. Since ozone is distributed in a layer and the stratosphere is held constant in our model, we treat band 8 as radiation from the surface at temperature T_s with a mean transmission given by

$$\bar{\tau} = 1 - [(W_{CO_2} + W_{O_3})/\Delta\nu_6] \tag{56}$$

where W_{CO_2} and W_{O_3} are the equivalent widths of the 9.4μ CO_2 and 9.6μ O_3 absorption bands respectively.

Assuming the ozone layer to be homogeneous with column density $\langle c\rho\rangle \ell = 3.68 \times 10^{-3}$ kg m^{-2}, $R_{O_3} = 1731.8$ cm^{-1}(kg m^{-2})$^{-1}$, and mean pressure $\langle p\rangle = 25.5$ mb have from Eq. (49).

$$W_{O_3} \approx 2R_{O_3} (\langle c\rho\rangle \ell)^{1/2} (\langle p\rangle/p_o)^{1/2} = 33 \text{ cm}^{-1} \tag{57}$$

Digitized by Google

The equivalent width of the 9.4μ CO_2 band is calculated as with the CO_2 in band 8 yielding $W_{CO_2} \approx 7\ cm^{-1}$ for $v_{CO_2} = 333$ ppm , $H = 8500$ m , and $S_{CO_2} = 1.2\ cm^{-1}\ (kg\ m^{-2})^{-1}$ at $T_s = 288$ K . Thus for the conditions of Table III-2 $\bar{\tau} = 0.6$ for band 6.

3. Temperature Profile

The temperature profile $T(z)$ is basically that of the U.S. Standard Atmosphere 1976. For a surface temperature T_s of 288°K the temperature profile is thus the solid line in Fig. III-1. For values of T_s other than 288°K the lapse rate is maintained constant at 6.5 K/km as is the tropopause temperature (217°K). The structure above the tropopause is assumed to remain that of Fig. III-1 regardless of surface temperature. Profiles for $T_s \neq 288$°K are illustrated by the dotted lines of Fig. III-1.

4. Comparison and Observations

We now compare the IR fluxes predicted by our model with satellite measurements of the IR radiation emerging from several different geographical areas. One set of such measurements - made by Hanel, et al. (1971) - from Nimbus 4, is shown in Fig. III-3. The thermal emission of the surface plus atmosphere emitted vertically upward was measured over a 95 km diameter circular area with a spectral resolution of 1.4 cm^{-1}. In each of the three graphs of Fig. III-3 the radiances of black bodies at various temperatures are shown for comparison. Also shown are the spectral bands of our model

Digitized by Google

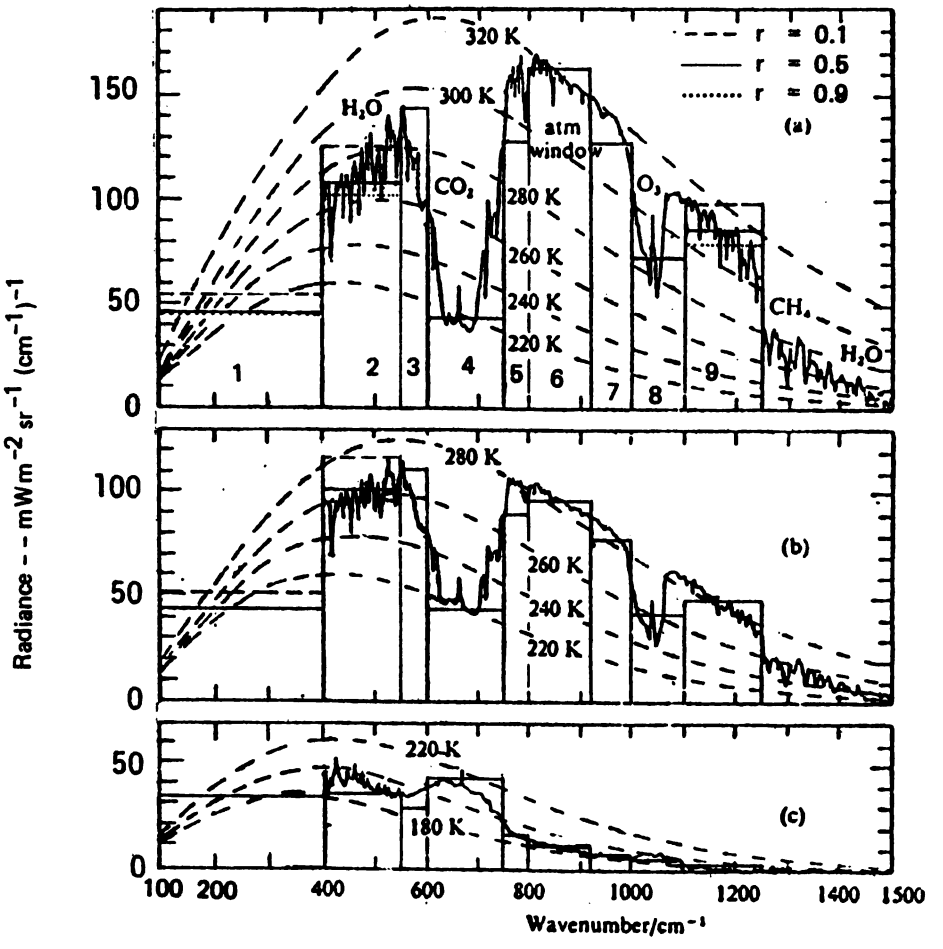

Figure III-3

THERMAL EMISSION FROM THE EARTH'S SURFACE AND ATMOSPHERE EMITTED VERTICALLY UPWARDS AND MEASURED BY HANEL et al. (1971) USING THE INFRARED INTERFEROMETER SPECTROMETER ON NIMBUS 4, (a) OVER SAHARA, (b) OVER MEDITERRANEAN AND (c) OVER ANTARCTIC

The radiances of black bodies at various temperatures are superimposed as dashed lines. Average radiances predicted by the seven band radiation model discussed in the text are given by the bar graphs. In each case model radiances are given for three relative humidities. The solid ——lines correspond to a relative humidity of 50% (r=0.5). The dashed - - - and dotted · · · · lines show changes for relative humidities of 10% and 90% respectively. The normalization factor a=1.

Digitized by Google

and the radiances predicted for each band. Model results are shown for relative humidities of 10, 50, and 90% (r - 0.1, 0.5 and 0.9). Here we have used v_{CO_2} = 326 ppm appropriate to 1970 when the observations were made.

For the Sahara desert case of Fig. III-3(a) we let T_s = 320°K corresponding to the black body temperature in the atmospheric window (band 6). The effective heights z_i and temperatures T_i, determined as above, are shown in Table III-3. The nine band model gives a reasonably good fit to the observational data. The agreement between model and observation is reassuring in that T_s = 320°K is an extreme case—some 20°K higher than the highest zonal average shown in Fig. III-4.

For the Mediterranean Sea case of Fig. III-3(b) we again estimate the surface temperature from the atmospheric window (band 6) yielding T_s = 283°K . A relative humidity of rather more than 50% seems appropriate as one could expect over water. Here again the model radiances are in reasonably good agreement with the observations.

In Fig. III-3(c), results are shown for the Antarctic. Here the black body temperature in the atmospheric window indicates T_s ~ 188°K (-85°C), very cold indeed. Since our temperature profile model calls for a constant tropopause temperature of 217°K, this indicates a temperature inversion and we assume a linear gradient of 5K/km from the surface to the 217°K level. The saturation water vapor pressure is

Digitized by Google

Table III-3

EFFECTIVE HEIGHTS AND TEMPERATURES FOR THE SURFACE CONDITIONS OF FIG. III-3

Band	Major	(a) T_s = 320 K, r = 0.5		(b) T_s = 283 K, r = 0.5		(c) T_s = 188 K, r = 0.5	
i =	Absorber	z_i (km)	T_i (K)	z_i (km)	T_i (K)	z_i (km)	T_i (K)
1	H_2O	14.9	223	10.3	217	0.0	188
2	H_2O	8.1	268	3.4	261	0.0	188
3	CO_2	4.1	293	2.0	270	0.0	188
4	CO_2	18.2	217	18.2	217	19.7	217
5	CO_2	3.9	294	2.1	269	0.0	188
6	None	0.0	320	0.0	283	0.0	188
7	CO_2	0.0*	320*	0.0*	283*	0.0*	188*
8	O_3/CO_2	0.0*	320*	0.0*	283*	0.0*	188*
9	H_2O	1.2	312	0.0	283	0.0	188

* Treated as optically thin.

Digitized by Google

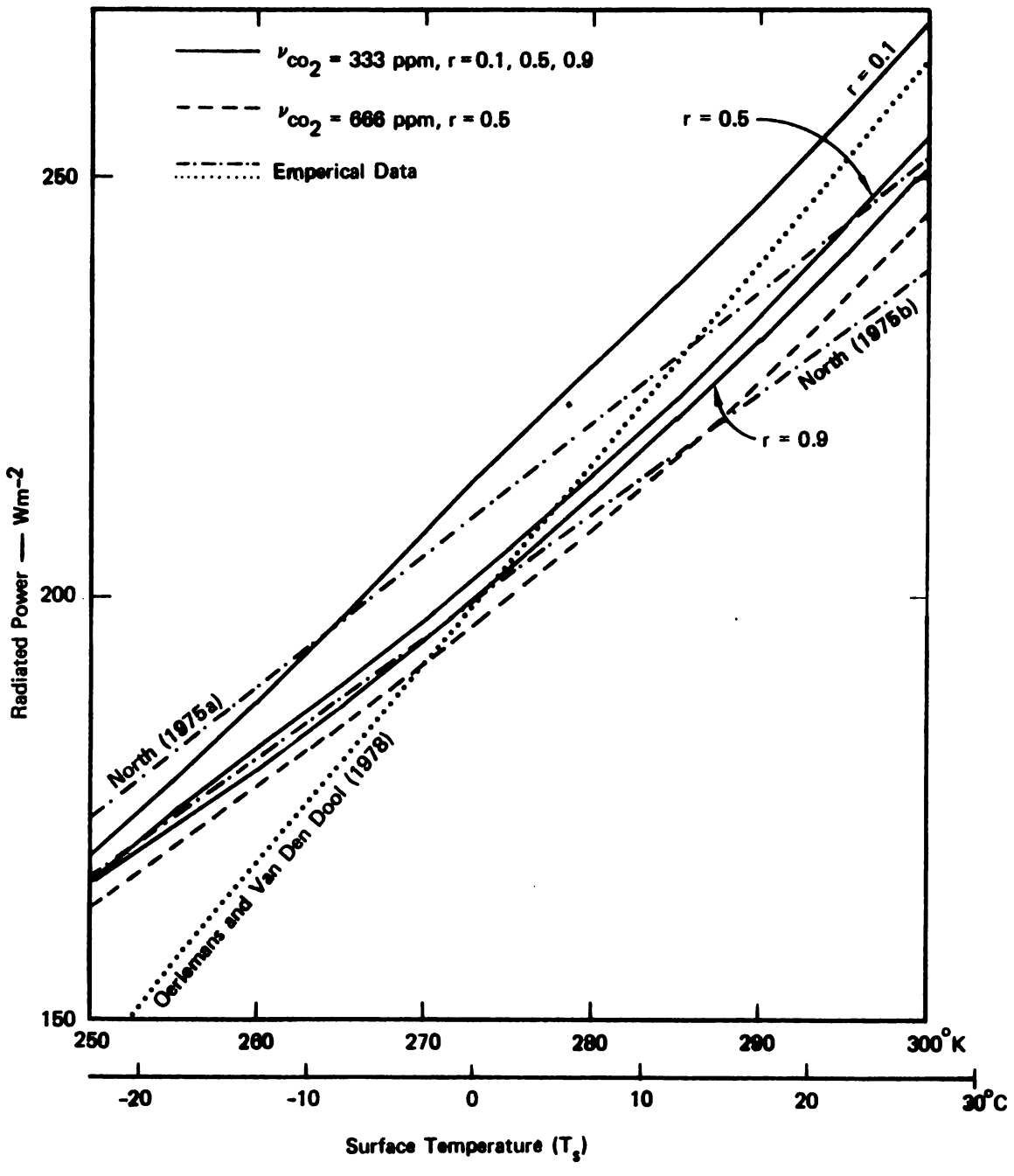

Figure III-4

ATMOSPHERIC RADIATION FLUX TO SPACE $F(T_s)$

Curves are given for the 9 band model for ν_{CO_2} = 333 ppm and relative humidities of r = 0.1, 0.5 and 0.9 (solid lines). A model curve is also given for CO_2 doubling to ν_{CO_2} = 666 ppm and r = 0.5. For comparison we include 3 curves (-·-·- and · · · · lines) which represent straight line fits to observational data. The model curves are normalized to the average of the emperical curves at T_s = 288°K, i.e., a = 0.949 in Eq. (45).

Digitized by Google

so low at this low temperature that even high values of relative humidity still do not cause significant water vapor absorption. Thus the effective radiating levels in bands 1, 2 and 9 are at the surface. The enhanced radiance in the 15μ CO_2 band arises because the temperature at the effective height (in our model) is actually greater than the very low surface temperature. Again the comparison shown in Fig. III-3(c) is reassuring in that the agreement between model and observation is reasonably good even in this very extreme case.

5. Radiated Flux

a. Average Atmosphere

As a first approximation, consider the Earth to have a homogeneous average atmosphere. This assumption allows us to extrapolate conclusions about an atmosphere with a single temperature profile, etc. to the Earth as a whole. Clearly the climate model investigated in Sec. IV of this report will yield more precise results, but this initial approximation is still worth making. For our average atmosphere we take the U.S. Standard Atmosphere, 1976 shown in Fig. III-1. Using this profile and an average relative humidity of 50%, Eq. (46) yields the sum of the average radiated flux in each of the nine bands. The IR flux in each band as well as the effective heights z_i and temperature T_i are shown in Table III-2. The total IR flux $F = 242\ Wm^{-2}$ when $a = 1$. This value of F is slightly too high to balance the incoming solar flux $F_\odot(1-A)/4 = 235\ Wm^{-2}$ calculated when the albedo A has the conventional value of 0.33. However, more recent work indicates A is

Digitized by Google

about 0.29, yielding an incoming flux of 249 Wm^{-2}. To make the outgoing flux from our assumed average atmosphere balance the incoming flux of 249 Wm^{2} we must let $a = 1.03$. Having $a > 1$ is to some extent justified in that some compensation should be made for IR flux which is not included within the 100-1250 cm^{-1} wavenumber band of the model, e.g., see the 1250-1500 cm^{-1} portion of Fig. III-3. Another way to make the incoming and outgoing fluxes balance is to let $a = 1$, but raise T_s from 288°K to about 290°K.

Although a is close to unity, it is not clear just what value a should take. From Fig. III-4 we note that the data of Oerlemans and Van den Dool (1978) indicate F is about 238 Wm^{-2} at $T_s = 288°K$ based on zonally averaged fluxes and temperatures. These data also indicate a difference of about 4 Wm^{-2} between the northern and southern hemispheres. If we take F as 238 Wm^{-2}, $a = 0.98$.

b. Variations in F with Changes in H_2O and CO_2 Content

The key item of interest so far as climate effects are concerned is the alteration of F by changes in atmospheric constituents such as water vapor and CO_2. Consider the average atmosphere discussed above where $v_{CO_2} = 333$ ppm , $T_s = 288°K$, relative humidity = 50%, $a = 1.03$ and hence $F = 249$ Wm^{-2} balancing the incoming solar flux (insolation). If the average relative humidity is reduced to 20% and other factors remain constant, F increases by 8.2 to about 257 Wm^{-2}. To regain balance with the incoming solar flux, the surface temperature

Digitized by Google

T_s would have to drop by about 3.9°K. If the average relative humidity were to increase to 80%, F decreases by 0.9% and a surface temperature rise of about 1.1°K would be required to regain balance with the insolation.

Again consider the aforementioned average atmosphere with $T_3 = 288°K$, $r = 0.5$ and $a = 1.03$. Doubling the carbon dioxide concentration from 333 to 666 ppm reduces F by 3.1% to 241 Wm^{-2}. To reestablish radiation balance with the atmospheric CO_2 content doubled, the surface temperature must rise by 3.8°K. A change in surface temperature could also imply a change in average relative humidity--probably an increase. If we increase the average relative humidity in our model from 50 to 60% in addition to doubling the CO_2 content, the new radiation balance is established at $T_s = 290°K$, an overall 4.3°K increase. If, on the other hand, the relative humidity increases to 40% in addition to CO_2 doubling, the new radiation balance would occur at $T_s = 288.2°K$, an overall increase of only 2.8°K. Thus changes in relative humidity which occur concurrently with changes in CO_2 content can serve to significantly enhance or diminish any CO_2 induced surface temperature changes.

The surface temperature increase predicted by our model for a doubling of atmospheric CO_2 content, namely 3.8°K, falls just above the range of 1.5 to 3°K suggested by Schneider (1975) as the range of reasonable values. He arrived at this range after reviewing

Digitized by Google

a number of model predictions. More recently he has suggested a range of 1.5 to 5°K which encompasses our result.

We note that the change in outgoing infrared flux induced by a doubling of CO_2 in our model is caused by changes in bands 3, 5, 7 and 8, i.e., the wings of the 15μ band and the weak 9.4 and 10.4μ absorption bands of CO_2. Doubling the CO_2 content causes the effective height in band 4, containing the core of the 15μ CO_2 band, to increase; but since the effective height remains in the tropopause region the effective temperature remains at 217°K and the flux radiated in band 4 remains unchanged.

c. Variations in F with Changes in Surface Temperature for Various Atmospheric Conditions

By summing the radiation flux to space in each of the nine bands according to Eq. (45) we arrive at a total flux F. In Fig. III-4 we have plotted F as a function of surface temperature (T_s) for several sets of atmospheric parameters namely average relative humidity and carbon dioxide concentration. For comparison we show three emperical curves for $F(T_s)$, which are straight lines fitted to observations. We have normalized the model curves by letting the model curve for $r = 0.5$ and $v_{CO_2} = 333$ ppm pass through the average of the emperical curves at $T_s = 288°K$, the Earth's average surface temperature, i.e., $a = 0.949$ in Eq. (45).

Digitized by Google

Perhaps the most striking feature of the model curves themselves, is the large effects caused by changes in average relative humidity (r), especially for $r \gtrsim 0.5$ and $T_s \gtrsim 270°K$. This serves to emphasize the importance of water vapor in the atmosphere and points out that changes in average relative humidity which might occur along with changes in CO_2 content could significantly alter predictions of CO_2 climate effects based on an unchanging water vapor content. The atmospheric radiation model considered here includes the increase in saturation water vapor pressure with temperature; hence, for a constant relative humidity, a CO_2 induced increase in surface temperature causes an increase in water vapor content and hence an additional surface temperature increment over and above that caused by CO_2 above.

We note that for $T_s \lesssim 280°K$, the three model curves for $F(T_s)$ converge. This occurs because the decreasing temperature decreases the water vapor content of the atmosphere for a given relative humidity. At low enough temperatures the water vapor absorption becomes negligible in bands 1, 2 and 9 and the model predicts the same flux regardless of r.

An interesting feature of the model $F(T_s)$ curve for $r = 0.5$ and $v_{CO_2} = 666$ ppm is that the difference relative to the $r = 0.5$, $v_{CO_2} = 333$ ppm curve is most pronounced at higher temperatures. This results from the temperature dependence of S in Eq. (54) for bands 7 and 8. S increases by more than a factor of two between 250 and 300°K;

Digitized by Google

hence the greater CO_2 absorption at high temperatures. This dependence of S on T in bands 7 and 8 would tend to mitigate CO_2 induced temperature changes at high latitudes.

Comparing the model curves with the observational curves we find that our model generally lies between the sets of observation data. In terms of the slope of the model curves, which is really the relevant comparison, the model curves for $r \gtrsim 0.5$ agree best with the Oerlemans and Van der Dool (1978) data at $T_s \gtrsim 280°K$ and with the North data for lower temperatures. The model curve for $r = 0.1$ is more closely in agreement with the Oerlemans and Van der Dool data over the entire temperature range.

d. Linear Approximations to $F(T_s)$

In connection with energy balance climate models it is convenient to approximate the atmospheric radiation flux to free space by a linear law of the form:

$$F(T_s^1) = A + BT_s^1 \tag{58}$$

where $T_s^{\prime}$ is the surface temperature in degrees centigrade. This law allows analytic solutions to a simple energy balance climate model as discussed elsewhere in this report. To provide an input to such models, we have used our nine band model to calculate A and B for varying CO_2 content with relative humidity held constant at 50% and $a = 0.949$. This value of a is the same as was used for normalization in Fig. III-4.

Digitized by Google

Table III-4 gives the values of A and B for CO_2 concentrations ranging from 300 to 1000 ppm. Comparing our values for A and B with those used by other authors, we find A = 209.9, 200.0 and 199.3 and B = 1.57, 1.45 and 2.40 for North (1975a), North (1975b) and Oerlemans and Van den Dool (1978) respectively. Comparing these values for A and B with our nine band model with v_{CO_2} = 333 ppm and r = 0.5 we see from Table III-4 that our model values fall near the center of the observational values.

6. Summary and Conclusions

Our hope was to include enough physics of the Earth's atmosphere and of the radiation processes involved to construct a reasonably useful model. The extent to which this goal was achieved is shown graphically in Figs. III-3 and III-4 where we compare model prediction with observational data. We conclude that our nine band radiation model, while far from complete, is useful in making at least crude estimates of the impact of increases in atmospheric CO_2 content on future climate especially when coupled with the energy balance climate model discussed in section IV of this report.

By assuming the Earth's atmosphere to be homogeneous with an average temperature of T_s = 288°K and an average relative humidity of 50%, we can estimate the change in surface temperature induced by a doubling of CO_2 content. Our result is a 3.8°K increase which falls

Digitized by Google

Table III-4

Linear Approximation for $F(T_s')$ Centered on $\overset{\circ}{\lambda}$°C, $F(T_s'$ in °C) = $A+BT_s'$

v_{CO_2} (ppm)	A (Wm^{-2})	B($Wm^{-2}C^{-1}$)
300	203.2	1.69
333	202.6	1.66
400	201.1	1.66
500	199.4	1.61
600	197.7	1.60
666	197.1	1.57
700	196.6	1.57
800	196.3	1.54
900	194.4	1.52
1000	194.3	1.49

Relative humidity = 50% and a = 0.949.

Digitized by Google

near the middle of the 1.5 - 5°K range suggested by Steven Schneider after a review of model calculations. The CO_2 doubling has its impact in the wings of the strong 15μ CO_2 absorption band and in the weak CO_2 absorption bands near 10.4 and 9.4μ (bands 7 and 8 in our model). In band 4 which contains the core of the strong 15μ CO_2 absorption no changes occur for a CO_2 doubling. In this case although absorption increases drive the effective radiating height upward, this height is in the constant temperature tropopause both before and after doubling; hence there is no change in radiated flux. Because we have neglected water vapor in bands 3 and 5, we expect that our figure of $\Delta T_s = 3.8°K$ (for the average surface temperature increase upon CO_2 doubling) is an overestimate. We have done a calculation in which the CO_2 in bands 3 and 5 was completely neglected. This resulted in a figure of $\Delta T_s = 1.4°K$, which we would regard as an underestimate. Since we expect the error in the larger figure to be smaller, we would correspondingly expect further refinements in our simple band model to lead to $\Delta T_s = 3°K$.

The above result of $\Delta T_s = 3.8°K$ surface temperature increase for a doubling of atmospheric CO_2 is in substantial agreement with the $\Delta T_s = 2.8°K$ deduced in Section III-A above. This is interesting because these similar results were obtained by quite significantly different approaches. Hence it lends credibility to the estimate of about 3°K as the average surface temperature increase in response to a doubling of atmospheric CO_2 content.

Digitized by Google

Certainly this nine band radiation model could be improved. For example in the handling of wavebands where there are two or more important absorbing constituents such as band 3 where both water vapor and CO_2 are important. However, one could easily question the wisdom of further model improvements in view of the reasonably good agreement with observations (Fig. III-3) and in the face of other uncertainties such as the response of water vapor to changes in surface temperature.

It is no secret that water vapor is presently the dominant constituent in determining the atmospheric radiation balance (see Fig. III-2). Hence changes in atmospheric water vapor content which occur along with increases in CO_2 content are clearly important and could be the dominant factor in the effect of CO_2 on climate. Our model can quantify this importance in the sense that we can calculate the changes in radiation balance due to given concurrent changes in both H_2O and CO_2 content. For example, if we assume that upon a doubling of CO_2 the average relative humidity also increases from 50 to 60%, our homogeneous atmosphere model implies a change in average surface temperature of 4.3°K, a nearly 15% higher temperature increase than with the relative humidity constant at 50%.

As shown by the dashed and solid lines in Fig. III-4, the difference in $F(T_s)$ caused by a doubling of CO_2 (with r held constant at 0.5) is not constant with variations in surface temperature. The difference increases with increasing T_s. This results from the temperature dependence of the CO_2 absorption coefficient in the weak 9.4 and 10.4μ bands.

Digitized by Google

While our nine band model is deficient in some respects, e.g., cloud variations are neglected, it does incorporate a modicum of atmospheric physics and agrees reasonably well with experimental data. Hence it provides some insight into the climatic effects of increased atmospheric CO_2 content. It also provides a radiative loss function dependent on average relative humidity and atmospheric CO_2 content for use in the energy balance climate model discussed elsewhere.

Digitized by Google

Digitized by Google

REFERENCES FOR SECTION III

1. Plass, G.: 1956, Tellus 8, 140-153.

2. Chamberlain, J.W.: 1978, Theory of Planetary Atmospheres, Academic Press, N.Y., 330.

3. Kondratyev, K.Y.: 1969, Radiation in the Atmosphere, Academic Press, N.Y., 912.

4. Schneider, S.H.: 1975, On the Carbon Dioxide - Climate Confusion, J. Atm. Sci., 32, 2060-2066.

5. Ramanathan, V.: 1975, Greenhouse Effect Due to Chlorofluoro-carbons: Climatic Implication, Science, 190, 50-51.

6. Wang, W.C., Yung, Y.L., Lacis, A.A., Mo, T., Hansen, J.E.: 1976, Greenhouse Effects Due to Man-made Perturbations of Tracer Gases, Science, 685-689.

7. Allen, C.W.: 1976, Astrophysical Quantities, 3rd ed., Univ. of London (Athlone Press).

8. Chamberlain, J.W.: 1978, Theory of Planetary Atmospheres, Academic Press, N.Y.

9. ESSA, NASA, USAR: 1966, U.S. Standard Atmosphere Supplements, 1966, U.S. Gov't Printing Office, Washington, D.C.

10. Goody, R.M.: 1964, Atmospheric Radiation, I. Theoretical Basis, Oxford Univ. Press.

11. Goody, R.M. and J.C.G. Walker: 1972, Atmospheres, Prentice-Hall, Englewood Cliffs, N.J.

12. Hanel, R.A., Schlachman, B, Rodgers, D., and D. Vanous: 1971, Nimbus 4 Michelson Interferometer, Applied Optics, 10, 1376-1382.

13. Houghton, J.T.: 1977, The Physics of Atmospheres, Cambridge Univ. Press.

14. Kondratyev, K.Y.: 1969, Radiation in the Atmosphere, Academic Press, N.Y.

15. Manabe, S. and R.T. Wetherald: 1975, The effects of doubling the CO_2 concentration on the climate of a general circulation model, J. Atm. Sci., 32, 3-15.

Digitized by Google

16. NOAA, NASA, USAF: 1976, U.S. Standard Atmosphere, 1976, U.S. Govt. Printing Office, Washington, D.C.

17. North, G.R.: 1975a, Analytic solution to a simple climate model with diffusive heat transport, J. Atm. Sci., 36, 1301-1307.

18. North, G.R.: 1975b, Theory of energy balance climate models, J. Atm. Sci., 32, 2033-2043.

19. Oerlemans, J. and H.M. Van den Dool: 1978, Energy balance climate models: stability experiments with a refined albedo and updated coefficients for infrared emission, J. Atm. Sci., 35, 371-381.

20. Paltridge, G.W. and C.M.R. Platt: 1976, Radiative Processes in Meteorology and Climatology, Elsevier, Amsterdam.

21. Schneider, S.H.: 1975, On the Carbon Dioxide - Climate Confusion, J. Atm. Sci., 32, 2060-2066.

22. Sellers, W.D.: 1966, Physical Climatology, Univ. of Chicago Press.

Digitized by Google

Appendix A to Section III

VIBRATIONAL BAND STRENGTHS

The vibrational modes of a molecule interact with electromagnetic radiation because there is a significant charge associated with some of its vibrating constituents. If electronic excitations are ignored the molecule may be described as a collection of atomic masses M_i, such with an effective charge Q_i, interacting among themselves through complicated potentials. A gas of such molecules has a frequency dependent dielectric constant which satisfies the Kramers-Kronig relation:

$$R\ell\ \varepsilon(\omega) - 1 = \frac{2}{\pi} P \int_0^\infty \frac{\mathrm{Im}\ \varepsilon(\omega')\ \omega'\ d\omega'}{\omega'^2 - \omega^2} \qquad \text{(A-1)}$$

[This statement, equivalent to the analyticity of the function $\varepsilon(z)$ in the upper half plane together with the condition, from physical considerations, that $\varepsilon(\omega) \to 1$ as $\omega \to \infty$, follows just from the fact that the molecule cannot respond to an external electric field before such a field is present.]

The response of the molecule to a sufficiently high frequency external electric field is independent of the interaction between the atom-like constituents and

$$\lim_{\omega\to\infty} \varepsilon(\omega) = 1 - \frac{4\pi n}{\omega^2} \sum \frac{Q_i^2}{M_i} \qquad \text{(A-2)}$$

Digitized by Google

when n is the number density of molecules. When the high frequency limit is taken for the RHS of Eq. (A-1) we obtain the sum rule:

$$4\pi n \sum \frac{Q_i^2}{M_i} = \frac{2}{\pi} \int_0^\infty \omega' \ \mathrm{Im}\ \varepsilon(\omega')\ d\omega' \tag{A-3}$$

The integrated line intensity over a molecular vibration band is expressed in terms of ε as

$$S = 2 \int_B \frac{\omega \mathrm{Im}(\varepsilon^{1/2})}{nc^2}\ d\omega \tag{A-4}$$

In a gas

$$\mathrm{Im}\ \varepsilon^{1/2} = \mathrm{Im}\ [1 + (R\ell\ \varepsilon - 1) + i\ \mathrm{Im}\varepsilon]^{1/2}$$

$$\sim \frac{1}{2}\ \mathrm{Im}\ \varepsilon$$

Then, because the integration range in Eq. (A-4) is less than that of Eq. (A-3), we have the inequality

$$S < 2\pi^2 \sum \frac{Q_i^2}{M_i c^2} \tag{A-5}$$

For $M_i = x_i x$ mass of a carbon atom and $Q_i = y_i e$ the inequality (A-5) is

$$S < 2 \cdot 10^{-16} \sum \frac{y_i^2}{x_i}\ \mathrm{cm.} \tag{A-6}$$

Digitized by Google

Only very rarely is the bonding between atoms in a molecule so ionic that $y_i \sim 1$. In such cases large dipole moments may be present of order $e(1\text{-}2\text{Å}) \sim 10^{-17}$ (cgs) = 10 D , as is found in FℓK , CℓK , BeK . In most bonds $D \sim 1$ corresponding to y_i much less than 1. Then for H-C bonds (where x_i would be of order 10^{-1}), or C-C bonds $y_i^2 << 1$. Values of S very much greater than a few $x10^{-16}$ cm would not be expected except in molecules where the number of relevant constituent atoms is so great that very many different vibrations in separate parts of the molecule have the same frequency.

Digitized by Google

Digitized by Google

IV CLIMATE MODELS

The radiative models discussed in Section III neglect the redistribution of the sun's energy by the movements of the atmosphere and oceans. The dynamics of the coupled ocean-atmosphere system remain an unsolved problem. In this section, we explore models in which the atmosphere and oceans are dealt with as a unit and the temperature of the earth is assumed to be a function only of latitude.

A. Energy Budget Climate Models

We wish to evaluate the effect of increased atmospheric concentrations of CO_2 on the climate, by examining simple climate models, the so called energy budget models.

The most elementary energy budget model, which we choose to call zero'th order, simply asserts:

$$\sigma \bar{T}_e^4 = \frac{Q}{4} (1 - \bar{\alpha}) \tag{1}$$

where

Digitized by Google

σ = Stefan Boltzmann constant

$\overline{T}_e$ = effective mean radiating temperature

Q = solar constant

$\overline{\alpha}$ = mean albedo of the earth.

From computations made at JASON 1978, we believe the relation between effective and surface temperature is given by

$$\overline{T}_s = (1 + 3\tau/4)^{1/4}\,\overline{T}_e$$

where τ is a measure of the opacity of the opacity of the atmosphere whose dependence on CO_2 concentration is described elsewhere in this report. For the current atmosphere, τ, computed from first principles, was found to be 0.75. Putting in conventional values of the remaining constants:

$\sigma = 5.6 \times 10^{-8}\ W/m^2\ (°K)^4$

$Q = 1360\ W/m^2$

$\overline{\alpha} = 0.3$

we get the quite acceptable figures $\overline{T}_e = 257°K$, and $\overline{T}_s = 288°K = 15°C$.

As a predictive equation, Eq. (1) suffers from an array of defects. Changing, for example, the solar constant alters $\overline{\alpha}$ in an unknown manner. A change in CO_2 concentrations affects the mean surface temperature, and

Digitized by Google

hence also $\bar{\alpha}$. Its effect on the biosphere, and hence again α , is, at the moment, a book of seven seals, needing intensive further investigation.

A first attempt to overcome these difficulties is present in First Order Models. In these, surface temperature T is permitted to vary with latitude θ , or one may imagine, if one prefers, that T is mean azimuthal temperature at latitude θ . Heat transport is introduced, and the governing equation has the general form

$$\mathcal{D} + \mathcal{I} = \frac{Q}{4}(1-\alpha) = q(1-\alpha)$$

where now

$\mathcal{D}$ = transport mechanism

$\mathcal{I}$ = outgoing radiative flux as function of T

α = (mean) albedo of earth at latitude θ as function of θ and T.

Various modellings of $\mathcal{I}$, $\mathcal{D}$, and α are possible. The simplest parametrization of $1 - \alpha$ is as follows: (It is convenient to introduce the variable $x = \sin\ \theta$, in place of θ .)

$$1 - \alpha = Z(x) \cdot \begin{cases} 0.7 \text{ if } T > -10°C \\ 0.4 \text{ if } T < -10°C \end{cases}$$

Digitized by Google

where $Z(x)$ is a correction for zenith angle, 0.7 is the co-albedo of land-sea, 0.4 that of ice-snow. In this way, ice albedo feedback is incorporated into the model.

Better modellings would take account of land-sea mix at given latitude, have smoother transition of albedo from ice to non-ice, worry about cloudiness, etc., but the above is adequate to reveal the general features of these models.

The radiative flux I may be modeled by permitting Eq. (1) to hold locally; thus

$$I = \sigma T_e^4 = \frac{\sigma}{1 + .75\tau} T^4$$

where τ can now be adjusted for CO_2 concentration.

It is convenient, but not essential, to modify I by linearizing about Celsium zero, to get $I = A + BT$, with T now in degrees Celsius. It appears, in practice, that A and B are then retrospectively adjusted to better fit current climate data, thus incorporating current cloudiness, for example. The effects of such a procedure should be obvious to the reader.

At the same time, there are large, and rather serious discrepancies in the literature concerning the magnitude of B, which significantly affect the sensitivity of the model to changes in the solar constant.

Digitized by Google

We owe the first consideration of first order energy budget models to Budyko and Sellers, independently. Subsequent work has been, in the main, variants of the schemes they contrived.

Budyko's choice of D was:

$$\mathcal{D} = \gamma(T - \overline{T}) \ ,$$

$\overline{T}$ is the mean surface temperature, and γ a phenomenological constant to be adjusted later.

Sellers (and others) used diffusive transport

$$\mathcal{D} = -\frac{d}{dx}\left[D(1 - x^2)\frac{dT}{dx}\right]$$

where D is, according to who you are reading, a constant, a function of x , a function of x and T , or even a function of x , T and $\frac{dT}{dx}$.

Some writers have used a linear mix of Budyko and Sellers type transports.

For the purposes of our immediate discussion, we will take

$$\mathcal{D} = -D\frac{d}{dx}\left[(1-x^2)\frac{dT}{dx}\right] = -D \text{ div grad } T \ ,$$

where D is a phenomenological constant to be determined later.

Digitized by Google

The first order energy budget equation becomes

$$-D \frac{d}{dx}\left[(1-x^2) \frac{dT}{dx}\right] + A + BT = qZ(x) \cdot \begin{cases} 0.7 \text{ if } T > -10°C \\ 0.4 \text{ if } T < -10°C \end{cases} \qquad (2)$$

Equation (2) includes Eq. (1) from two points of view, so we may expect Eq. (2) to give reasonable mean surface temperatures. On the one hand as D gets large (more energetic diffusion), T gets more nearly constant and Eq. (2) becomes a version of Eq. (1). On the other hand, if Eq. (2) is integrated from -1 to $+1$, the diffusive term vanishes, and what remains is a version of Eq. (1).

Equation (2) is not a bad differential equation except for the driving term, which is a function of both the independent and dependent variable. It is usually solved as follows. Assume T is a decreasing function of x for $0 \leq x \leq 1$, and even. Postulate x_i, $0 \leq x_i \leq 1$, the position of the northern ice line where $T(x_i) = -10$. Now the differential equation is an ordinary inhomogeneous one, requiring no boundary conditions, which can be solved by variation of parameters, or eigenfunction expansions.

With the solution obtained, Q and D must be adjusted so that $T(x_i) = -10$, and monotonicity and evenness verified.

If one supposes that for current climate, $x_i = 0.95$, and $q = \frac{Q}{4} = 340$, D is determined uniquely. With D so determined, and q still fixed at 340, one finds three positions altogether of the ice line meeting the

Digitized by Google

assumed requirements of evenness and monotonicity of $T(x)$, to wit: the normal, a heavily glaciated, and all ice. The heavily glaciated is not stable.

With D fixed by the current climate, one may also investigate the effect of changes in S . A decrease of Q on the order of 2 to 3% is enough to give only an ice covered earth as solution, still on the assumption of evenness and monotonicity of $T(x)$.

The results quoted above are mainly extracts from North[8,9], though they are in general accord with the results of others[1,2,4]. An outstanding exception occurs in Ref. 6, where a different determination of the constant B in the radiative mechanism I leads to strikingly distinct conclusions.

There is one consideration on the methodology above which we feel is important to further consideration of such models. It concerns the role of the constant D , which is determined by matching current climate. It would be particularly desirable to give an a-priori estimate of D , or at least to present a persuasive argument that D is indeed constant over a reasonable range of the other parameters present. Otherwise, any predictions from the model of climatic response to change of the other parameters are highly suspect.

This remark applies, mutus mutandi, to phenomenological constants in any model.

Digitized by Google

We have some further comments on the hidden or implicit assumptions in the procedure for solving Eq. (2). There is the assumption of evenness of $T(t)$, (i.e., symmetry about the equator), as well as the assumption that T falls as one moves from equator to pole. There is nothing in the differential Eq. (2) requiring these assumptions, and as soon as one foregoes them, some interesting and provocative possibilities emerge.

Let us for the moment assume that T rises in passing from equator to pole, but is an even function. One may, as before, solve the differential equation and hope the solution fits our assumptions. With some limited computer work, we found one such solution with the same D as for current climate, with the ice line at 30° latitude, but with a solar constant of 1680. This kind of solution, which we choose to call an anti-climate, seemed at first glance to be merely an aberrant, of no particular physical meaning or significance. Subsequently, it was discovered, however, that during the Permian era there was extensive glaciation in equatorial regions, but none in Antarctica, and anti-climates took on somewhat greater significance. Our geologic knowledge of Permian glaciation is, unfortunately, confounded by uncertainty as to the location of the continents. But aside from their possible relevance for ancient climates, we believe there is a variety of other anti-climates, though we must confess that our limited computer effort has not to date found any with the current solar constant and acceptable values of D. The computation to date does suggest, however, that there are many ice-band solutions, or ice-striped earths, in which one has a band of ice followed by a band of ice-free surface, etc.

Digitized by Google

There are, almost certainly, solutions of the differential equation not symmetric about the equator. These may find their physical realization in ice-age conditions, when the southern ice line remained in place, while the northern moved equatorward.

It is conceivable that better understanding of First Order Models may be attained by trying to match well-documented ancient climates.

We have not investigated stability of any of the bizarre climates alluded to above. We might add, however, that the possibility of bifurcation of the ice line does raise a question about the extant stability analysis of conventional climates.

One of the most surprising features of First Order Models is how well they match current temperature profiles with such naive modelling of transport, radiation, and incoming energy. See, for example, the JASON Climate Model data elsewhere in this report. While this is a very pleasing development from one point of view, it is quite unfortunate from another. What it means, of course, is that only marginal evidence will be available for the correctness of more sophisticated modelling of the important mechanisms. Bad further modelling may, nevertheless, reveal its nature very readily.

We will address the question of testing more sophisticated effects in First Order Models presently. For the moment, we want to comment on the level of modelling incorporated in, say, Eq. (2). The I-R radiative

Digitized by Google

flux I should be nailed down as much as possible, and the constants A and B determined with greater precision. The modelling of the albedo can probably be improved; and we want to emphasize that, which is generally conceded by researchers, the effects of cloudiness must be assessed and incorporated into both the albedo and radiative flux. Since the relation between cloudiness and ground tempearture is unknown, speculations and investigations on the nature of cloudiness may, when incorporated into these models, produce feedback mechanisms with dramatic effects, or with very stabilizing effects.

A word or two about the transport mechanism is in order. One of the more interesting features of these models is how little they appear to depend on the choice of transport mechanism. This is probably partly due to the freedom in choosing phenomenological constants, but if really so, should be explained on a-priori grounds. If the affirmative argument cannot be adduced, then efforts should be made to separate the distinct transport mechanisms on the basis of more sophisticated modelling, or any other reasonable tests.

Finally, we want to indicate where we think these other tests may come from. Clearly, what is needed is data on other experiments which nature has performed for us. An obvious possibility, already mentioned, is the well-documented ancient climates. A richer source, probably, will come from examining seasonal and diurnal variations. A time dependent first order model will take the form

Digitized by Google

$$C \frac{\partial T}{\partial t} + \mathcal{D} + \mathcal{I} = q(1 - \alpha)$$

where C is an unknown heat capacity. An estimate of C may be obtained by simply looking at a time dependent zero'th order model

$$C \frac{d\overline{T}}{dt} + A + B\overline{T} = q(1 - \overline{\alpha})$$

at a seasonal level, where $\overline{T}$ is mean temperature in the Northern hemisphere, as a function of time of year, and q and $\overline{\alpha}$ are known periodic functions of time of year. For each choice of C, the unique periodic solution may be compared with known seasonal temperature data in the Northern hemisphere to arrive at an optimal selection of C.

The constant C so determined may then be utilized in a time dependent first order model:

$$C \frac{\partial T}{\partial t} + \mathcal{I} + \mathcal{D} = q(1 - \alpha)$$

to be analyzed first at the level of seasonal variation. The right hand driving terms would be parametrized as known functions of x, t, and the unknown periodic $x_i(t)$. It is easy to imagine iterative processes converging to the correct solution. One could, for example, postulate $x_i(t)$ as constant, solve the differential equation, use the solution to get another version of ice-line as function of time, and iterate.

Digitized by Google

In order to get realistic results, it may be necessary to build lapse times for melting of ice and freezing of water into this model. In general, it is quite difficult to see the consequences of pursuing this area of research, yet it is easy to see that it might be extraordinarily fertile.

As a next step in a research program, it would be useful to explore time dependent first order models at the level of diurnal variation.

Beyond this lie second order models with a two-dimensional earth, and third order with an atmosphere. At the end of the line we have the G.C.M.s.

B. JASON Climate Model

To assess in a quantitative fashion the effects on climate of increasing the CO_2 concentration we have constructed and analyzed an energy balance climate model of the kind described in the previous section. The ingredients in an energy balance model are specifications of

1) Incoming solar radiation and absorption by land and water: Insolation
2) Outgoing radiation by the earth and by the atmosphere
3) Transport of energy poleward by the ocean currents, by latent heat and by sensible heat.

Digitized by Google

More precisely we write

$$C \frac{\partial T}{\partial t} = \text{Insolation} - \text{Outward Radiation} - \text{Transport}$$

where C is some "heat capacity" which sets the time scale for the response of the temperature T to changes in any of the quantities on the right hand side of this equation. In principle, C can be a function of longitude, latitude and even time.

Let us look at the three basic energy quantities listed above:

1. <u>Insolation</u>

This is the easiest and in many ways the most well established of the ingredients in our climate stew. The form of insolation is

$$\frac{Q}{4} Z(x) a(x, x_c) \tag{4}$$

where Q is the solar constant

$$Q \approx 1380 \text{ watts/m}^2$$

and $Z(x)$ is a zenith angle factor giving the mean annual distribution of insolation over latitude. x is the sine of the latitude and

$$\begin{aligned} Z(x) &= 1 - 0.482 P_2(x) \\ &= 1 - \frac{1}{2} P_2(x) \end{aligned} \tag{5}$$

Digitized by Google

with $P_2(x) = \frac{1}{2}(3x^2 - 1)$, the second order Legendre polynomial. The factor $a(x,x_c)$ represents the absorption of the solar radiation by land sea and ice. We will use the idea of Budyko (1969) that $a(x,x_c)$ varies with x for $x \leq x_c$ at which latitude the hemisphere is permanently ice covered and $a(x,x_c)$ $x \geq x_c$ is a constant. Actual values for $a(x,x_c)$ are not precisely agreed upon by all workers, but we adopted the following values from North (1975b):

$$x_c = 0.95 \quad , \quad \text{Latitude} = 71.8° \quad ;$$

for $x > x_c$

$$a(x,x_c) = 0.38 \quad , \quad \text{albedo} = 0.62 \tag{6}$$

for $x < x_c$

$$a(x,x_c) = 0.697 - 0.0779P_2(x) \tag{7}$$

which gives an average albedo of ≈ 0.3 including land, water, and ice.

Two comments are in order here: (1) we use zonally averaged quantities so that azimuthal or longitudinal dependence is washed out. This is an important simplification of the real two dimensional geometry of the earth's surface. However, following the orginators of energy balance models we are convinced it is an adequate starting point.

Digitized by Google

(2) The particular values represented in Eqs. (5), (6) and (7) are, of course, important, but variations over small domains are unlikely to significantly affect our discussion or conclusions.

2. Outgoing Radiation

We desire a representation of the infrared radiation escaping the earth at each latitude as a function of the ground temperature. There appears to be agreement among workers that a linearized formula

$$\text{Radiation} = A_R + B_R T(x) \tag{8}$$

is quite adequate. The coefficients A_R and B_R are, of course, independent of $T(x)$ but may depend on cloudiness and other climatological features. Cess (1976) has reviewed the situation and his results derived from satellite observation are presented in Tables IV-1 and IV-2 where A_c is the cloud cover fraction.

Table IV-1

SUMMARY OF ZONAL ANNUAL CLIMATOLOGICAL DATA FOR THE NORTHERN HEMISPHERE
The Units of F are W m^{-2}

Latitude (°N)	T_s (°C)	A_c	F Observed	F Eq. (8)	Error (%)
5	26.3	0.51	250	252	0.8
15	26.3	0.44	257	259	0.8
25	23.2	0.41	259	256	-1.2
35	15.9	0.47	241	239	-0.8
45	8.4	0.57	220	218	-0.9
55	2.2	0.64	204	202	-1.0
65	- 5.5	0.64	191	190	-0.5
75	-12.7	0.61	181	182	0.6
85	-18.0	0.55	179	179	0
Average	15.0	0.51	233	234	0.4

Digitized by Google

Table IV-2

SUMMARY OF ZONAL ANNUAL CLIMATOLOGICAL DATA FOR THE SOUTHERN HEMISPHERE
The Units of F are W m^{-2}

Latitude (°S)	T_s (°C)	A_c	F Observed	F Eq. (8)	Error (%)
5	26.2	0.50	257	263	2.3
15	24.6	0.47	266	263	-1.1
25	21.4	0.47	262	258	-1.5
35	16.6	0.54	243	245	0.8
45	9.7	0.65	224	225	0.5
55	2.8	0.79	206	202	-1.9
65	-6.0	0.77	188	190	1.1
75	-33.0	0.56	163	164	0.6
85	-43.8	0.47	154	154	0
Average	13.4	0.57	236	237	0.4

Using his values of average cloud cover we find for the Northern Hemisphere A_R = 210.59 watts/m^2 and B_R = 1.57 watts/m^2-°C while for the Southern Hemisphere A_R = 215.83 watts/m^2 and B_R = 1.59 watts/m^2-°C . In our actual calculations we adopted the values of North (1978) of A_R = 211.2 watts/m^2 and B_R = 1.55 watts/m^2-°C .

Now as discussed above, the variation of A_R and B_R with CO_2 concentration or the concentration of any atmospheric constituent is given by

$$A_R = \alpha / \left(1 + \frac{3}{4} \tau_g\right) \qquad (9)$$

Digitized by Google

and

$$B_R = \beta / \left(1 + \frac{3}{4} \tau_g\right) \tag{10}$$

with τ_g the net opacity at the ground and α and β some constants. By using the relation between ground temperature, T, and the skin temperature T_e needed to radiate back the net insolation

$$T = \left(1 + \frac{3}{4} \tau_g\right)^{1/4} T_e \tag{11}$$

we determine that $\tau_g \approx 3/4$ for $T_e = 257°K$ and $T = 288°K$ - the global average temperature.

As the opacity of the atmosphere to the infrared radiation entering in Eq. (8) increases, the radiation coefficients A_R and B_R will decrease and the average global temperature must increase. To get a feeling for this note that if we are in a steady state and integrate the energy balance equation over the globe it reads

Infrared Radiation Out = Insolation

As we change CO_2 concentration, say, the net insolation is more or less constant (it is constant in our simple models if the ice line at x_c doesn't change) so $A_R + B_R \langle T \rangle$ is constant. $\langle T \rangle$ is the global average temperature. Using the rules from Eqs. (9 and 10) we find, on the basis of the radiative transport theory presented before, that doubling the CO_2

Digitized by Google

concentration from today's value of 332 ppm would result in a change in global average temperature of

$$\left\langle T_{\text{Doubled } CO_2} \right\rangle - \left\langle T_{\text{Today}} \right\rangle = +2.4\ ^\circ C \tag{12}$$

This is a number consistent with a wide variety of other models, simple and complicated, and emerges because global energy balance really does represent the basic gross structure of our planetary temperature. Precisely how this energy is transported about the globe does not affect in a dramatic fashion these global averages. Details of any climate model, including the one we are discussing here, will differ in how this 2°-3°C change is distributed over the globe.

3. Energy Transport

Variations of temperature over space and time are governed by energy transport mechanisms. We restrict ourselves in our models to transport in the latitudinal directions only; so, to repeat, we have averaged over longitude. The heat flux from the equatorial region toward the pole comes in three main forms: ocean currents, latent heat, and sensible heat. Figure IV-1 shows these fluxes as recorded by Sellers (1965), Chapter 8.

Following the ideas expressed by Stone (1973) with a somewhat different emphasis we have chosen to view this figure as representing several varieties of heat transport cells. For example, suppose we consider the net heat flux R_g shown in Figure IV-1. It vanishes at

Digitized by Google

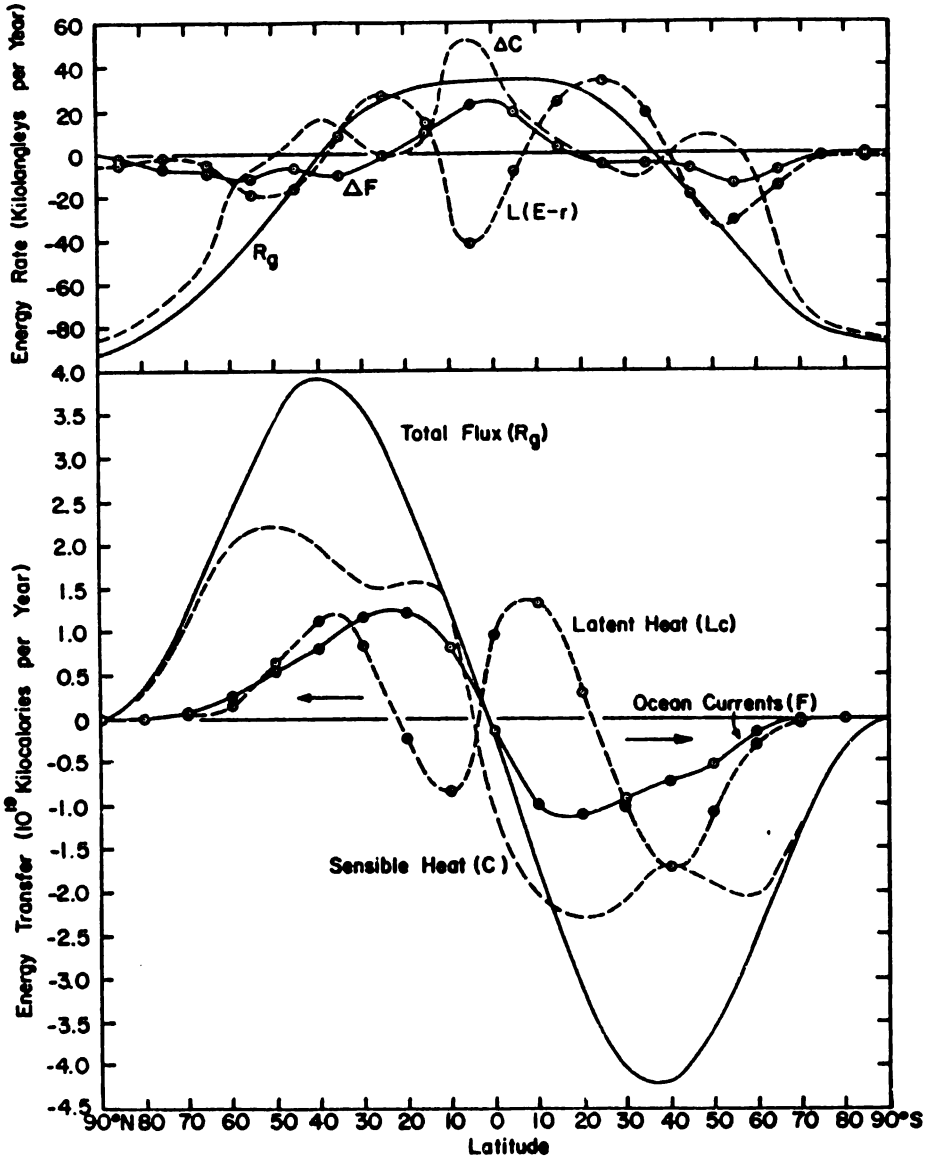

Figure IV-1

THE AVERAGE ANNUAL LATITUDINAL DISTRIBUTION OF THE COMPONENTS OF THE ENERGY BALANCE OF THE EARTH-ATMOSPHERE SYSTEM IN KLY YEAR^{-1} (top) AND OF THE COMPONENTS OF THE POLEWARD ENERGY FLUX IN 10^{19} KCAL YEAR^{-1} (bottom)

Digitized by Google

$x = 0$ and $x = 1$ and peaks around $x \approx 0.6$. We can parametrize this by imagining a net heat flow which is

$$- K \frac{d}{dx}\left[x(1 - x) \frac{dT}{dx}\right] \tag{13}$$

where K is an "eddy diffusion constant" and the heat flux $-Kx(1 - x)dT/dx$ vanishes at $x = 0$ and $x = 1$ while peaking at $x \sim 0.6$ when dT/dx behaves as $\approx x^{3/4}$. Really this is a representation of the actual heat flow by a lumped diffusion law with one overall constant K which sets the scale of the flow.

If one wanted to make a finer kind of cellular structure, it is easy to imagine constructing several cells corresponding to latent heat alone or ocean currents alone, etc. For example, consider ocean currents. The sea surface temperature, call it T_o , is different from the ground temperature T we have been considering heretofore. The heat flow due to ocean currents in the Northern Hemisphere is poleward from the equator to about $x = 0.94$. One could try a representation of the ocean currents as

$$-K_o \frac{d}{dx}\left[x(0.94 - x) \frac{dT_o}{dx}\right] \tag{14}$$

with K_o another "eddy diffusion constant" setting the scale for the kind of heat transport being considered--here ocean currents.

Digitized by Google

For latent heat in the Northern Hemisphere we would assign an effective temperature $T_L(x)$ to each latitude. Next note that the latent heat flow is negative for $0 \leq x \leq 0.37$ with a peak at $x \approx 0.17$ and positive for $0.37 \leq x \leq 0.94$ peaking at $x \approx 0.59$. For this flux we would write

$$-K_{1L} \frac{d}{dx}\left[(0.94 - x)(x - 0.37)\frac{dT_L}{dx}\right] + K_{2L} \frac{d}{dx}\left[x(0.37 - x)\frac{dT_L}{dx}\right] , \quad (15)$$

with the "eddy diffusion constants" $K_{iL} > 0$, $i = 1,2$. A rule relating or coupling T_o, T_L and T would have to be constructed to complete this scheme.

The general zone lying between $\alpha \leq x \leq \beta$ has the flux

$$-K \frac{d}{dx}\left[(\beta - x)(x - \alpha)\frac{dT}{dx}\right] . \quad (16)$$

Here we will take one heat transport cell for each hemisphere and one diffusion constant K for each hemisphere.

The climate model we have arrived at for the Northern Hemisphere, say, is

$$C \frac{\partial T}{\partial t} - K \frac{\partial}{\partial x}\left[x(1-x)\frac{\partial T}{\partial x}\right] + A_R + B_R T(x,t) = \frac{Q}{4} Z(x)a(x,x_c) . \quad (17)$$

Digitized by Google

We will refer to this and its generalizations as JASON Climate Models (JCM).

Our first concern is with the allowed steady state versions of (14):

$$-K \frac{d}{dx}\left[x(1 - x)\frac{dT}{dx}\right] + A_R + B_R T(x) = \frac{Q}{4} z(x)a(x,x_c) \quad . \tag{18}$$

In this set $z = 1 - 2x$ which turns (18) into

$$\frac{d}{dz}\left[(1 - z^2)\frac{dT}{dz}\right] + \sigma(\sigma + 1)T(z) = -\frac{1}{K}\left[\frac{Q}{4} z(x)a(z,z_c) - A\right] = -S(z) \tag{19}$$

with

$$\sigma(\sigma + 1) = -B_R/K \tag{20}$$

or

$$\sigma = -\frac{1}{2} + i\sqrt{\frac{B_R}{K} - \frac{1}{4}} \tag{21}$$

This is the Legendre equation. $\{$A heat transport cell with flux given by (16) becomes Legendre's equation with $z = [(\alpha + \beta) - 2x]/(\beta - \alpha)\}$. The solution to (19) is

$$T(z) = P_\sigma(z) \int_{-1}^{z} dw\, Q_\sigma(w)S(w)$$

$$+ Q_\sigma(z) \int_{z}^{1} dw P_\sigma(w)S(w) + \xi P_\sigma(z) + \eta Q_\sigma(z) \quad , \tag{22}$$

Digitized by Google

where $P_\sigma(z)$ and $Q_\sigma(z)$ are the usual and second kind of Legendre function of index σ. ξ and η are integration constants. The function $Q_\sigma(z)$ is logarithmically singular at $z = \pm 1$ as is $P_\sigma(z)$ at $z = -1$. We must choose ξ and η so the temperature $T(z)$ is finite for all z. Finiteness at $z = 1$ requires $\eta = 0$, while at $z = -1$ it is satisfied only when

$$\xi = -\frac{\pi \cot \sigma\pi}{2} \int_{-1}^{1} dw S(w) P_\sigma(w) \quad . \tag{23}$$

To derive these results we need

$$Q_\sigma(z) = \frac{\pi}{2 \sin \sigma\pi} \left[P_\sigma(z) \cos \sigma\pi - P_\sigma(-z) \right] \tag{24}$$

for z along the real axis between -1 and 1. The result for $T(z)$ is finally

$$T(z) = -\frac{\pi}{2 \sin \pi\sigma} \left\{ P_\sigma(z) \int_{-1}^{z} dw S(w) P_\sigma(-w) \right.$$

$$\left. + P_\sigma(-z) \int_{z}^{1} dw S(w) P_\sigma(w) \right\} \quad . \tag{25}$$

The solution for $T(z)$ inside any heat transport cell has just this form with the $\sigma = -1/2 + i\sqrt{B_R/K_i - 1}$ and K_i the transport coefficient for that cell and $z = (\alpha + \beta - 2x)/(\beta - \alpha)$ in that cell.

Digitized by Google

It is important to note that we need require no conditions on $T(z)$ or its derivatives except finiteness of $T(z)$ throughout each cell. The "boundary conditions" discussed by North (1975a,b) and others are unnecessary.

To determine K, the eddy diffusion coefficient in the JCM, we proceed by setting Q, A_R, B_R and $z_c = 1 - 2x_c$ to their present day values given above. Then K is varied until $T(z_c)$ achieves a definite value, conventionally chosen to be -10°C. This yields a $K = 1.37$ watts/m^2-°C. This diffusion coefficient is much larger than the value 0.59 watts/m^2 °C found by North (1975b, 1978) when he considered a single heat transport cell running from pole to pole. Our heat flux proportional to $x(1 - x)$ is quite inhibited in transporting heat near the equator, while North's transport is proportional to $1 - x^2$ which is still sizeable near $x = 0$. It is natural to expect the transport coefficient here to be larger since it is from the equatorial region that heat must be pumped.

Once we have K such that $T(z_c) = -10°C$ we may calculate $T(z)$ for today's climate. This is given in Figure IV-2.

This should be compared to the data recorded in Cess (1976) for both the Northern and Southern hemispheres (Figure IV-3). The JCM gives temperatures too low in midlatitudes, but rather reasonable at high and low latitudes. An effect like this should be expected from our discussion of the structure of heat transport cells in the actual earth-atmosphere-ocean system. Because of the zeroes in latent heat transport

Digitized by Google

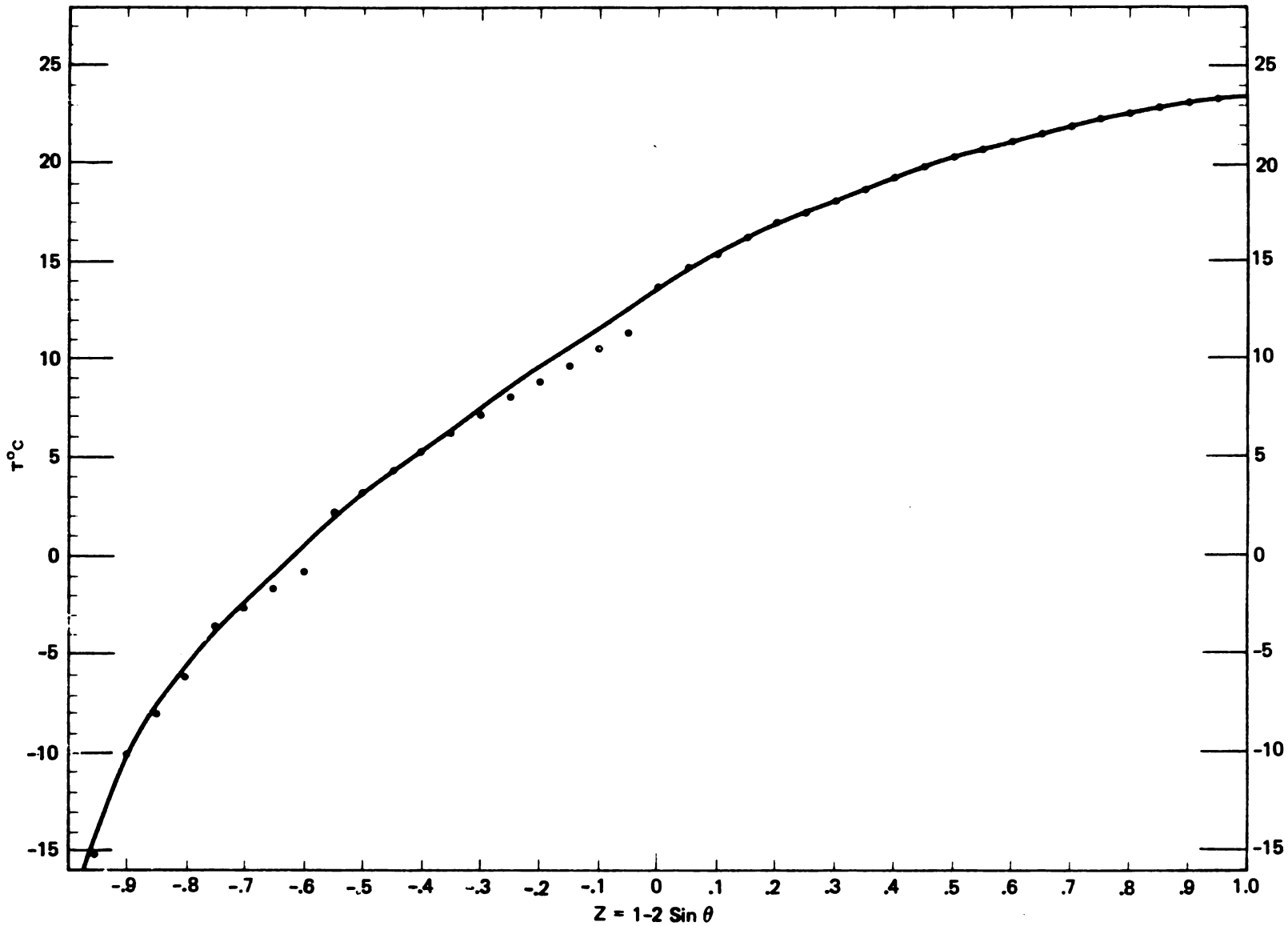

Figure IV-2

PREDICTION OF THE JASON MODEL FOR VARIANCE IN TEMPERATURE WITH LATITUDE (o) AND A CO_2 CONCENTRATION OF 332 ppm

Today's Climate

$1 = 211.2 + 1.55\,T$ $\quad f_{co_2} = 332$ ppm $\quad K = 1.37\ W/m^{2o}C$ $\quad Z_o = 0.9$

Digitized by Google

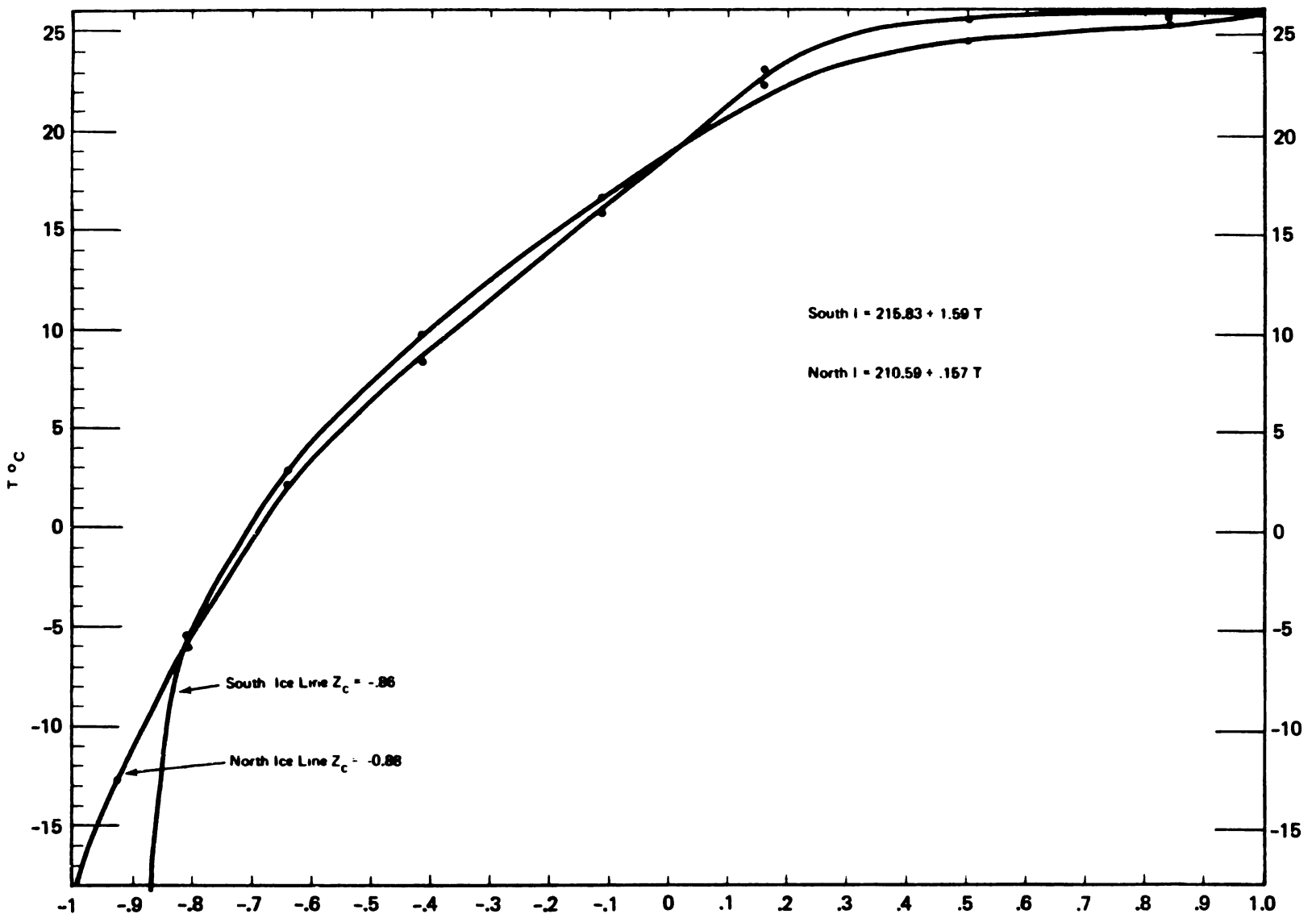

Figure IV-3

OBSERVATION DATA TAKEN FROM CESS (1976) FOR NORTHERN & SOUTHERN HEMISPHERES (0 is the latitude)

Digitized by Google

and dips in sensible heat transport in midlatitudes, less heat, in fact, is transported out of those latitudes than the simplest JCM would indicate. So a many celled JCM will push up the mid-latitude temperature as desired.

The response of the JCM to changes in CO_2 concentration is examined by changing A_R and B_R according to (9) and (10). Using the results from earlier sections, we find a doubling of CO_2 in the atmosphere to 664 ppm will lead to values of $A_R = 207.7$ watts/m^2 and $B_R = 1.524$ watts/m^2-°C . Since we have fixed our eddy diffusion parameter K , we adjust z_c so $T(z_c) = 10°C$. We find that $z_c = -1$ for this A_R and B_R , which means the ice line has retreated to the pole (see Figure IV-4). So a doubling of CO_2 concentration according to the one heat transport cell/hemisphere JCM is likely to cause the ice caps to melt.

The rate of increase of CO_2 concentration has been 4.3%/yr of the industrial contribution. Taking 285 ppm as the preindustrial level we see that the fraction of CO_2 in ppm increases as

$$f_{CO_2} = 285 \text{ ppm} + (1.043)^N \cdot 47 \text{ ppm} \quad ; \qquad (26)$$

N is in years from today. So a doubling of CO_2 to 664 ppm should occur as soon as 50 years hence. If the ice line instantaneously follows the $T = 10°C$ line as is assumed in energy-balance models, the ice line should retreat and disappear as CO_2 doubles.

Digitized by Google

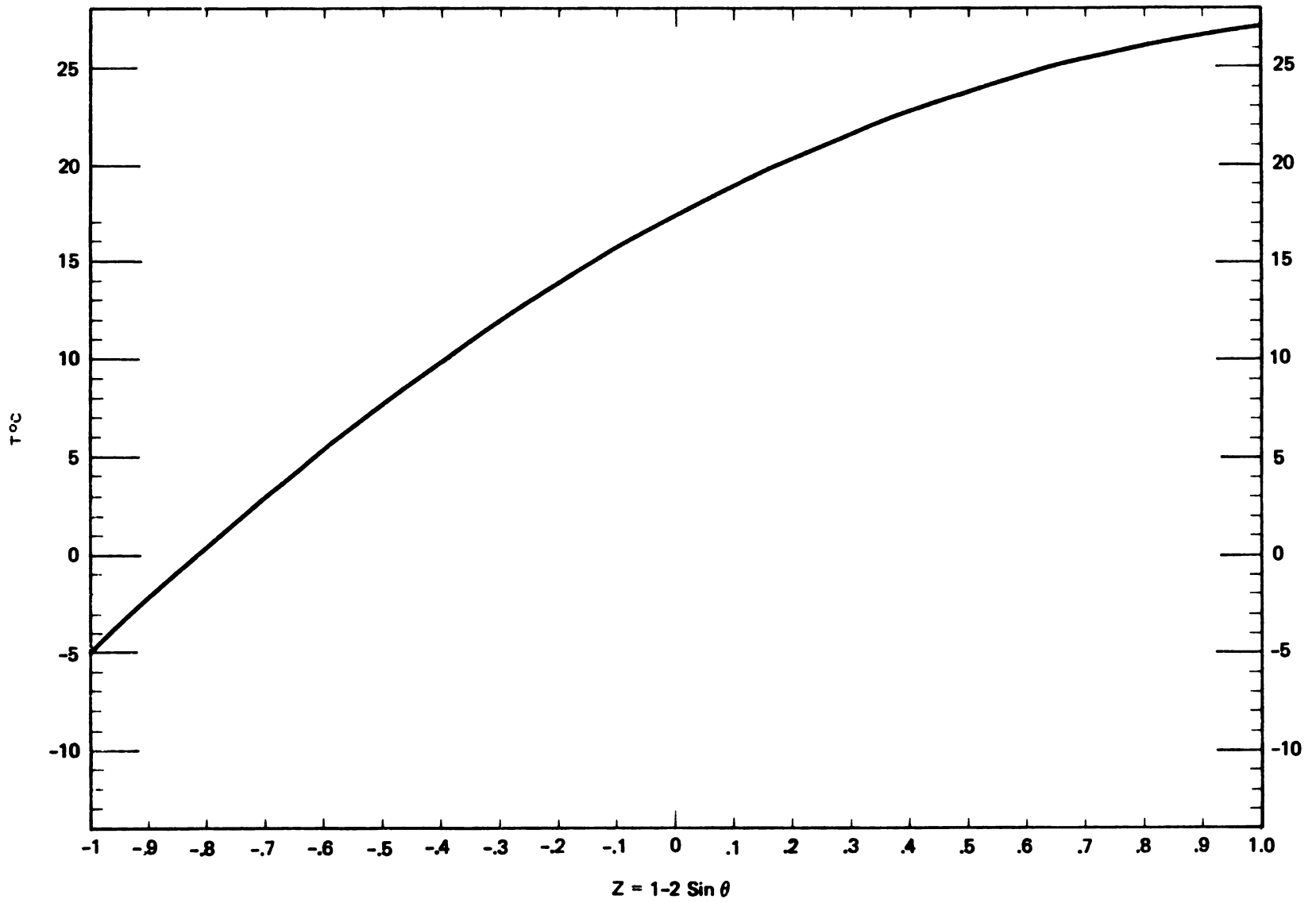

Figure IV-4

PREDICTION OF THE JASON MODEL FOR VARIANCE IN TEMPERATURE WITH LATITUDE (0), AND ASSUMING A DOUBLING OF THE CO_2 CONCENTRATION FOR PRESENT LEVELS

$Z_c = -1.0$ $f_{CO_2} = 664$ ppm 50 yrs hence at 4.3%

$1 = 207.7 + 1.524\ T$ $K = 1.37\ W/m^{2\,o}C$

Digitized by Google

Comparing Figures IV-2 and IV-4 we see that the average rise in T is slightly more than the 2.4°C evaluated from the conservation of $AR + B_R T$. This is clearly because of the retreat of the ice line, and this is emphasized by the large rise in T in the polar region.

These results are the essence of our analysis of the JCM. We have not explored to any extent questions such as the variation of the ice line as the solar constant varies or the sensitivity to the values of A_R, B_R, albedo, x_c, or the assumption that $T(x_c) = -10°C$. These are interesting issues and important for one's confidence in the general scheme represented by the JCM. We feel it is rather clear that our heat transport cell description of heat flow in the earth-ocean-atmosphere system promises a realistic version of the actual complicated processes involved yet within the attractive simplicity of the energy balance models.

An important issue we have not yet been able to explore in depth concerns the time dependence of the JCM. The problem is to study the solutions of Eq. (17) when A_R, B_R, x_c and possibly Q depend on time. This is important since the stability of the time independent or equilibrium states explored above is governed by the time dependent solutions.

In (17) introduce $\theta(x,t)$ as

Digitized by Google

$$T(x,t) = \exp\left[-\frac{1}{C}\int_0^t du B_R(u)\right]\theta(x,t) \quad , \tag{27}$$

so $\theta(x,t)$ satisfies

$$C\frac{\partial\theta}{\partial t} - K\frac{\partial}{\partial x}\left[x(1-x)\frac{\partial\theta}{\partial t}\right] = \left[\frac{Q}{4}Z(x)a(x,x_c(t)) - A_R(t)\right]$$

$$\times \exp\frac{1}{C}\int_0^t du B_R(u) \equiv S(x,t) \ . \tag{28}$$

Now go over to the Laplace transform of θ

$$\tau_p(x) = \int_0^\infty dt e^{-pt}\theta(x,t) \tag{29}$$

which satisfies

$$-K\frac{d}{dx}\left[x(1-x)\frac{d\tau_p}{dx}\right] + Cp\tau_p(x) = S_p(x) - T(x,o) \quad , \tag{30}$$

where

$$S_p(x) = \int_0^\infty dt e^{-pt}S(x,t) \quad , \tag{31}$$

Digitized by Google

and we have noted $T(x,o) = \theta(x,o)$.

This equation is precisely of the form studied above:

$$\frac{d}{dx}\left[x(1-x)\frac{d\tau_p(x)}{dx}\right] + \eta(\eta+1)\tau_p(x) = -S_p(x) \tag{32}$$

with

$$\eta = -\frac{1}{2} + i\sqrt{c_p - \frac{1}{4}}$$

and

$$S_p(x) = [S_p(x) - T(x,o)]/K \quad . \tag{33}$$

So we know the solution, finite at $z = \pm 1$, to be $(z = 1 - 2x)$

$$\tau_p(z) = -\frac{\pi}{2\sin\pi\eta}\left\{P_\eta(z)\int_{-1}^{z} dw S_p(w)P_\eta(-w)\right.$$

$$\left. + P_\eta(-z)\int_{z}^{1} dw S_p(w)P_\eta(w)\right\} \quad . \tag{34}$$

The temperature $T(x,t)$ is recovered from

$$T(x,t) = \exp\left[\frac{1}{C}\int_0^t du B_R(u)\right]\left(\int_{\alpha-i\infty}^{\alpha+i\infty} \frac{dp}{2\pi i} e^{pt}\tau_p(z)\right) \tag{35}$$

Digitized by Google

where $\mathrm{Re}\alpha > 0$. This is the usual Laplace inversion formula and emphasizes the point that the analytic structure of $\tau_p(x)$ in the p plane governs the stability of solutions to the JCM. Now what is attractive about this result is that given the temperature distribution at $t = 0$, $T(x,o)$, the subsequent development of $T(x,t)$ is governed by solutions to the same differential equation as the static JCM with the response dictated by the value of C .

Furthermore the very important question of <u>seasonal variations</u> and their effect on accumulations of ice cover or cumulative effects on climate modification can now be explored. Seasonal variations are known for many of the ingredients to our model. North (1978) notes that the albedo factor entering $z(x,x_c)$ has a variation

$$\alpha(x,t) = 0.319 + P_1(x)\left[0.071 \cos 2\pi t/t_o + 0.055 \sin 2\pi t/t_o\right] + 0.202P_2(x) \quad , \tag{36}$$

with $P_1(x) = x$ and $t_o = 1$ year. Also the zenith angle factor entering the insolation behaves as

$$Z(x,t) = 1 - 0.796 \cos 2\pi t/t_o P_1(x) - 0.477P_2(x) \quad . \tag{37}$$

These ingredients can be straightforwardly folded into the time dependent JCM which may include as well a time dependence for the radiation parameters A_R and B_R resulting from CO_2 effects. The time scale of A_R

Digitized by Google

and B_R variations will be slow compared to $t_o/2\pi \approx 1$ month , so as a first approximation they could be taken constant. Detailed exploration of all this has yet to be carried out.

One last note about $T(x,t)$ in these models. The determination of $z_c(t)$ must be done in a self-consistent fashion by looking at

$$T(z_c(t),t) = -10°C \tag{38}$$

Since $T(x,t)$ is a functional of $z_c(t)$, this is a non-linear recursive procedure which can in principle be carried out, though in practice it may be tedious.

C. Sensitivity of Climate Models

A normal procedure for assaying the degree of reality of a model in general and a climate model in particular is to test the sensitivity of the model to reasonable variations in its parametric makeup.

In the following we use the notation of the preceding sections and for convenience we adopt the simplest energy balance model, i.e. that of North where the heat transport is given by

$$-D \frac{\partial}{\partial x} (1-x^2) \frac{\partial T}{\partial x} \tag{39}$$

Digitized by Google

Purely for consistency we keep this value of D constant, but again for convenience, following North we treat the radiated energy I as the dependent variable with a correspondingly different D which will be allowed to vary.

In the expression for the absorbed solar heating

$$Q[1+S_2P_2(x)] \begin{cases} \bullet\ b_o & x > x_s \\ \bullet\ [a_o+a_2P_2(x)] & x < x_s \end{cases} \tag{40}$$

we hold the parameters Q , b_o , a_o , a_2 fixed.

Since our problem is the sensitivity of climate to variation in CO_2 of the atmosphere in the expression for the radiated energy

$$A + BT \tag{41}$$

A and B will be varied in accordance with the discussion on the effect of CO_2 on the radiant energy. This means that A and B will vary proportionately over a range of about 1% and D in the equation for I will vary inversely. Increases in A and B will therefore imply a colder earth.

Digitized by Google

We repeat the following initial values of the parameters:

A	211.2	watts/m^2
B	1.55	watts/m^2 deg C
D	0.382	
b_o	0.38	
a_o	0.697	
a_2	-0.0799	
x_2	0.95	

The ice line temperature remains -10°C. There will be a slight inconsistency. North's value of D, 0.382, is only approximately, but closely, computed from the constants. Our computation will be exact to the figures given.

The approach is to perturb the constants A, B, and D and find the new values of x_s, $\bar{T}$ (average T). and of course if needed, the new temperature profile. What emerges is an extraordinary sensitivity of the ice line to slight variations in A and B.

Digitized by Google

The table is an indication of this sensitivity.

Table IV-3

A/A_o	x_s	$\overline{T}$
1.02	0.80	5.45
1.01	0.87	9.82
1.00	0.935	13.81
0.9975	0.958	14.92
0.996	0.980	15.79

A/A_o of course is the fractional perturbation.

The point of special interest is that the current climate corresponds to a sin latitude = 0.95, very close to ice free. A very small perturbation, 0.5% in the effect of CO_2 on the radiated flux, will drive the climate to an ice free regime.

In the other direction the area of the ice zone moves rapidly southward.

Digitized by Google

The curves shown in Fig. IV-5 are sample plots of the temperature variation for sample cases. For comparison an ice free regime $A/A_o = 0.98$ is shown although the formal solution for this case ($x_s = 1$) is trivial, consisting as it does of the sum of terms with P_o, P_2, and P_4 of x as factors.*

A number of obvious and curious conclusions can be drawn from these results. Perhaps the most interesting and possibly fruitful one is relative to the stability of the constants A and B. If the model has any validity at all this would mean that the real climate behavior must depend heavily on some specific processes that damp the effect of excursions in energy radiation or lock in the values of A and B in some fashion.

---

* This is why the 2-mode model works as well as it does. The assumed ice-line, $\mu = .95$, represents a very small ice area: the exact solution for the ice-free situation is a good approximation to the "real case."

Digitized by Google

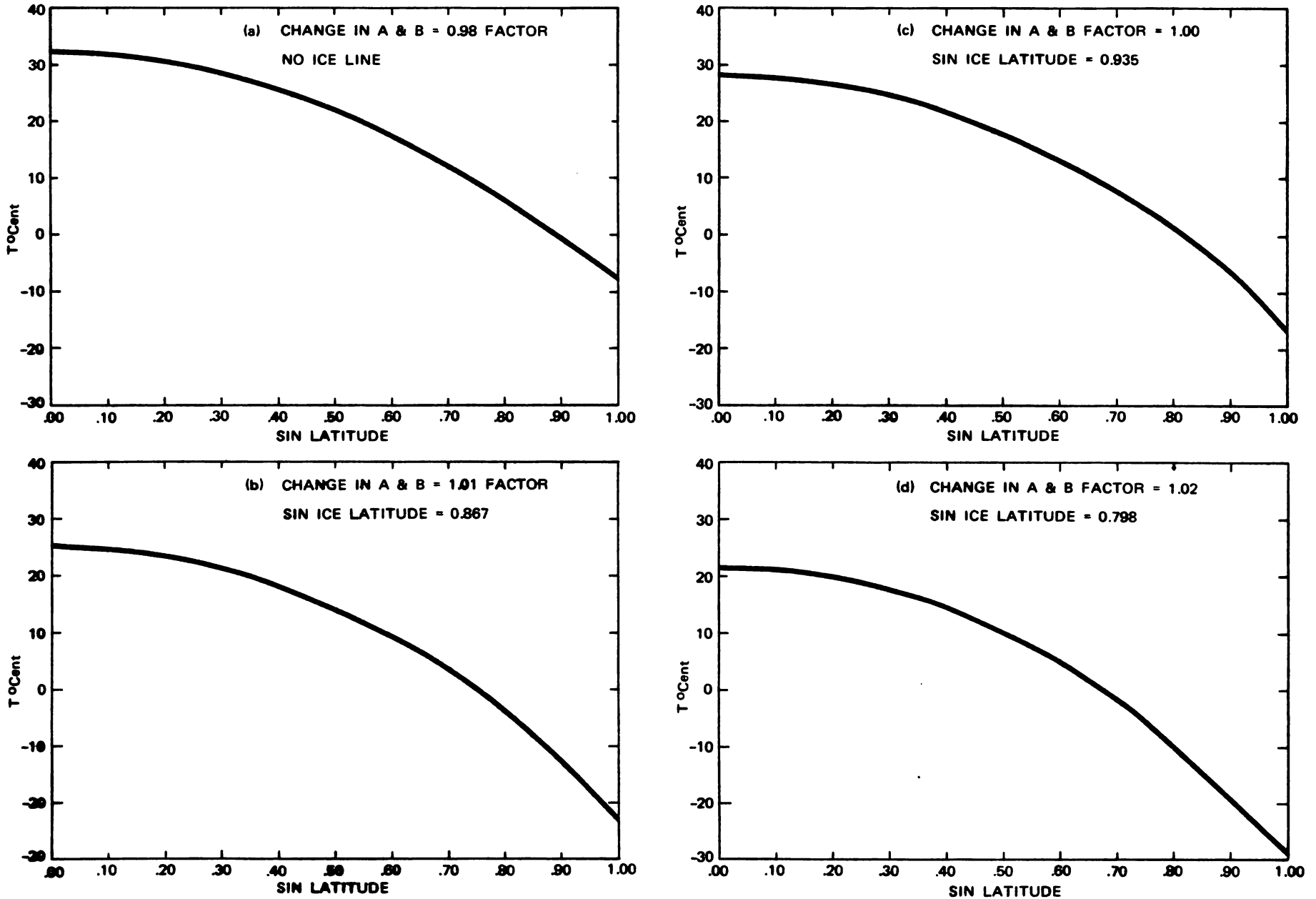

Figure IV-5

SAMPLE PLOTS OF TEMPERATURE VARIATION FOR SAMPLE CASES

Digitized by Google

D. Sensitivity of Energy Budget Models to Changes in Albedo

We briefly review the influence of such factors as albedo, infrared emissivity and cloud cover on climate. Although satellite data are now available there is some disagreement among various authors[16-18] on how the data are to be interpreted.

We first consider the arguments of Ref. 16, wherein ice-albedo feedback is ignored. Using the global energy balance equation

$$F = \frac{1}{4} S(1 - \alpha_p) \tag{42}$$

where F is the outward radiation flux, S the solar constant and αp the global albedo, we may write the "sensitivity parameter" $\beta = S\, dT_s/dS$ in the form

$$\beta = \frac{F}{\frac{dF}{dT_s} + \frac{S}{4}\frac{d\alpha_p}{dT_s}} \tag{43}$$

where T_s is the mean surface temperature.

We note that in the case of constant albedo, β depends entirely on the IR feedback, giving $\beta = 70°C$ for an IR emissivity of .6, $F = 233\ W/m^2$ and $T_s = 288°K$. The change of surface temperature due to a change in the solar constant of ΔS

$$\Delta T_s = \beta\frac{\Delta S}{S} \tag{44}$$

Digitized by Google

is in this case .7°C per 1% change in S (note for reference that $dF/dT_s = 3.3$) . Consideration of a more complete dynamics, with differing feedback properties, produces β values from 35° to 400° C.

The dependence of the infrared emissivity on surface temperature T_s and cloud cover fraction A_c has been parametrized by Budyko as

$$F = 223 + 2.2\ T_s - (47 + 1.6\ T_s)\ A_c \tag{45}$$

again with F in W/m^2 and T_s in °C.

The most sensitive climates ($\beta \approx 400°C$) were found by Budyko[19] and Sellers[20]; however, Ref. 18 claims that such sensitivity is greatly decreased if correct satellite data are used. All authors cited here use zonally averaged variables.

The planetary albedo is decomposed as

$$\alpha_p = \alpha_c A_c + \alpha_s (1-A_c) \tag{46}$$

where α_s is the clear sky albedo and α_c the cloud cover albedo. Nobody seems willing to predict the temperature dependence of A_c . Assuming that α_c and α_s are independent of T_s , β is

$$\beta = \frac{F}{\frac{\partial F}{\partial T_s} + \left[\frac{\partial F}{\partial A_c} + \frac{S}{4}(\alpha_c - \alpha_s)\right] \frac{dA_c}{dT_s}} \tag{47}$$

Digitized by Google

Cess[16] writes this as ($-\delta$ = [ ] in Eq. (47))

$$\beta = \frac{F}{\frac{\partial F}{\partial T_s} - \delta \frac{dA_c}{dT_s}} \tag{48}$$

and argues that except near the poles δ is sufficiently small (for subsequently deduced bounds on dA_c/dT_s) the cloud cover correction is very small. However, the value obtained by Cess for δ is small by virtue of cancellation between two large numbers. Using his fit ($F = 257 + 1.6\ T_3 - 91\ A_c$ for the northern hemisphere), along with $\alpha_c = .44$, $\alpha_s = -0.18$ gives $\delta = 91 - 88.4 = 2.6$. Budyko's fit, Eq. (45), gives (for $T_s = 15°C$) $\delta = 71 - 88.6 = -17.6$, indicating greater sensitivity. Clearly the cloud cover effect is very sensitive to the model and is therefore to be regarded at present as unreliable. It should be mentioned that the influence of cloudiness on albedo is completely ignored in Ref. 18. These authors disagree with Cess on the dependence of F on T_s even though the same satellite data were used. The "correction" to Cess is held responsible for the climate being more stable to changes in S than claimed by Budyko and Sellers.

The satellite fits cited above rely on comparison of different latitudinal zones. Thus the temperatures T_s are average annual values suitable to different latitudes. Cess also discussed the seasonal temperature dependence of F and α for a fixed zone, chosen to avoid complications due to snow and ice (35°N). His motive for doing this was the apparent independence of the atmospheric feedback mechanisms on latitude (except possibly at high latitude). Again F and α are well fit to a linear dependence on T_s :

Digitized by Google

$$F = 185 + 3.5\ T_s$$

$$\alpha_p = 0.441 - 0.0086\ T_s \tag{49}$$

These results are derived from monthly mean values of F and α_p. If we use the values Eq. (49) blindly in Eq. (43) we get a very large value $\beta = 410°$, very different from the value $\beta = 145°$ obtained from Eq. (48) with negligible cloud feedback.

Cess proposes to interpret this difference as due to a strong positive seasonal feedback mechanism which does not occur for the long-term global climate change. His candidate for this is an effective temperature dependence of α_c, to be estimated from the observed latitudinal dependence of α_c. Consideration of Eq. (46) then gives

$$\frac{d\alpha_p}{dT_s} = \left(\frac{d\alpha_p}{dT_s}\right)_{\text{seasonal}} - A_c \left(\frac{d\alpha_c}{dT_s}\right)_{\text{eff.}} \tag{50}$$

which restores agreement with β reckoned on an annual basis.

Finally, we mention Cess' estimates of dA_c/dT_s. From Eq. (46) we find

$$\frac{dA_c}{dT_s} = \frac{1}{\alpha_c - \alpha_s} \frac{d\alpha_p}{dT_s} \quad . \tag{51}$$

Using Eq. (50) one finds values of -0.013, -0.020, -0.014 $(°C)^{-1}$ for 25°N, 35°N and 45°N latitude, suggesting that the annual cloud cover

Digitized by Google

decreases with increasing T_s. In this and other matters it is not clear whether latitude and temperature dependence have been correctly disentangled.

Ice-albedo feedback was re-evaluated in Ref. 17 and was found to be substantially smaller than originally thought.[19,20]

Digitized by Google

Digitized by Google

REFERENCES FOR SECTION IV

1. P. Chylek and J. A. Coakley, Jr., "Analytical analysis of a Budyko-type climate model; Journ. Atmos. Sci., 32, 1975, No. 675-679.

2. M. Ghil, "Climate stability for a Sellers-type model," Journ. Atm. Sci., 33, 1976, pp 3-20.

3. M. Hantel, "Polar boundary conditions in zonally averaged global climate models," Journ. App. Meteor, 13, 1974, 752-759.

4. I. M. Held and M. J. Suarez, "Simple albedo feedback models of the icecaps," Tellus, 36, 1974, pp 613-629.

5. M. S. Liam and R. D. Cess, "Energy balance climate models--a reappraisal of ice-albedo feedback," Journ. Atm. Sci, 34, 1977, pp 1058-1062.

6. J. Oerleman and H. M. van den Dool, "Energy balance climate models: stability experiments with a refined albedo and updated coefficients for I-R emission", Journ. Atm. Sci., March 1978, pp 371-381.

7. W. D. Sellers, "A new global climate model," Journ. App. Meteor, 8, 1973, pp 241-254.

8. G. North, "Analytical solution to a simple climate model with diffusive heat transport", Journ. Atmos. Sci., 32, 1975, pp 1301-1307.

9. G. North, "Theory of energy balance climate models", Journ. Atmos. Sci., 32, 1975, p 2033-2093.

10. G. R. North, "Simple Mathematical Models of the Climate," unpublished lecture notes (1978).

11. G. R. North, "Analytical Solution to a Simple Climate Model with Diffusive Heat Transport," J. Atmos. Sci., Vol. 36, pp. 1301-1307 (1957a).

12. M. I. Bodyko, "The Effect of Solar Radiation Variations on the Climate of the Earth," Tellus, Vol. 21, pp. 611-619 (1969).

13. G. R. North, "Theory of Energy-Balance Climate Models," J. Atmos. Sci., Vol. 32, pp. 2033-2043 (1975b).

Digitized by Google

REFERENCES FOR SECTION IV (Cont.)

14. W. D. Sellers, Physical Climatology University of Chicago Press, 4th Edition, 1974) (1965).

15. P. H. Stone, "The Effect of Large-Scale Eddies on Climatic Change," J. Atmos. Sci., Vol. 30, pp. 521-529 (1973).

16. R. D. Cess, J. Atmos. Sci. 33, 1831 (1976).

17. M. S. Lian and R. D. Cess, J. Atmos. Sci. 34, 1058 (1977).

18. J. Oerlemans and H. M. van den Dool, J. Atmos Sci. 35, 371 (1978).

19. M. I. Budyko, Tellers 21, 611 (1969)

20. W. D. Sellers, J. Appl. Meteor. 8, 392 (1969).

Digitized by Google

V RESEARCH NEEDS
A CRITIQUE OF "A COMPREHENSIVE PLAN FOR CARBON DIOXIDE EFFECTS RESEARCH AND ASSESSMENT"

A. General

In May 1978, the Department of Energy's Office of Carbon Dioxide Effects Research and Assessment published a plan for research into the Global Climate Cycle and Climatic Effects of Increasing Carbon Dioxide. The Plan was the basis of a number of Research Program Development Papers prepared by specialists in various areas of carbon dioxide research. Our comments on the plan derive from our own research efforts as well as many discussions with scientists interested in the carbon dioxide question.

The Department of Energy's plan is comprehensive and represents the results of a vigorous and wide-ranging effort to assess the opinions and ideas of those experts who have worked in the general area. It is useful as a compendium of possible research activities, but it can hardly be termed a research plan since the priority recommendations do not provide the overall guidance for the total effort. In particular, the plan does not indicate how the evolution of the program will depend on the results derived in any particular research effort. For example, until some rough estimate of the contribution of the biosphere is made, it is difficult to assess how much effort, if any, should be devoted to obtaining further detailed information on the biosphere.

Digitized by Google

The goal of the program should be to obtain a sufficiently good understanding of the carbon cycle and of the atmosphere to be able to predict with a high level of confidence climatic effects over time intervals of decades to centuries due to changes in atmospheric carbon dioxide concentration. Since there is not empirical evidence of the coupling between the observed increase in atmospheric carbon dioxide and the current climate, we must turn to theory and indirect observations.

With respect to an improved climate prediction capability, this difficult problem has attracted the attention of many outstanding scientists for a number of years, but progress has been slow. We believe that more effort along conventional lines will not lead to a timely resolution of the CO_2 problem. The Plan does refer to simplified climate models based on heat budget consideration, but does not give them a high priority. We believe that basically new approaches are needed, not necessarily based on simple energy budget models or complex General Circulation Models to deal with the CO_2 question.

The carbon cycle problem is more complicated. Some parts of the cycle have been studied for a long time, others only recognized recently. For example, the living carbon content of the oceans is relatively small, on the order of two Gtons, but the turnover time is short, about a week, far less than the terrestrial equivalent. The "box" models of the ocean tell us very little in that they are parametrically insensitive. Much the same is true for the tracer approaches.

Digitized by Google

When a new one is introduced, it carries with it its own set of uncertainties leaving the situation with one more equation, but also one more variable. The research program should recognize the limitations of eddy diffusive models and emphasize the content of the organic pools and turnover rates in both the ocean and terrestrial environments.

B. Priorities

Our set of priorities differs significantly from those given in the Plan. In our view, the primary problem in understanding the increase of carbon dioixde in the atmosphere is to determine the sign and magnitude of the biosphere contributions. If this contribution is close to zero as some chemical oceanographers would argue, then a good semi-quantitative description for changes in carbon dioxide is available and further research will only be a refinement. If, on the other hand, the biosphere is as important as others have maintained, then we are far from understanding the sinks for the carbon based fuel injected into the atmosphere. Because of these considerations, first priority should be given to improved estimates of the contribution of the biosphere to recent changes in carbon dioxide, especially through the use of carbon isotopes.

Digitized by Google

Our list of priorities, in order of importance is as follows:

- improved estimates of the contribution of the biosphere to recent changes in CO_2, especially through the use of carbon isotopes;

- detailed planning of oceanographic survey to assess the rate of transfer of the carbon species from the surface water to the deeper oceans;

- investigations of more sophisticated energy budget models and statistical models of climate;

- expansion of observing network to determine variation in the trace molecule composition of the atmosphere and the carbon isotope ratios;

- feasibility studies of directly determining future changes in both vegetation and especially soil carbon; and the ways these are being influenced by ground leasing and agricultural practices;

- investigation of the possibility of shallow-water sedimentation and dissolution contributing to the ocean CO_2 balance;

- investigation of the <u>seasonal</u> variation of CO_2 in the mixed layer in order to obtain better data on the turbulent diffusion parameters.

Digitized by Google

We would give an improvement of the industrial source terms a much lower priority since these are known to within about 10%. We would also give research on the buffering factor a low priority. It does not make much difference at present just where in the range 1/7 to 1/11 the value lies. We do not believe that refinements of the gas-exchange rate across the air-sea interface be given high priority. C^{14} measurements show that this rate is fast enough to insure spproximate atmosphere-mixed layer equilibrium on a time scale on order of magnitude less than that for CO_2 growth or mixed layer residence times. The precise value does not enter into any prediction or interpretation of CO_2 sources and sinks.

In the area of improving climate prediction, the plan calls for support of coupled ocean-atmosphere General Circulation Models. We believe that the complexity of the models may be so great as to hide the underlying physics and that the numerical methods employed may distort long term integrations. Research into models intermediate in complexity between the heat budget models and the GCM may provide useful insights into the prediction problem.

C. Management Issues

The research plan avoids questions of program management. We do have, however, serious reservations about housing program management within the Office of the Assistant Secretary of the Environment. The study of carbon dioxide is going to be a many-year effort of basic

Digitized by Google

research, involving a wide range of disciplines. The Office of the Assistant Secretary of the Environment is faced with a vast variety of day-to-day issues which may prevent adequate consideration of the longer term questions. The Office of Research has had a long history of managing multi-disciplinary long term efforts and is directly responsible for the National Laboratories. Because of their long involvement in basic research, the Office of Research would provide a more congenial home than the Office of the Assistant Secretary of the Environment.

- Responsibility within the Department of Energy for the management of the carbon dioxide research and assessment program should be given to the Office of Research.

The Plan refers to the international aspects of the carbon dioxide research program. We believe that the international nature of the program has received inadequate attention. Cooperation of other countries as well as such organizations as WMO and UNEP will be essential if the goal of the program is to be achieved.

- International aspects of CO_2 research should receive high priority.

Digitized by Google

DISTRIBUTION LIST

ORGANIZATION	NO. OF COPIES
Dr. Henry D.I. Abarbanel Lawrence Berkeley Laboratory Berkeley, CA 94720	1
Philip H. Abelson Science 1515 Massachusetts Ave., NW Washington, D.C. 20005	1
Theodore M. Albert Div. of Environmental Impacts Office of Technology Impacts U.S. Department of Energy Washington, D.C. 20545	1
J.A.S. Adams Geology Department Rice University Houston, TX 77005	1
L.H. Allen, Jr. USDA-ARS-SWAP Project 304 Newell Hall Agronomy Department University of Florida Gainesville, FL 32611	1
C.C. Amundsen University of Tennessee Department of Ecology 408 Tenth Street Knoxville, TN 37916	1
Neil R. Andersen Marine Chemistry National Science Foundation Washington, D.C. 20550	1
Anders W. Andren Department of Water Chemistry University of Wisconsin Madison, WI 53706	1
Lynn Anspaugh Lawrence Livermore Laboratory Box 868 Livermore, CA 94550	1
R. Keith Arnold Asst. Vice President for Research University of Texas/Austin University Station, Box Y Austin, TX 78712	1
W.C. Ashby Department of Botany Southern Illinois University Carbondale, IL 62903	1
P.M. Attiwill University of Melbourne Melbourne AUSTRALIA	1
Dr. Paul Auvil Department of Physics Northwestern University Evanston, IL 60201	1
Robert Bacastow Scripps Institution of Oceanography University of California/San Diego La Jolla, CA 92093	1
Wilfrid Bach Applied Climatology, Department of Geography University of Munster D 4400 Munster WEST GERMANY	1
Dr. James Bailey Office of Naval Research Code 462 Arlington, VA 22217	1
D. Ballantine Div. of Biomedical & Environmental Research U.S. Department of Energy Washington, D.C. 20545	1
N.F. Barr Div. of Biomedical & Environmental Research U.S. Department of Energy Washington, D.C. 20545	1

Digitized by Google

ORGANIZATION	NO. OF COPIES
David Barry, Dean The Graduate School University of Toledo 2801 Bancroft Street Toledo, OH 43606	1
Roger P. Belanger Southeastern Forest Experiment Station Athens, GA 30601	1
W. Belter U.S. Department of Energy Washington, D.C. 20545	1
Carl M. Bernstein Timber Management Research 811-RPE 12th & Independence Avenue Washington, D.C. 20250	1
Eugene Bierly Climate Dynamics National Science Foundation Washington, D.C. 20550	1
W. Dwight Billings Department of Botany Duke University Durham, NC 27700	1
W. Bischof Institute of Meterology University of Stockholm Stockholm SWEDEN	1
O. Bjorkman Department of Plant Biology Carnegie Institute of Washington Stanford University Palo Alto, CA 94305	1
Lawrence C. Bliss Department of Botany University of Washington Seattle, WA 98185	1
Bert Bolin Department of Meterology Arrhenius Laboratory University of Stockholm FACK, S-104-05 Stockholm SWEDEN	1

ORGANIZATION	NO. OF COPIES
Herbert Bormann School of Forestry Yale University New Haven, CT 06520	1
Vaughn Bowen Woods Hole Institute of Oceanography Woods Hole, MA 02543	1
Stephen G. Boyce Southeastern Forest Experiment Station Asheville, NC 28807	1
Dr. Max E. Britton U.S. Geological Survey National Center (MS 106) 12202 Sunrise Valley Drive Reston, VA 22092	1
Wallace S. Broecker Lamont-Doherty Geological Observatory of Columbia University Palisades, NY 10964	1
H. Brooke 217 Pierce Hall Harvard University Cambridge, MA 02138	1
J. Brooks Biological & Environmental Research National Science Foundation Washington, D.C. 20550	1
Jerry Brown Cold Regions Research & Engineering Laboratory Box 282 Hanover, NH 03755	1
R.A. Bryson Institute for Environmental Studies University of Wisconsin Madison, WI 33706	1
Robert E. Buckman Deputy Chief, Research Forest Service Washington, D.C. 20250	1

Digitized by Google

ORGANIZATION	NO. OF COPIES
R.W. Burling Institute of Oceanography University of British Columbia Vancouver, B.C., V6T 1W5 CANADA	1
K.W. Butzer Department of Geography University of Chicago Chicago, IL 60637	1
John Cairns, Jr. Center for Environmental Studies Virginia Polytechnic Institute Blacksburg, VA 24060	1
Melvin Calvin Laboratory of Chemical Biodynamics University of California Berkeley, CA 94720	1
Dr. Gregory H. Canavan Director of Internal Fusion M.S. C-404 U.S. Department of Energy Washington, D.C. 20545	1
J. Cantlon Provost Office Michigan State University East Lansing, MI 48823	1
Joseph M. Caprio Department of Plant & Soil Science Montana State University Bozeman, MT 59715	1
Dr. Peter Carruthers Los Alamos Scientific Laboratory Post Office Box 1663 Los Alamos, NM 87545	1
Mary E. Cárter, Director Southern Regional Research Center USDA/ARS 1100 Robert E. Lee Boulevard P.O. Box 19687 New Orleans, LA 70179	1
Dr. Joseph W. Chamberlain 18622 Carriage Court Houston, TX 77058	1

ORGANIZATION	NO. OF COPIES
Keith Chave University of Hawaii Hawaii Institute of Geophysics Honolulu, HI 96822	1
Dr. Robert Chervin National Center for Atmospheric Res. P.O. Box 3000 Boulder, CO 80307	1
William W. Chilcote Department of Botany Oregon State University Corvallis, OR 97331	1
Dr. Robert F. Christy California Institute of Technology 340-32 Pasadena, CA 91125	1
Eloise E. Clark Biological & Medical Sciences National Science Foundation Washington, D.C. 20550	1
Harlan Cleveland Program in International Affairs Aspen Institute for Humanistic Studies P.O. Box 2829 Princeton, NJ 08540	1
Ron Collis SRI International/L2110 333 Ravenswood Avenue Menlo Park, CA 94025	1
Charles Cooper Ecology Program San Diego State University San Diego, CA 92182	1
R.D. Cooper Integrated Assessment U.S. Department of Energy Washington, D.C. 20545	1
Harmon Craig Scripps Institution of Oceanography A-020 University of California/San Diego La Jolla, CA 92093	1

Digitized by Google

ORGANIZATION	NO. OF COPIES
Kermit Cromack U.S. Forest Service Laboratory Corvallis, OR 97330	1
Dr. Paul Dalrymple National Defense Institute Research Directorate Ft. McNair, W.D.C. 20319	1
Kenneth W. Davis Vice President Bechtel Power Corporation P.O. Box 3965 San Francisco, CA 94119	1
Dr. Ruth Davis DUSDRE (R&AT) The Pentagon, Room 3E114 Washington, D.C. 20301	1
E.S. Deevey, Jr. Florida State Museum University of Florida Gainesville, FL 32611	1
Wayne L. Decker Department of Atmospheric Sciences University of Missouri Columbia, MO 65201	1
Egon T. Degens Geologisch-Palantologisches Institute University of Hamburg Bundesstrabe 55 2000 Hamburg 13 FEDERAL REPUBLIC OF GERMANY	1
Constance C. Delwiche Soils and Plant Nutrition University of California Davis, CA 95616	1
H.R. Deselm Department of Botany University of Tennessee Knoxville, TN 37916	1
Dr. John Deutch Director, Office of Energy Research U.S. Department of Energy Washington, D.C. 20545	1
Josephine Doherty Division of Applied Research National Science Foundation Washington, D.C. 20550	1
Warren Doolittle Associate Deputy Chief Forest Service, USDA 3007 South Building 12th & Independence Ave., SW Washington, D.C. 20250	1
John Eddy High Altitude Observatory Box 1558 Boulder, CO 80302	1
Dr. David Elliott SRI International/L2053 333 Ravenswood Avenue Menlo Park, CA 94025	1
Dr. William Elliott NOAA/ARL Resources Laboratory 8060 - 13th Street Silver Spring, MD 20910	1
C. Emiliani Marine & Atmospheric Science University of Miami Coral Gables, FL 33124	1
A.H. Emmons Vice President for Research University of Missouri Route 4, Box 210B Columbia, MO 65201	1
E. Eriksson University of Uppsala Uppsala SWEDEN	1
Col. E.W. Finday OUSDRE/ELS The Pentagon, Room 3D129 Washington, D.C. 20301	1
Dr. Manuel Fliadeiro Department of Geology & Geophysics Yale University P.O. Box 261, Yale Station New Haven, CN 06520	1

Digitized by Google

ORGANIZATION	NO. OF COPIES
H. Flohn Meterological Institute Bonn University WEST GERMANY	1
Dr. Henry M. Foley Department of Physics Columbia University New York, NY 10017	1
Director National Security Agency Ft. Meade, MD 20755 ATTN: Dr. Richard Foss FAN III, A42	1
Dr. Robert Fossum Director Advanced Research Projects Agency 1400 Wilson Boulevard Arlington, VA 22209	1
J. Franklin U.S. Forest Service Laboratory Corvallis, OR 97330	1
R.E. Franklin Div. of Biomedical & Environmental Research U.S. Department of Energy Washington, D.C. 20545	1
David Freeman Tennessee Valley Authority Knoxville, TN 37902	1
J.C. Frye Executive Secretary Geological Society of America 3300 Penrose Place Boulder, CO 80301	1
Richard R. Gardner Deputy Assistant Administrator Office of Coastal Zone Management 3300 Whitehaven Street, NW Washington, D.C. 20235	1
R.M. Garrels Department of Geology Northwestern University Evanston, IL 60201	1

ORGANIZATION	NO. OF COPIES
Dr. Richard L. Garwin IBM, TJWatson Research Center Post Office Box 218 Yorktown Heights, NY 10598	1
William R. Gasser National Defense University Research Directorate Fort McNair, W.D.C. 20319	1
David M. Gates Division of Biological Sciences University of Michigan Ann Arbor, MI 48109	1
W. Lawrence Gates Department of Atmospheric Science Ag Hall Oregon State University Corvallis, OR 97331	1
J.H. Gibbons Environmental Center University of Tennessee Knoxville, TN 37916	1
Robert A. Goldstein Electric Power Research Institute 3412 Hillview Avenue P.O. Box 10412 Palo Alto, CA 94304	1
Frank B. Golley, Jr. Institute of Ecology, Rockhouse University of Georgia Athens, GA 30601	1
A.J.P. Gore Monks Wood Experimental Station Natural Resources Research Council Abbots Ripton Hunts UNITED KINGDOM	1
Col. John Hager OUSDRE (R&AT) The Pentagon, Room 3E121 Washington, D.C. 20301	1
Dr. Ralph W.F. Hardy Central Research & Development Dept. E.I. Dupont Wilmington, DE 19898	1

Digitized by Google

ORGANIZATION	NO. OF COPIES
Steven Hanna NOAA Atmospheric Turbulence & Diffusion Laboratory Oak Ridge, TN 37830	1
Kirby Hanson Environmental Research Laboratories NOAA Boulder, CO 80302	1
Wayne Hanson Los Alamos Scientific Laboratory P.O. Box 1663 Los Alamos, NM 87544	1
James D. Hays Lamont-Doherty Geophysical Laboratory of Columbia University Palisades, NY 10964	1
Allen Hecht Climate Dynamics National Science Foundation Washington, D.C. 20550	1
Joan Hett c/o College of Forestry University of Washington Seattle, WA 98195	1
H.R. Hickey Environmental Planning Tennessee Valley Authority Chattanooga, TN 37401	1
J.B. Hilmon Director Southeastern Forest Experiment Sta. Asheville, NC 28807	1
Charles J. Hitch President Resources for the Future 1755 Massachusetts Ave., NW Washington, D.C. 20036	1
J.P. Holdren Energy & Resources Group University of California 100 T-4 Berkeley, CA 94720	1

ORGANIZATION	NO. OF COPIES
Crawford S. Holling Institute of Animal Resource Ecology The University of British Columbia 2075 Wesbrook Place Vancouver, B.C., V6T 1W5 CANADA	1
H. Hollister U.S. Department of Energy Washington, D.C. 20545	1
Raymond P. Hosker, Jr. Atmospheric Turbulence & Diffusion Lab. NOAA P.O. Box E Oak Ridge, TN 37830	1
Peter House U.S. Department of Energy Washington, D.C. 20545	1
Wallace E. Howell Assistant to the Chief Division of Atmospheric Water Resources Mgmt. Bureau of Reclamation P.O. Box 25007, DFC Denver, CO 80225	1
Dr. Benjamin Huberman National Security Council Old Executive Office Building Washington, D.C. 20506	1
Mr. James Hughes Office of Naval Research Code 465 Arlington, VA 22217	1
G.E. Hutchinson Yale University New Haven, CN 06520	1
John Imbrie Department of Geological Science Brown University Providence, RI 02912	1
Carl Jordan c/o Institute of Ecology University of Georgia Athens, GA 30601	1

Digitized by Google

ORGANIZATION	NO. OF COPIES
J. Jordan Climate Dynamics National Science Foundation Washington, D.C. 20550	1
Charles D. Keeling Scripps Institution of Oceanography University of California/San Diego La Jolla, CA 92093	1
W.W. Kellogg National Center for Atmospheric Res. P.O. Box 3000 Boulder, CO 80303	1
B.H. Ketchum Woods Hole Inst. of Oceanography Woods Hole, MA 02543	1
Donald King, Director Office of Environmental Affairs Department of State Washington, D.C. 20520	1
Kenneth R. Knoerr School of Forestry and Environmental Studies Duke University Durham, NC 27706	1
Dr. Eugene Kopf Deputy Director Advanced Research Projects Agency 1400 Wilson Boulevard Arlington, VA 22209	1
V. Kovda Moscow State University Moscow USSR	1
Helmut Landsberg University of Maryland College Park, MD 20740	1
J.A. Laurmann Division of Applied Mechanics Stanford University Stanford, CA 94305	1

ORGANIZATION	NO. OF COPIES
Ray Leadabrand SRI International/L1053 333 Ravenswood Avenue Menlo Park, CA 94025	1
Dr. Edgar R. Lemon Microclimate Project 1020 Bradfield Hall Cornell University Ithaca, NY 14853	1
Estella Leopold Quaternary Research Center University of Washington Seattle, WA 98195	1
Leona Libby Engineering School University of California/LA Los Angeles, CA 90024	1
Rothamsted Experimental Station ATTN: Library Harpenden, Herts ENGLAND	1
Tennessee Valley Authority ATTN: Library Knoxville, TN 37902	1
Great Lakes Fishery Laboratory ATTN: Library U.S. Bureau of Sport Fisheries and Wildlife Ann Arbor, MI 49904	1
University of Michigan Biological Station ATTN: Library Ann Arbor, MI 48109	1
G. Likens Ecology & Systematics Cornell University Ithaca, NY 14850	1
J.L. Liverman Deputy Asst. Secretary for Environment U.S. Department of Energy Washington, D.C. 20545	1

Digitized by Google

ORGANIZATION	NO. OF COPIES
Robert S. Loomis Agronomy & Range Science University of California Davis, CA 95616	1
Orie Loucks The Institute of Ecology Holcomb Institute Butler University Indianapolis, IN 46208	1
Arial Lugo Council on Environmental Quality 722 Jackson Place, NW Washington, D.C. 20006	1
L. Machta Air Research Laboratory NOAA Silver Spring, MD 20910	1
Director National Security Agency Ft. Meade, MD 20755 ATTN: Mr. Robert Madden	1
John J. Magnuson Limnology Laboratory University of Wisconsin Madison, WI 53706	1
Jack Major Department of Botany University of California Davis, CA 95616	1
Alexander Malahoff National Ocean Survey NOAA Rockville, MD 20852	1
T. Malone The Institute of Ecology Holcomb Institute Research Butler University Indianapolis, IN 46208	1
Syuhoro Manabe Geophysical Fluid Dynamics Lab. NOAA P.O. Box 308 Princeton, NJ 08540	1

ORGANIZATION	NO. OF COPIES
Bryan Mar Department of Civil Engineering FX-10 University of Washington Seattle, WA 98195	1
G.I. Marchuk USSR Academy of Science Leninskiy Prospect Moscow USSR	1
Dr. Clifford Mass Department of Atmospheric Science AK-40 University of Washington Seattle, WA 98195	1
William D. McElroy Chancellor University of California/San Diego La Jolla, CA 92093	1
Samuel McKee Office of the Foreign Secretary National Academy of Sciences 2101 Constitution Avenue, NW Washington, D.C. 20418	1
D.H. Miller Department of Geological Sciences University of Wisconsin Milwaukee, WI 53201	1
J.M. Mitchell Environmental Data Service NOAA Silver Spring, MD 20910	1
Tom Moss c/o George Brown Rayburn Office Building U.S. House of Representatives Washington, D.C. 20515	1
Robert J. Mulholland E.S. 303 Oklahoma State University Stillwater, OK 74074	1

Digitized by Google

ORGANIZATION	NO. OF COPIES
Dr. Gordon J. MacDonald The MITRE Corporation MITRE C^3 Division 1820 Dolley Madison Boulevard McLean, VA 22102	5
Dr. Walter H. Munk M.C. A025 IGPP University of California/San Diego La Jolla, CA 92093	1
Jerome Namias Research Meterologist, A024 Room 2252, Sverdrup Hall Scripps Institution of Oceanography University of California/San Diego La Jolla, CA 92093	1
J. Neuhold Ecology Program Utah State University Logan, UT 84321	1
Reginald Newell Department of Meterology M.I.T. Cambridge, MA 02139	1
Dr. William A. Nierenberg Scripps Institution of Oceanography University of California/San Diego La Jolla, CA 92093	1
Dr. Gerald North Department of Physics 517 Benton Hall University of Missouri 8001 Natural Bridge Street St. Louis, MO 63121	1
E.P. Odum Institute of Ecology University of Georgia Athens, GA 30601	1
H.T. Odum Environmental Engineering University of Florida Gainesville, FL 32601	1
W.T. Odum Environmental Sciences University of Virginia Charlottesville, VA 22903	1
Dr. Hans Oeschger Physics Institute University of Bern Sidlerstr. 5 3000 Bern SWITZERLAND	1
H. Gote Ostlund School of Marine & Atmospheric Science University of Miami 4600 Rickenbacker Causeway Miami, FL 33149	1
The Honorable William Perry Under Secretary of Defense (RE) The Pentagon, Room 3E1006 Washington, D.C. 20301	1
The Honorable Frank Press Director Office of Science & Technology Policy Executive Office of the President Washington, D.C. 20500	1
S.I. Rasool c/o Code E-1 NASA Headquarters Washington, D.C. 20546	1
W.A. Reiners Biological Sciences Dartmouth College Hanover, NH 03755	1
Elmar Reiter Department of Atmospheric Science Colorado State University Fort Collins, CO 80521	1
Dr. Roger Revelle Scripps Institution of Oceanography University of California/SD La Jolla, CA 92093	1

Digitized by Google

ORGANIZATION	NO. OF COPIES
Gordon A. Riley Institute of Oceanography Dalhousie University Halifax, Nova Scotia CANADA	1
M. Reilly Fossil Fuels U.S. Department of Energy Washington, D.C. 20545	1
G.D. Robinson Center for the Environment & Man 275 Winsor Street Harford, CN 06120	1
Dr. Oscar Rothaus 106 Devon Road Ithaca, NY 14850	1
Eugene Ruane Main P.O. Box 1925 Washington, D.C. 20013	1
Dr. Malvin A. Ruderman 29 Washington Square, West New York, NY 10011	1
The Honorable James Schlesinger Director U.S. Department of Energy Washington, D.C. 20545	1
Dr. Mike Schlesinger Department of Atmospheric Science Ag Hall Oregon State University Corvallis, OR 97331	1
William Schlesinger Department of Biology University of California Santa Barbara, CA 93106	1
Dr. Stephen Schneider National Center for Atmospheric Res. P.O. Box 3000 Boulder, CO 80307	1

ORGANIZATION	NO. OF COPIES
R.C. Schnell Mt. Kenya Project Box 30218 Nairobi, Kenya AFRICA	1
Dr. William D. Sellers Institute for Atmospheric Research University of Arizona Tucson, AZ 85721	1
N.J. Shackleton University of Cambridge 5, Salisbury Villas Station Road Cambridge CB1 2JF ENGLAND	1
Ray Siever Hoffman Laboratory Harvard University Cambridge, MA 02138	1
S. Fred Singer Professor, Environmental Sciences University of Virginia Clark Hall Charlottesville, VA 22903	1
Dr. David Slade Director Office of CO_2 Effects Research & Assessment Office of Asst. Sec./Environment U.S. Department of Energy Washington, D.C. 20545	5
J. Smagorinsky Geophysical Fluid Dynamics Laboratory NOAA Princeton, NJ 08540	1
Frederick E. Smith Graduate School of Design Harvard University Cambridge, MA 02138	1

Digitized by Google

ORGANIZATION	NO. OF COPIES
Samuel C. Snedaker Associate Professor School of Marine & Atmospheric Sci. University of Miami 4600 Rickenbacker Causeway Miami, FL 33149	1
Dr. Fred Snell Department of Atmospheric Science Ag Hall Oregon State University Corvallis, OR 97331	1
Dr. Joel A. Snow Associate Director Office of Research Policy Office of Energy Research U.S. Department of Energy Washington, D.C. 20545	5
Walter O. Spofford, Jr. Director Quality of the Environment Division Resources for the Future 1755 Massachusetts Avenue, NW Washington, D.C. 20036	1
Forest Stearns Department of Botany The University of Wisconsin Milwaukee, WI 53201	1
Klaus Steinbeck School of Forest Resources University of Georgia Athens, VA 30601	1
Earl L. Stone Agronomy Department Cornell University Ithaca, NY 14850	1
Boyd R. Strain Botany Department Duke University Durham, NC 27706	1
Minze Stuiver Quaternary Research Center M.S. AK-60 University of Washington Seattle, WA 98195	1
Hans E. Suess Department of Chemistry University of California/SD Code B-017 La Jolla, CA 92093	1
Taro Takahashi Lamont Doherty Geological Observatory of Columbia University Palisades, NY 10964	1
John D. Tenhunen University of Michigan Biological Station Ann Arbor, MI 48109	1
E.G. Terhune Policy Analysis National Science Foundation Washington, D.C. 20550	1
Werner H. Terjung Department of Geography University of California Los Angeles, CA 90024	1
Larry Tombough National Science Foundation Washington, D.C. 20550	1
K. Van Cleve Forest Soils Laboratory University of Alaska Fairbanks, AK 99701	1
Dr. John F. Vesecky Center for Radar Astronomy Stanford University Stanford, CA 94305	1
P.E. Waggoner Connecticut Agricultural Experiment Station New Haven, CN 06501	1
Warren Washington National Center for Atmospheric Res. P.O. Box 3000 Boulder, CO 80303	1

Digitized by Google

ORGANIZATION	NO. OF COPIES
Kenneth Watt Division of Environmental Studies University of California Davis, CA 95616	1
Thompson Webb, III Department of Geological Sciences Brown University Providence, RI 02912	1
A.L. Weinberg Institute for Energy Analysis Oak Ridge Associated Universities Oak Ridge, TN 37830	1
Gilbert F. White Institute of Behavioral Science University of Colorado Boulder, CO 08302	1
R.H. Whittaker Department of Ecology & Systematics Cornell University Ithaca, NY 14850	1
Carroll L. Wilson Department of Urban & Regional Planning M.I.T. Cambridge, MA 02139	1
J. Wilson Division of Environmental Impacts U.S. Department of Energy Washington, D.C. 20545	1
Dr. S.H. Wittwer 101 Agriculture Hall Michigan State University E. Lansing, MI 48824	1
G. Woodwell Marine Biological Laboratory Woods Hole, MA 02543	1
Dr. Fredrick Zachariasen 1 Ch. de Tavernay 1218 Grand Saconnex Geneva SWITZERLAND	1

ORGANIZATION	NO. OF COPIES
Academy of Natural Sciences of Philadelphia Department of Limnology Nineteenth & Parkway Philadelphia, PA 19405	1
Air Force Air Weather Service AWD/DNTI Air Weather Service Scott Air Force Base, IL 62225	1
Battelle Memorial Institute ATTN: R.S. Davidson Columbus Laboratories 505 King Street Columbus, OH 43201	1
Battelle Memorial Institute Technical Information Section Pacific Northwest Laboratory P.O. Box 999 Richland, WA 99352	1
Brookhaven National Laboratory Upton, NY 11973	1
Florida State Energy Office ATTN: Carlos S. Warren State Energy Director 108 Collins Building Tallahassee, FL 32304	1
Hudson Institute ATTN: Project Manager Quaker Ridge Road Croton-on-Hudson, NY 10520	1
Lawrence Livermore Laboratory ATTN: Program Manager for Environmental Biology P.O. Box 808 Livermore, CA 94551	1
NASA ATTN: Library Goddard Space Flight Center Greenbelt, MD 20770	1
NASA ATTN: Library Johnson Space Center Houston, TX 77058	1

Digitized by Google

ORGANIZATION	NO. OF COPIES
NASA ATTN: Library Langley Research Center Hampton, VA 23665	1
National Coal Association ATTN: Carl Bogge, President 1130 - 17th Street, NW Washington, D.C. 20030	1
NOAA ATTN: Robert Kay Office of Marine Technology National Ocean Survey Executive Boulevard NOA/OMT Code C-6 Rockville, MD 20852	1
National Park Service ATTN: Office of Chief Scientist 1100 "L" Street, NW Washington, D.C. 20240	1
Oak Ridge Associated Universities ATTN: Library Institute of Energy Analysis P.O. Box 117 Oak Ridge, TN 37830	1
U.S. Department of Agriculture ATTN: Library	1
Agriculture Research Service	1
Office of the Secretary for Research & Education Washington, D.C. 20250	1
U.S. Department of Agriculture National Agricultural Library Current Serial Record Beltsville, MD 20705	1
U.S. Department of Commerce ATTN: Energy Programs Division	1
Business Awareness Division, Rm. 3011, Off. Energy Prog.	1
James Curlin	1
Asst. Secretary of Commerce for Research & Devel. Washington, D.C. 20230	1

ORGANIZATION	NO. OF COPIES
U.S. Department of Commerce NOAA ATTN: Richard Lehman Office of Ecology & Environmental Conservation Rm. 5815, Main Commerce Building Washington, D.C. 20230	1
U.S. Department of Energy ATTN:	
Div. of Basic Energy Sciences	1
Div. of Biomedical & Environmental Research, Physical & Technological Programs	1
Coal Conversion & Utilization Fossil Energy	1
Div. of Environmental Control Technology	1
Div. of Fossil Energy Research	1
Div. of Fossil Energy Research, Environment & Safety	1
Asst. Director, Div. of Interprogram Applications	1
Asst. Director, Nuclear Energy Assessment, Div. of Nuclear Research & Application	1
Director, Div. of Oil, Gas & Shale Technology	1
Chief, Program Planning, Div. of Operational & Environmental Safety	1
Library, M.S. G-043	1
Asst. General Counsel for Patents	1
Asst. Administrator for Planning & Analysis	1
Dr. Leonard Topper, Director, Div. of Research & Technology Assessment, Office Energy Res. Washington, D.C. 20545	7
U.S. Department of Energy Reports Control Clerk Nevada Operations Office P.O. Box 14100 Las Vegas, NV 89114	1
U.S. Department of Energy ATTN: Management Officer Pittsburgh Energy Research Ctr. 4800 Forbes Avenue Pittsburgh, PA 15213	1

Digitized by Google

ORGANIZATION	NO. OF COPIES
U.S. Department of Energy ATTN: Technical Information Richland Operations Office P.O. Box 550 Richland, WA 99352	1
U.S. Department of Energy 1333 Broadway Oakland, CA 94612 ATTN: Fusion Energy & Physical Research Division	1
Procurement Div., Technical Information Specialist	1
U.S. Department of Energy P.O. Box 808 Livermore, CA 94550 ATTN: Office of Patent Counsel	1
U.S. Environmental Protection Agency 401 "M" Street, SW Washington, D.C. 20460 ATTN: Technical Information	1
Stephen Gage	1
Stephen Platkin	
U.S. Fish & Wildlife Service ATTN: Allan Hirsch Office of Biological Services Washington, D.C. 20240	1
U.S. Naval Postgraduate School ATTN: Library Monterey, CA 93940	1
U.S. Nuclear Regulatory Commission ATTN: Library Washington, D.C. 20555	1
University of California ATTN: Library, Bldg. 50, Rm. 134 Lawrence Berkeley Laboratory Berkeley, CA 94720	1
University of California/SD ATTN: S.S. Penner, Director Energy Center La Jolla, CA 92093	1

ORGANIZATION	NO. OF COPIES
University of Oklahoma Science & Public Policy 601 Elm Avenue Room 432 Norman, OK 73019	1
University of South Florida College of Engineering Tampa, FL 33620	1
University of Washington ATTN: Stanley Gessel College of Forestry Seattle, WA 98195	1
West Virginia University ATTN: J. Renton	1
A.C. Donaldson	1
F.T.C. Ting Geology & Geography Dept. Morgantown, WV 26506	1
Woods Hole Oceanographic Inst. ATTN: John Ryther	1
Senior Scientist, Dept. of Physical Oceanography Woods Hole, MA 02543	1
Mei-Kao Liu Systems Applications, Inc. 950 N. Gate Drive San Raphael, CA 94903	1

Digitized by Google

Digitized by Google

13
6C184-B

Digitized by Google

Digitized by Google

THE UNIVERSITY LIBRARY • UNIVERSITY OF CALIFORNIA, SAN DIEGO
Digitized by Google

THE UNIVERSITY LIBRARY • UNIVERSITY OF CALIFORNIA, SAN DIEGO

Digitized by Google

Digitized by Google